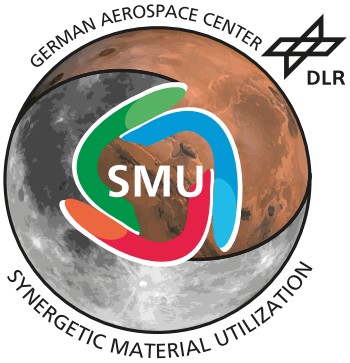

Master Thesis

Experimental optimisation of lunar regolith beneficiation for the production of an ilmenite-rich feedstock

Submitted to the

Faculty of Mechanical Engineering and Transport Systems

Institute of Aeronautics and Astronautics

Chair of Space Technology

Author: Kunal Kulkarni

Matr. Nr.: 0463795

Course of Study: Master of Space Engineering

Supervisors:

Prof Dr.-Ing. Enrico Stoll
Head of Chair of Space Technology
Technische Universität Berlin

M.Sc. Joel Patzwald
Technische Universität Berlin

Berlin, July 2023

Kulkarni, Kunal:
Experimental optimisation of lunar regolith beneficiation for the production of an ilmenite-rich feedstock
Master Thesis, Technische Universität Berlin, 2023.

Declaration of Authorship

I hereby certify that this thesis has been composed by me and is based on my own work, unless stated otherwise. No other person's work has been used without due acknowledgement in this thesis. All references and verbatim extracts have been quoted, and all sources of information, including graphs and data sets, have been specifically acknowledged.

Berlin, 11.07.2023 — Kunalk.

Place, Date — Signature

Agreement on rights of ultilization

The Technische Universität Berlin, represented by the Chair of Space Technology, may use the results of the thesis at hand in education and research. It receives simple (non-exclusive) rights of utilization as according to § 31 Abs. 2 Urheberrechtsgesetzt (Urhg). This right of utilization is unlimited and involves content of any kind (e.g. documentation, presentations, animations, photos, videos, equipment, parts, procedures, designs, drawings, software including source code and similar).

An eventual commercial use on part of the Technische Universität Berlin will only be carried out with approval of the author of the thesis at hand under appropriate share of earnings.

Berlin, 11.07.2023

Place, Date

Kunalk.

Signature

Professor Dr.-Ing Enrico Stoll
Head of the Chair of Space Technology

Abstract

In recent years, significant progress has been made in the space industry to pave the way for long-term human space exploration missions. The Moon has emerged as a focal point of interest, driving technology development and serving as a crucial stepping stone for future exploration endeavours throughout our solar system and beyond. To ensure the sustainable settlement of humans in space, the development of In-situ Resource Utilisation (ISRU) technologies is imperative to enable self-sufficiency in long-duration space missions. The lunar regolith contains essential minerals that hold promise for supporting human space settlements. Amongst them, ilmenite is of significant value for in-situ oxygen production on the lunar surface due to the higher oxygen yield that it provides compared to other minerals. However, the distribution of ilmenite is not uniform across the lunar surface and thus, the raw regolith requires additional processing to achieve sustainable extraction efficiency. This pre-processing is called beneficiation which encompasses activities that help in concentrating a raw material with the mineral of interest using different strategies depending on the material properties. Although being an essential part of ISRU, beneficiation as a research area has often been overlooked, while the attention of the scientific community mainly focused on the preceding and subsequent steps, i.e., excavation and extraction.

The Synergetic Material Utilization research group at DLR Bremen has been working on the development of ISRU technologies to support sustainable human space exploration in the future. In this research group, a laboratory-scale multi-stage lunar regolith beneficiation test bed has been developed for producing an ilmenite-rich feedstock for the subsequent oxygen extraction process. Along with them, the Exploration and Propulsion Group at TU Berlin is also involved in the development of ISRU technologies. An integral part of their research is the production of lunar simulants that allow for the testing of the ISRU technologies. The research produced in this work is an outcome of collaboration between both research groups.

This research begins with an extensive review of prior scientific research on lunar regolith beneficiation to establish a comprehensive understanding of the process. The stages of the testbed are then discussed, highlighting the crucial process parameters necessary for achieving optimisation. Experimental analysis is conducted using different configurations of these parameters to determine the one that produces the desired beneficiation results. To ensure result repeatability, experiments are performed using LMS-1 simulant and TUBS-M based modular regolith simulant. Additionally, secondary results, such as total energy consumption and material residuals, are analysed to gain insights into the system's overall performance and behaviour during continuous operation. The primary objective of this research is to validate and optimise the beneficiation testbed, ensuring the production of the desired output feedstock. Furthermore, this work strives to address existing knowledge gaps in the field of beneficiation and lay the groundwork for future advancements.

Keywords: ISRU, ilmenite, lunar regolith beneficiation, oxygen production

Aknowledgements

I would like to express my deepest gratitude to several individuals and groups who have contributed to the completion of this thesis. First and foremost, I am thankful to the SMU research group in DLR Bremen and my supervisor Dr Paul Zabel for giving me the opportunity to work on this project. I would also like to extend my sincere appreciation to Prof Dr Thorsten Gesing, from the Solid State Chemical Crystallography Department at the University of Bremen, and his PhD student Md. Izzuddin Hanafi, for their assistance in performing the X-ray Diffraction Analysis of the experiment samples. Their expertise in crystallography and their willingness to share their knowledge have significantly helped in this study.

I would like to thank my supervisor at TU Berlin Joel Patzwald for his guidance and support throughout the project. I am also grateful to Cem Avsar from TU Berlin and the entire MSE team for their continuous and prompt support, coordination, and provision of necessary resources. Their efforts have facilitated a smooth and efficient administrative process. I would like to acknowledge Prof. Dr.-Ing Enrico Stoll, the Head of the Chair of Space Technology, for his support in pursuing this research topic.

To my friends and colleagues, I extend my heartfelt thanks for their companionship, stimulating discussions, and motivation throughout this academic endeavour. Their support and camaraderie have made the research experience more enjoyable and fulfilling. Last, but certainly not least, I am profoundly grateful to my family for their unwavering love, encouragement, and understanding. Their continuous support and belief in me have been my driving force. This would be incomplete without a special mention of my grandfather, Suhas Thakur, who sadly passed away last year. I am sure that he would have cherished witnessing me reach this milestone in my life, and I am immensely grateful for his blessings. May he rest in peace.

To all those mentioned above and to anyone else who has contributed in any way, I offer my deepest appreciation. This work would not have been possible without your support and guidance.

Contents

List of Figures

List of Tables

List of Abbreviations

ISRU	In-Situ Resource Utilisation
NASA	National Aeronautics and Space Administration
DLR	Deutsches Zentrum für Luft- und Raumfahrt
LSPS	Lunar Soil Particle Separator
XRD	X-Ray Diffraction
ICDD	International Center for Diffraction Data
ESA	European Space Agency
GCR	Galactic Cosmic Radiations
LIED	Lunar Ilmenite Enrichment Demonstrator
ISS	International Space Station

Chapter 1

Introduction

In recent years, the global space industry has dedicated significant efforts to develop technologies that facilitate long-duration human space exploration missions. A primary focus of these endeavours is the utilisation of resources found in space. Dava Newman, the Ex-Deputy Administrator of NASA stated that "Space resources are the gold of the future, holding the potential to revolutionise our economies, open up new frontiers of exploration, and provide the means for sustained human presence beyond Earth". Recognising the importance of space resources, the industry acknowledges that the establishment of infrastructure for such purposes is crucial for enabling sustainable space exploration and, ultimately for the realisation of human settlements in space as shown in Figure 1.1 [1].

Figure 1.1: Rendered image for future lunar settlement [2]

The Artemis Missions, led by the National Aeronautics and Space Administration (NASA), serve as the foremost catalyst for advancing these efforts. Through these missions, NASA strives to return humans to the lunar surface, aiming to establish a sustainable and enduring presence on the Moon [3]. The main obstacle in such a venture, beyond the inhospitable space environment, lies in the ability to provide support and ensure the long-term survival of human life in space. The International Space Station (ISS) remains our sole reference for long-duration manned missions. Despite some astronauts having stayed in the ISS for nearly a year, it is important to note that the required provisions such as food, medicine, consumables for life support systems, and other

necessary equipment are regularly delivered to the ISS through re-supply missions conducted every few months [4]. However, as we venture further away from the Earth, the feasibility of relying on re-supply missions diminishes due to the increasing time and costs associated with them. As a consequence, there will be a constraint on the maximum duration of all future manned missions if we depend on these re-supply missions. To avoid this restriction on exploration activities, it is necessary to shift our focus beyond Earth and explore alternative sources of essential supplies. This drives the motivation to utilise space resources for advancing exploration endeavours which brings into focus the topic of In-situ Resource Utilisation (ISRU) which deals with technologies that harness the available resources in the lunar regolith for the production of necessary supplies. Figure 1.2 illustrates the interrelationships among various ISRU systems, which demonstrates that advancements in one system can provide valuable insights for the rest of the ISRU infrastructure. The choice of destination for space exploration will directly influence the ISRU infrastructure and its output requirements.

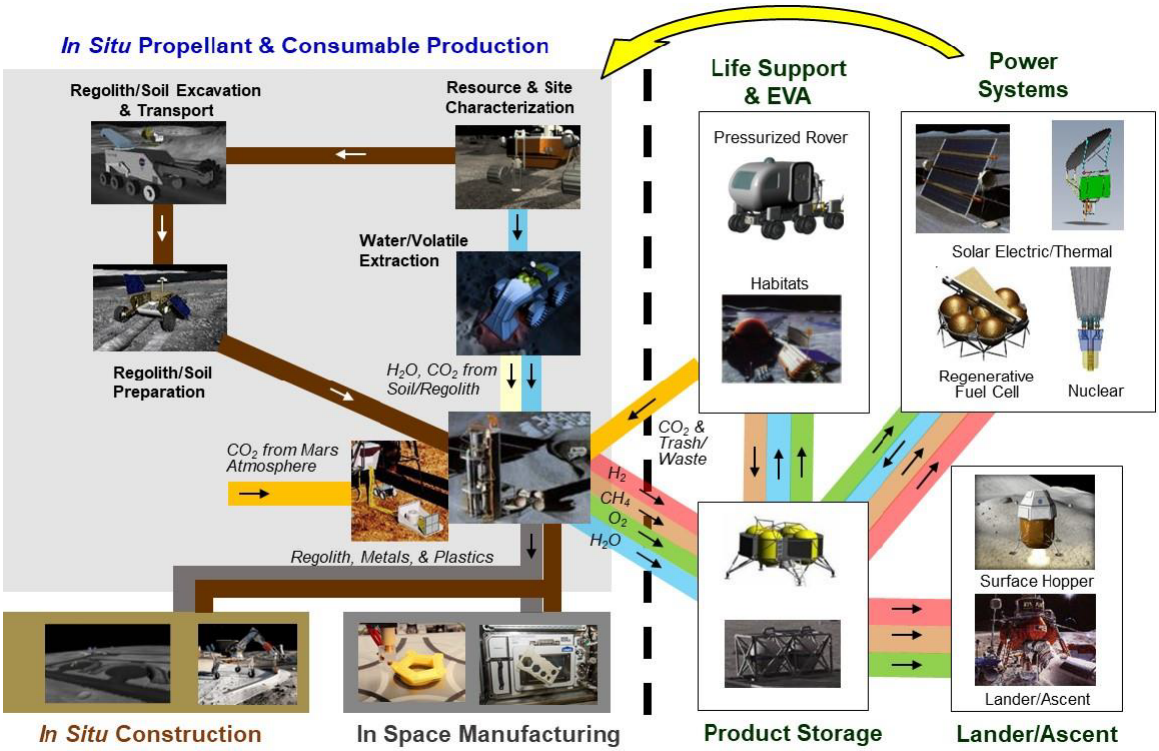

Figure 1.2: Interrelationships in ISRU infrastructure [5]

The choice of the Moon as the destination for Artemis missions is primarily due to its greater accessibility compared to other celestial bodies, the in-situ experience gained during the Apollo missions and the resources present in the lunar regolith that can be extracted and used for space exploration activities. Initially, the Moon was perceived to be bone-dry and devoid of any valuable resources [6]. However, this perception rapidly changed upon analysing the Apollo mission samples, revealing substantial quantities of various minerals [7, 8]. This availability of minerals in the lunar regolith offers opportunities for producing essential supplies to sustain human life on the lunar surface. Among the fundamental requirements for human life are food, water, and oxygen. Remarkably, the lunar regolith contains a substantial amount of oxygen embedded primarily within its silicate and oxide minerals [9]. This oxygen can be extracted and utilised for various purposes, including the production of breathable air, water, and even rocket fuel, thereby enabling self-sufficiency on the lunar surface [9, 6].

Out of the available minerals, ilmenite has the highest yield of oxygen per unit mass which makes it a prime candidate for in-situ oxygen production [10]. However, the availability of ilmenite on the lunar surface is relatively scarce and non-uniform. The concentration of ilmenite in the lunar regolith ranges from less than $0.1\ wt.\%$ to more than $10\ wt.\%$ across different regions of the Moon [7]. The higher preference for ilmenite as a source of oxygen is limited to feedstock with high ilmenite content. A previous study published by NASA about the analysis of power requirements for a small lunar base camp suggests that there exists an inverse relationship between energy consumption for ilmenite-based oxygen extraction and the total ilmenite content present in the lunar regolith [11]. This claim is also validated by another analytical study which shows the decreasing amount of regolith needed with increasing ilmenite content for producing the same amount of oxygen [12]. Therefore, the higher the ilmenite content, the lower the overall energy demand for oxygen production, thereby influencing the efficiency of the extraction system. In order to achieve higher efficiency, a pre-processing of the lunar regolith is necessary to increase its ilmenite content. This pre-processing step is called beneficiation.

Beneficiation refers to the process of extracting and enhancing valuable minerals and resources in a raw material [13]. Without beneficiation of the raw regolith, ilmenite which not only contains oxygen but also metals such as titanium and iron cannot be utilised with sustainable efficiency. This makes beneficiation an important part of the space resources value chain. This importance of beneficiation has also been highlighted by the European Space Agency (ESA) in their ISRU Gap Assessment report published in 2021 [5]. It describes the knowledge gaps in beneficiation activities such as the possible degree of separation for the mineral of interest, the energy expenditure of beneficiation, the system's operational life and the effects of wear on its operational life. Understanding the importance of in-situ oxygen production on the lunar surface and considering ilmenite as a preferred source for extraction, the beneficiation of lunar regolith to enrich it with ilmenite drove the motivation for this thesis.

The *Deutsches Zentrum für Luft- und Raumfahrt (DLR)*, specifically the *Institute of Space Systems (DLR RY)*, has formed a dedicated research group called *Synergetic Material Utilization (SMU)* focussing on exploring the synergies between space resource utilisation activities and life support systems. The team has been actively engaged in developing a beneficiation test bed specifically designed for enriching ilmenite in the lunar regolith. The testbed has been assembled and is currently operational at their facility in Bremen. In the context of this thesis, it is referred to as the Lunar Ilmenite Enrichment Demonstrator (LIED). The primary objective of this research is to conduct an experimental evaluation of LIED to produce a feedstock with higher ilmenite content compared to the input unprocessed simulant. This ilmenite-enriched feedstock will serve as the input for oxygen production processes.

To achieve an optimised beneficiation process, the preliminary goal of this work is to review previous scientific work related to the beneficiation of lunar regolith using different methods and accordingly, make decisions about the optimisation experiments. The processes of beneficiation used in LIED have been well documented by a previous master thesis based on its development process and are made available to the author [14]. The beneficiation of regolith simulant in LIED is achieved using multiple stages that each have their own process parameters which affect the properties of the produced feedstock at the output. The experiments seek to analyse the influence of these parameters on the beneficiation output and determine their optimal configuration for achieving efficient beneficiation performance. The research also aims to identify and quantify any dependencies of the beneficiation results on the simulant properties by assessing the reliability and repeatability of the results across different simulant systems. Future efforts to enhance the LIED system could then prioritise the improvement of beneficiation output by implementing experimental and design modifications.

Thesis structure

The following is an outline of the research produced in this thesis.

Chapter 2 provides an extensive discussion on the theoretical foundation that underpins this research, offering valuable insights into beneficiation processes and analysis techniques relevant to the conducted experiments. Moving on to Chapter 3, a detailed description of the LIED system and its associated processes is presented, emphasising the crucial process parameters that exert influence on the experimental outcomes. Moreover, the chapter delves into the multi-phase optimisation strategy employed to achieve the experimental objectives, offering an elaborate explanation of the methodologies employed for the optimisation experiments and subsequent analyses. Figure 1.3 illustrates the optimisation roadmap followed for the experiments conducted within the scope of this thesis. Building upon this, Chapter 4 offers a comprehensive analysis of the experimental results obtained from LIED, accompanied by a detailed examination of the methodology adopted for the optimisation experiments and discussing the effects of these procedures on the experimental results. Finally, in Chapter 5, the research concludes by summarising the experimental findings, outlining essential considerations for future optimisation efforts, and providing an outlook on the future of beneficiation technologies within the space resources infrastructure.

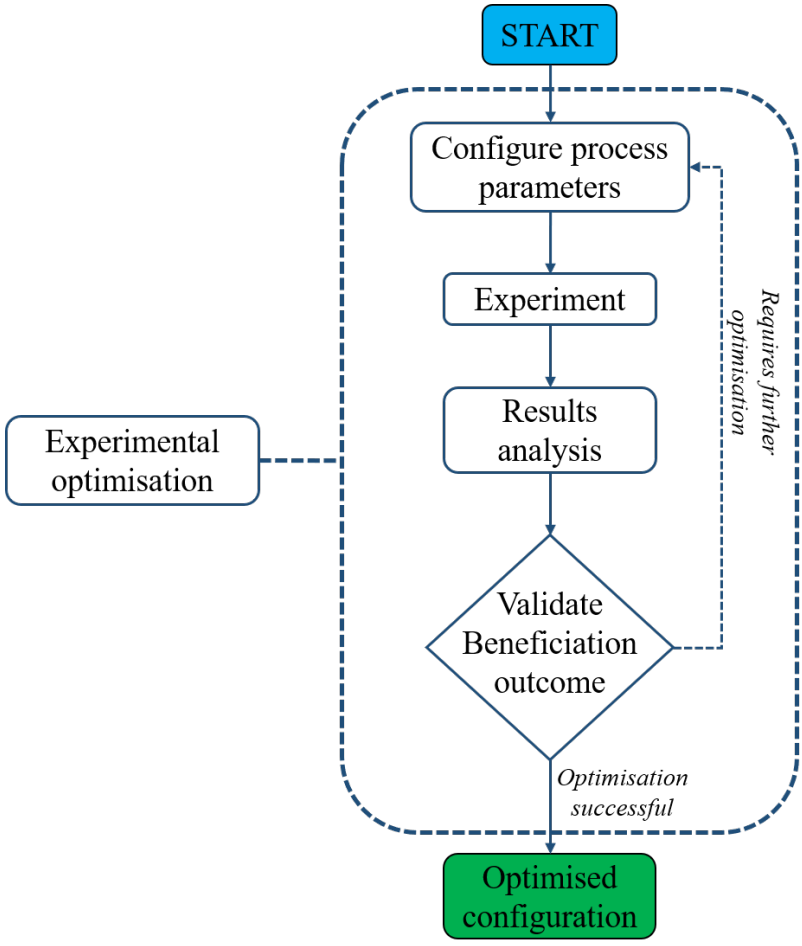

Figure 1.3: Process followed for optimisation of LIED

Chapter 2

Literature Review

This chapter discusses previous scientific work and research that is used as a basis for conducting experiments and analysis within the scope of this thesis. The sections in this chapter give the reader more information about previous lunar exploration missions that led to revelations about the lunar environment as well as the lunar regolith. Furthermore, ISRU on the Moon is discussed with a focus on beneficiation technologies for the production of oxygen using ilmenite on the lunar surface. The goal of this chapter is to provide the reader with a solid foundation for understanding the experimental optimisation of the lunar regolith beneficiation process to produce an ilmenite-rich feedstock, which is the primary objective of this thesis.

2.1 Lunar exploration

In 1960, the United States of America successfully initiated the exploration of the lunar surface with their Ranger missions, aiming to obtain closer images of the Moon [15]. Subsequently, Roscosmos conducted the LUNA missions, which involved sending probes to the Moon, while NASA's Apollo missions achieved the remarkable feat of landing humans on the lunar surface. These significant milestones propelled the Moon to the forefront of planetary objects of interest for space exploration and scientific research activities [16, 15]. Other government space agencies also embarked on their own lunar missions, including SMART-1 by ESA, SELENE by JAXA, CHANG'E by CNSA, and CHANDRAYAAN-1 by ISRO [17, 18, 19, 20]. To further the exploration efforts, NASA deployed the LCROSS and LRO payloads to the Moon, capturing high-resolution images of the lunar surface and conducting spectroscopic analyses. The LCROSS mission also included an impactor payload that struck the lunar surface, generating a fragmented plume of rocks that were analysed to glean additional insights about the composition and characteristics of the lunar regolith [17, 21].

As a result of these lunar missions, the perspective on the lunar surface has changed completely. Moon, the only natural satellite of Earth which was previously considered to be just a rock floating in space transformed into a resourceful location for future space exploration missions [22, 23]. These missions and their outcomes paved the way for NASA along with the ESA and other space agencies for going back to the Moon with an intention to establish a long-term human settlement there with the Artemis missions [24]. To achieve this next giant leap, efforts have been made to thoroughly understand the available lunar surface data and analyse it with a consideration of applying it for sustained operations in space. This has led to important discoveries about the lunar environment, the lunar regolith, its composition as well as its characteristics that can support human space settlements in the future. The following sections in this chapter will dive

deeper into these discoveries as they will outline the operational conditions for all future ISRU missions to the Moon.

2.1.1 The Lunar Environment

The Earth and Moon are intrinsically linked to each other. Not only are their formation stages connected but the Moon is virtually locked onto the rotation of the Earth, triggering tides, eclipses, etc. [25]. Despite sharing some similarities in their formation processes, the Earth and Moon also exhibit noteworthy differences that warrant careful consideration. Understanding and quantifying these differences is crucial for establishing a sustainable and enduring presence on the Moon.

The most notable distinction lies in the near absence of an atmosphere on the lunar surface. As shown in table 2.1, the atmosphere on Earth is very dense which helps in supporting natural ecosystems as opposed to that on the Moon. The presence of an atmosphere on Earth provides protection against small to medium-sized meteoroid impacts that would otherwise directly strike the surface, resulting in the formation of craters as observed on the Moon throughout its history. Scientists have extensively studied the formation and distribution of these craters across the lunar surface to gain insights into the lunar environment and its influence on the lunar regolith [7, 26]. Primary reasons for the absence of an atmosphere on the lunar surface are attributed to its low gravity which is almost six times lower than that on the Earth and the lack of a strong polar magnetic field [7].

Table 2.1: Comparison of physical properties between the Moon and Earth [7]

Property	**Moon**	**Earth**
Mass	$7.353x10^{22}$ kg	$5.976x10^{34}$ kg
Radius (spherical)	1738 km	6371 km
Surface area	$37.9x10^{6}$ km^2	$510.1x10^{6}$ km^2
Flattening*	0.0005	0.0034
Mean density	3.34 g/cm^3	5.517 g/cm^3
Gravity at equator	1.62 m/s^2	9.81 m/s^2
Escape velocity at equator	2.38 km/s	11.2 km/s
Sidereal rotation time	27.322 $days$	23.9345 hr
Inclination of equator/orbit	$6°41'$	$23°28'$
Mean surface temperature	$107°C$ (Day) -153°C (Night)	$22°C$
Temperature extremes	-233 °C to 123 °C	-89 °C to 58 °C
Atmosphere	10^4 $molecules/cm^3$ day ; $2x10^5$ $molecules/cm^3$ night	$2.5x10^{19}$ $molecules/cm^3$ (STP)
Moment of Inertia $(1/MR^2)$	0.395	0.3315
Heat flow (average)	-29 mW/m^2	63 mW/m^2
Seismic energy	$2x10^{10}$ (or 10^{14}) J/yr**	$10^{17} - 10^{18}$ J/yr
Magnetic field	0 (small paleofield)	$24 - 56$ A/m
* (Equatorial-ideal)/ideal radii. ** These estimates account for moonquakes only and do not account for seismicity from meteoroid impacts		

The lunar surface temperatures also pose a significant challenge for exploration missions on the Moon. The lunar day and night cycle is on average a 15-day cycle (15 days followed by 15 nights) in the equatorial regions of the Moon [27]. However, the duration of the lunar day and night cycle varies in different regions of the Moon. For instance, in regions surrounding the lunar south pole, the longest continuous night may last for approximately only 2.5 days. [28]. Nevertheless, the temperature ranges during the day and night follow a similar trend on the lunar surface although the average temperatures at the lunar south pole might differ [27]. The Apollo 15 and 17 missions measured the temperature at their respective landing locations. Their measurements found that the mean daytime temperature is around $374\ K$ while the temperatures at night dip to a minimum of $92\ K$ [29]. These temperatures change depending on the relative positions of the Moon and the Sun [29]. The measurements also discovered large differences between the surface temperatures and those measured at a depth. For example, the mean surface temperature was $45\ K$ lower than the temperature measured at a depth of $35\ cm$ at the Apollo 15 site [30]. A similar difference of $40\ K$ was observed at the Apollo 17 site [30]. This difference in temperatures was associated with the poor thermal conductivity of the lunar regolith. The overall temperature range on the Moon is too extreme for sustaining human beings without any protection. Therefore a major area of research in ISRU is to develop in-situ thermal protection using lunar regolith due to its insulating properties [31].

Apart from the lack of atmosphere compared to Earth, the Moon has another concerning environmental effect that is absent on Earth thanks to the strong polar magnetic field. This is the effect of ionizing radiations. There are two major categories of ionizing radiations that are detected on the lunar surface [32]. The first category consists of ionizing radiations from the cosmic rays also called the Galactic Cosmic Radiations (GCR). The second category of radiation is the radiation emitted by the Sun. The Sun emits particle radiations continuously which are known as the Solar wind. The intensity of radiation from the Sun varies during the 11-year solar cycle ranging between 10^{10} to $10^{12}\ particles\ cm^{-2}sr^{-1}$ [32]. Without proper shielding, these radiations may prove harmful to humans on the lunar surface. The radiation measurements made during previous lunar missions show that the annual exposure to GCR on the lunar surface ranges between $110 - 380\ mSv$ while the exposure to radiations due to Solar Particle Events (SPE) varies drastically and in worst cases may be up to to $1\ Sv$ [32]. To put that into perspective, the annual dose of natural ionizing radiation on the Earth's surface is about $2.4\ mSv$. This data concludes that the radiation dose on the lunar surface can be extremely fatal and have long-lasting risks like a higher risk of developing cancer, damage to DNA in cases of SPE, etc. which need to be considered for all future lunar missions.

The lunar regolith is present in abundance on the lunar surface and is therefore considered an important resource for all ISRU activities. The lunar environment and lunar regolith are closely related as the regolith formation is a consequence of the lunar environment. The finer particles of lunar regolith, otherwise known as the lunar dust pose a threat for exploration missions on the lunar surface. Due to reduced gravity and lack of atmosphere, the lunar dust can suspend for longer times in the extremely sparse lunar atmosphere which can easily cause problems with technologies implemented on the lunar surface such as a rover, habitat modules, astronaut suits, etc. This was also reported by the Apollo astronauts. They said that "After lunar liftoff, a great quantity of dust floated free within the cabin. This dust made breathing without the helmet difficult, and enough particles were present in the cabin atmosphere to affect our vision. The use of a whisk broom prior to ingress would probably not be satisfactory in solving the dust problem, because the dust tends to rub deeper into the garment rather than to brush off", [7, 33]. This lunar dust also creates challenges for future deployments of solar arrays as it can eventually get deposited on the solar arrays and reduce their effective Sun exposure. This is concluded from the experiences gathered during martian rover missions such as Opportunity, Curiosity, etc [34].

Another major reason for the sticking of lunar dust to the astronaut suits and equipment is the inherent charged nature of the dust particles. This was demonstrated by sensor measurements made during the Apollo 17 mission [7]. They concluded that the surface particles in the lunar dust carry a high electrostatic charge which causes them to stick to the astronaut suits and other equipment. This is a conflicting situation where the lunar regolith, a natural resource on the Moon, is very useful but at the same time also a potential threat to technologies if not accounted for in the design considerations. However, the results concluded from previous missions can provide insights into making dust-safe components and spacesuits to allow for the manipulation and utilisation of the lunar regolith.

This brings us to the next topic of discussion, which is, the lunar regolith. It forms the top layer of the lunar surface and is an abundant natural resource on the Moon. It holds the key resources that can be utilised in the short-term for ISRU activities on the Moon [7]. The next section discusses more about the lunar regolith in detail.

2.1.2 The Lunar Regolith

The word regolith is a geological term for the layer of fragmented and unconsolidated rock material, that is either residual or transported, has a high variance in character and covers the bedrock nearly everywhere on the surface of the land. [35]. All previous lunar missions have confirmed the presence of regolith over the entire lunar surface except for a few steep-sided walls of craters. This makes regolith an area of interest due to its natural abundance on the Moon.

The formation of lunar regolith was a multi-stage process and a direct consequence of the environmental conditions present on the Moon. In the early stages of formation, the regolith layer was relatively thin and thus vulnerable to meteoroid impacts of all sizes [7]. This resulted in the excavation of underlying bedrock and exposed it to the lunar environment. Eventually, with exposure to radiation and more meteoroid impacts, this newly exposed bedrock was crushed resulting in the formation of regolith and the process continued. As time went on the thickness of the upper regolith surface kept increasing thereby reducing the effect of smaller meteoroids on the bedrock. Only the larger impacts could then penetrate the regolith layer and expose the new bedrock. Eventually, the regolith layer that we see today was formed after millions of years [7]. This is also a reason why the regolith thickness is not uniform everywhere on the lunar surface as it depends on the number and size of impacts in the respective region. The current scientific consensus is that the layer of regolith is approximately around 4-5 m thick in the mare region and about 10-15 m thick in the highlands regions which indicates that the lunar highlands are much older than the lunar mare regions [7].

The lunar regolith has different layers with increasing depth however, our current in-situ and spectroscopic knowledge is restricted to its top-most layer due to limitations on the previous lunar missions. The top layer of the lunar regolith is a grey-coloured, fine-grained, loose, somewhat cohesive material originating primarily from the fragmentation of basaltic and/or anorthositic rocks. According to the analysis of Apollo samples, the regolith has a grain size in the range from $40 - 800\ \mu m$ with an average between $60 - 80\ \mu m$ [7]. Although the regolith chemical composition is not constant throughout the lunar surface, the overall physical properties follow a similar trend according to the analysis of Apollo samples collected from different regions on the Moon [7]. The petrographic studies of Apollo samples show that the lunar regolith is a mixture of mineral fragments, pristine crystalline rock fragments, glasses of various kinds, breccia fragments, and unique lunar constructional particles called agglutinates [7]. These agglutinates are a special component of the lunar regolith and are sourced from either the regolith or the

bedrock components. The agglutinates which are made up primarily of regolith breccia and different types of glasses are the outcomes of impacts on regolith surfaces and are thus characterised as the fused soil component. The second type of agglutinates that are composed of igneous rocks and other bedrock components are a consequence of impacts on the bedrock and are thus characterised as bedrock-derived agglutinates. Beneath the top layer of regolith, there is a possibility for the "True" regolith to exist, which supposedly is a complex zone that may consist of large-scale ejecta or other fractions created from impacts over the years [36]. This part of the regolith is known as Megaregolith and is believed to have larger rocks [7].

The Apollo missions brought back samples of the real lunar regolith. These samples are very important as they provided us with only in-situ data about the Moon. Upon analysis, these samples provided insights into the mineralogical composition of the lunar regolith. The lunar surface has two major geological regions known as the highlands and the mare regions. An important finding of this analysis shows that the highlands and mare lunar regolith differ from each other chemically as well as petrologically [37]. The soil samples collected from the transition zones of mare to highlands show a mixture of two lithologies [37]. The highlands regions have high concentrations of anorthositic rocks while the mare regions show basaltic rock compositions [7]. According to petrological studies of Apollo samples, the most abundant minerals in the lunar regolith, which make up about 90 % by volume of most lunar rocks are silicate minerals composed primarily of silicon and oxygen [7]. The most common silicate minerals are pyroxene, plagioclase feldspar, and olivine. An important observation of the mineral content of these samples is the complete absence of minerals that contain water like micas, amphiboles, and clays [7]. The next in abundance after silicate minerals in the lunar regolith are the oxide minerals which are particularly concentrated in the mare regions. These oxide minerals are primarily composed of metals and oxygen and they make up as much as 20 % by volume of the mare rocks. [7]. The lunar regolith also contains free native iron but shows no presence of any oxidised iron (Fe^{3+}). There also exist some rare lunar minerals in very low concentrations like Apatite which contains Fluorine or Chlorine and its associated minerals like whitlockite. Some lunar rock samples have also shown the existence of rare sulphides, phosphides and carbides [7]. Table 2.2 shows the composition of lunar regolith samples collected during the Apollo and Luna missions.

Table 2.2: Mineral composition in the lunar regolith samples collected during Apollo (A) and Luna (L) missions [7]

Mineral	A-	A-	A-14	A-(H[1])	A-(M[2])	A-16	A-(H[1])	A-(M[2])	L-16	L-20	L-24
Plagioclase	21.4	23.2	31.8	34.1	12.9	69.1	39.3	34.1	14.2	52.1	20.3
Pyroxene	44.9	38.2	31.7	38.0	61.1	8.5	27.7	30.1	57.3	27.0	51.6
Olivine	2.1	5.4	6.7	5.9	5.3	3.9	11.6	0.2	10.0	6.6	17.5
Silica	0.7	1.1	0.7	0.9	-	0.0	0.1	-	0.0	0.5	1.7
Ilmenite	6.5	2.7	1.3	0.4	0.8	0.4	3.7	12.8	1.8	0.0	1.0
Mare Glass	16.0	15.1	2.6	15.9	6.7	0.9	9.0	17.2	5.5	0.9	3.4
Highland Glass	8.3	14.2	25.0	4.8	10.9	17.1	8.5	4.7	11.2	12.8	3.8
Others	-	-	-	-	2.3	-	-	0.7	-	-	
Total	99.9	99.9	100.0	100.0	100.0	99.9	99.9	99.8	100.0	99.9	99.9

[1] *H refers to the lunar highlands samples*

[2] *M refers to the lunar mare samples*

In conclusion, the lunar regolith contains useful minerals like plagioclase, pyroxene, ilmenite and silica that can be used as alternative sources of minerals and resources such as oxygen, hydrogen as well as metals on the lunar surface. This can prove helpful for future space exploration missions to reduce dependencies on supplies from Earth. In order to make use of these available resources, technologies need to be developed that can efficiently extract and process these resources into usable end products. This has driven the development of In-situ resource utilisation ISRU technologies which are explained in the next section.

2.2 In-situ Resource Utilisation on the Moon

The lunar regolith consists of minerals containing iron, titanium, oxygen, etc. [7]. Upon careful analysis and characterisation of these mineral deposits, it was concluded that they have the potential to be used for applications such as the production of oxygen, hydrogen, water, etc. on the Moon [7]. The in situ process of acquisition, extraction and application of the resources found in space is known as In-situ Resource Utilisation (ISRU). ISRU technologies are of vital importance in making long-term human space exploration missions a reality as they have the potential to create alternative sources for essential supplies in space that are necessary to sustain astronauts and their habitat systems for a longer duration without depending on re-supply from Earth.

A major challenge on the Moon is to enable human life in the harsh and extremely hostile lunar environment. Humans depend on many resources on Earth which are not readily available in space. The major technological gap in the advancement of human space exploration is the development of technologies to extract and use resources found on planetary surfaces instead of depending on supplies from Earth. This is not only important for economic feasibility but also for the long-term sustainability of the mission. The resources available in space, if processed with the correct methods, can become alternative sources for essential supplies in space. The complete ISRU value chain consists of multiple stages of processing that lead to a usable end product. These stages are discussed further in this section.

ISRU Value Chain

The entire ISRU value chain can be simplified into a 5-stage process that starts with prospecting resources and ends with the desired end product in storage for further use. The stages are illustrated in Figure 2.1.

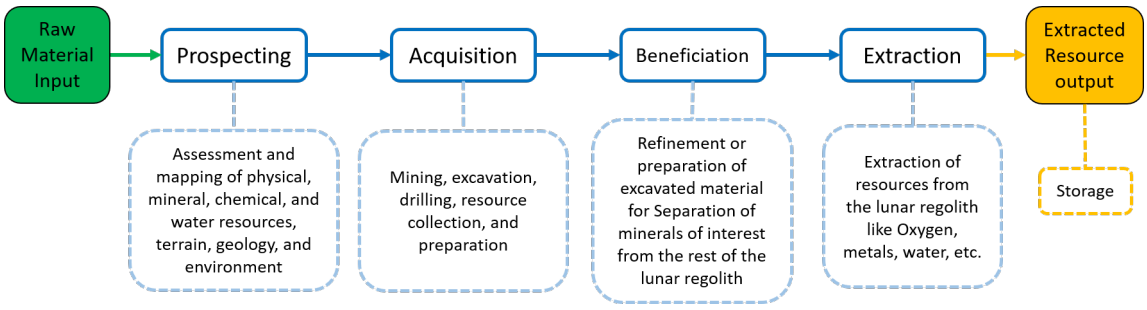

Figure 2.1: ISRU value chain [5]

1. **Prospecting**

   The first step of any ISRU process consists of the identification and characterisation of available resources, called Prospecting. It involves the discovery of mineral deposits that would usually lead to the economic development of the respective mining operation [38]. Upon the discovery of a mineral deposit, the characterisation of feedstock properties along with the overall geology of the location takes place [5]. This is achieved using various methods such as sending rovers and/or orbiters with special spectrometers, manned missions such as the Apollo missions to collect samples, etc. The process of prospecting is one of the most important stages in any mining operation as it gives key information about the estimated total available mineral reserve, the phases of minerals present, the distribution of minerals in the area, other mineral phases present, etc. which help in defining requirements for future mining operations.

2. **Acquisition**

   Upon successful prospecting of a mineral deposit, the next step is to excavate and collect the regolith containing minerals of interest for processing, which is referred to as Acquisition. It involves various processes such as excavation, drilling, hauling, conveying, etc. of the mineral deposit in order to gather it in a specific location for further processing. The method of acquisition depends on the type of mineral deposit as well as the state of minerals to be extracted. For example, the methods used for the acquisition of regolith containing ilmenite will be different than that used for the acquisition of regolith containing volatiles such as water vapour. Although the methods change, the fundamental principle, that these materials need to be collected to prepare them for extraction, remains the same. The excavation technologies employed on the lunar surface also need to take into consideration the abrasive nature of the lunar regolith and its effects on the expected life of the equipment [34, 5]. This brings us to the next stage in the ISRU process flow called Beneficiation.

3. **Beneficiation**

   Beneficiation is a terrestrial mining term that deals with the pre-processing of raw materials chemically or physically to improve the effectiveness of further extraction processes. For example, if the raw material is low-grade iron ore, there is a requirement for pre-processing this ore to increase the iron content and remove any unnecessary gangue particles to have an efficient extraction of iron. Without this pre-processing, the extraction would be too inefficient to be sustainable and consequently affect the profitability of the respective mine. Similarly, lunar minerals like ilmenite need enrichment before they are used for the extraction of useful resources from them. Beneficiation is thus, an important step in the ISRU value chain and will be the main topic of discussion in the Chapter 4 of this thesis.

4. **Extraction**

   Once the beneficiated feedstock is ready, it is taken to the next step of Extraction where the minerals of interest are liberated from the feedstock. This is an important stage in the ISRU value chain as it defines the system requirements for the remaining stages like the types of ores that can be processed and need to be collected by the excavators, feedstock requirements from the beneficiation process, the type of end products created that will determine the kinds of storage facilities needed, etc. The choice of extraction method will primarily depend on the mineral of interest because the mineral properties will influence the type, time, cost and energy expenditure of extraction. The efficiency of extraction is generally influenced by the input feedstock properties, thereby making beneficiation an integral part of the ISRU value chain.

5. **Supply**

   In a full-scale ISRU plant, the produced minerals may not be used instantly. Also, as the ISRU process generally follows a sequential approach of processing, there may be some dwell times between processes when the material needs to be stored until the next stage is ready for further processing. This creates a need for intermediate and end products to be stored safely until their need arises again. This is particularly important to consider while working on the Moon. Special storage facilities may be needed for the safe storage of some minerals to avoid any damage to them during their handling in the lunar environment. The storage facilities should also be equipped with interfaces to allow for the transfer of stored products as per requirement. The storage and supply of end products complete the ISRU process flow.

This discussion concludes that the entire ISRU process chain is interdependent and the quality of produced output is not only a function of the minerals of interest but also of the methods selected for mineral processing at every stage.

2.2.1 In-situ oxygen production on the Moon

Moon being the destination for many upcoming space missions makes it an ideal location for validation and demonstration of the ISRU technologies. The most important resources for sustaining human life are oxygen, water and food. These three are fundamental requirements apart from the environmental protection that will be required on the lunar surface. oxygen is a common denominator for many ISRU activities such as supplies for life support systems, in-situ water production, in-situ propellant production, etc. [39, 40]. This makes oxygen the resource of focus in the discussion about ISRU activities on the lunar surface.

In order to extract oxygen from minerals in the lunar regolith, two types of lunar minerals are proposed for the production of oxygen: ilmenite and silicates such as anorthite [41, 42]. According to the analysis of Apollo samples, these minerals are available in the top layer of the lunar regolith that is accessible for conducting mining activities [43, 7]. As discussed earlier, the silicates are present in much more abundance than ilmenite across the lunar surface which promotes their use for the in-situ production of oxygen. The process of extracting oxygen from silicate minerals is however challenging due to the necessary high reduction temperatures of $1100\ ^{\circ}C$ or more using the molten-phase electrolysis [44]. Another alternative method for this purpose is processing the silicate minerals using plasma or electrolysis processes but these need even higher temperatures [41]. Some of these procedures like the electrolysis process use consumable materials such as fluxing agents which will depend on replenishment from Earth [44]. At such high temperatures, there is also a risk of higher degradation of the electrodes which would eventually need replacements [43]. Overall, the sustainability factor of an in-situ oxygen production plant using silicates as raw materials over a longer duration is quite poor.

In contrast to this, processing ilmenite for extraction of oxygen can be accomplished at a comparatively lower temperature of $1000\ ^{\circ}C$ or even less [43]. This is not only energy efficient but also has relatively less degradation of the component systems leading to longer operational life. A major challenge is the natural abundance of ilmenite on the lunar surface which is much lower than that of the silicate minerals as discussed earlier in table 2.2. However, this can be overcome using various beneficiation techniques which have shown that the ilmenite concentrations can be increased from $5\ wt.\%$ to about $90\ wt.\%$ [45]. This is the reason for ilmenite being considered for oxygen production in spite of its less natural abundance.

In the case of using ilmenite as a source of oxygen, effective beneficiation is vital for the operational feasibility and efficiency of the extraction system. Without beneficiation, the overall advantage of using ilmenite will vanish. In order to understand the beneficiation processes used for ilmenite enrichment of lunar regolith, it is necessary to first understand more about ilmenite as a mineral and its properties that have a significant influence on the beneficiation process. The next part of this section will discuss more about ilmenite in detail.

Ilmenite

Ilmenite is a mineral that is commonly found in igneous and sedimentary rocks [46]. It is a black opaque iron-titanium oxide with the chemical composition of $FeTiO_3$. It is one of the primary ores of titanium with several high-performance applications and is generally formed during the slow cooling of magma chambers and is then concentrated by the process of magmatic segregation [46]. It is generally a weakly paramagnetic material and its magnetic nature also depends on the composition of the parent magma. If we extrapolate this knowledge about the formation of ilmenite to lunar geology, it can be concluded that the concentrations of ilmenite in the lunar regolith depend on the composition of the parent magma that led to the crystallisation and formation of lunar ilmenite [47, 48, 49]. Table 2.3 shows the general physical properties of ilmenite.

Table 2.3: Physical properties of ilmenite [46]

Physical Properties of ilmenite	
Chemical Classification	Oxide
Color	Black
Streak	Black
Luster	Metallic, submetallic
Diaphaneity	Opaque
Cleavage	None
Mohs Hardness	5.5 to 6
Specific Gravity	4.7 to 4.8
Diagnose Properties	Streak; sometimes weakly magnetic
Chemical Composition	Iron titanium oxide - $FeTiO_3$. Sometimes has significant amounts of magnesium and manganese in solid solution with the iron to yield a composition of $(Fe, Mg, Mn)TiO_3$
Crystal System	Trigonal
Uses	The primary ore of titanium. A minor source of iron. Used to make titanium dioxide.

Ilmenite content in the lunar regolith is neither high nor uniform across different regions as illustrated earlier in table 2.2. According to the analysis of Apollo 11 and 17 samples from the high-Ti mare regions, the ilmenite particle size ranges from $10 - 850\ \mu m$, however, the mean particle size lies in the range of $17 - 131\ \mu m$ which is important for deciding the appropriate beneficiation methodologies [50]. Despite the natural occurrence of ilmenite being low, research has shown that it can be effectively concentrated to increase the overall process efficiency [51, 52]. Ilmenite when treated with the appropriate processing stages can provide up to $10.5\ \%$ oxygen per mass unit [6]. Researchers have also performed experimental investigations of the

various beneficiation techniques and provided encouraging results [45]. The net result is however dependent on the effectiveness of the beneficiation methods implemented. The next part of this section will give more information about the beneficiation of lunar regolith for ilmenite enrichment.

2.2.2 Beneficiation of lunar regolith for ilmenite enrichment

As discussed earlier, beneficiation is the most important stage for the extraction of oxygen from ilmenite as the consideration of ilmenite being a more energy-efficient source of oxygen is dependent on the assumption that the beneficiation methods implemented will be effective enough to produce a high-grade feedstock. As shown in table 2.2, the highest measured ilmenite content in lunar regolith is 12.8 % by weight which is not enough for an efficient and profitable extraction process [7, 13]. Therefore, the lunar regolith needs pre-processing in order to achieve an efficient extraction of oxygen. The previous research on the beneficiation of lunar regolith for the enrichment of ilmenite has identified three major categories of beneficiation which are gravitational, magnetic and electrostatic beneficiation respectively [13]. These are discussed further in detail.

Gravitational beneficiation

The major role of gravitational beneficiation is to separate particles based on their sizes. Gravity-based separation is widely used in mineral beneficiation practices for its lower relative costs, ease of operation and control, and eco-friendly nature [53]. In terrestrial mining, this is achieved using many different methods. Out of all the methods available, the froth flotation technique to segregate particles is prevalent for many decades in traditional mining applications [54]. However, involving a process fluid on the lunar surface for particle sizing is out of the question due to its implied need for replenishment and pressurised installation for its operation. This is why dry separation is a better candidate for particle sizing on the lunar surface. One of the most widely used techniques for gravitational beneficiation of dry powder minerals are stationary screening, dynamic screening, cyclones, rotating cone separator and slotted ramp separator [14].

There is limited research available on gravitational beneficiation independently as it is usually involved in a multi-stage beneficiation test bed and is not the primary beneficiation technique that is used. However, some previous research gives an insight into the primary aspects of gravitational beneficiation with respect to dry separation methods [13]. Every dry separation method for particle sizing is fundamentally governed by the same equation of forces acting upon the particles. The net force acting on a particle undergoing dry separation is given by the sum of all forces acting on the particle [13],

$$\vec{F}_{net} = \vec{F}_g + \vec{F}_{ad} + \vec{F}_{vdW} + \vec{F}_{char} \tag{2.1}$$

where, $\vec{F}_{net}$ is the total net force acting on the particles, $\vec{F}_g$ is the gravitational force, $\vec{F}_{ad}$ is the adhesive force which is a force of attraction between the material's charged and uncharged particles, $\vec{F}_{vdW}$ is the van der Waal's force of attraction which is a distance-dependent force between particles that arises due to their fluctuating polarization [13]. These forces are independent of the process of particle separation. $\vec{F}_{char}$ is the characteristic force which is applied by the apparatus used and is also dependent on the material properties [13].

The experimental optimisation of a gravitational beneficiation process thus concerns itself with the properties of a material like the material density, particle size distribution of the mineral of

interest, and the available technology of beneficiation. The choice of dry separation method will influence characteristic forces acting on the material and thus, it will also have effects on the output characteristics. Also, the process parameters of the gravitational beneficiation setup will be an important parameter to consider. For example in the case of a vibratory sifter, the selection of sieve size will be influenced by the mineral of interest and its particle size distribution. For the process of ilmenite enrichment, the particle size distribution of ilmenite needs to be taken into account. Another consideration for the selection of the size of particles to be separated is the particle size requirement from the next stage of beneficiation (if any). These decisions depend on the specific mineral to be enriched and the beneficiation apparatus available. A trade-off will be necessary between filtering out all possible size fractions of the mineral of interest while maintaining the minimum particle size requirement from the next stages of beneficiation. However, these considerations need to be made for the successful optimisation of gravitational beneficiation.

Magnetic beneficiation

Magnetic separation methods have been around in the terrestrial material processing industry since the 19^{th} Century [55]. The effectiveness of these methods is a function of the magnetic properties of the material that needs to be separated from the feedstock. However, their application for lunar regolith beneficiation was a new discovery that was made after successful analysis of Apollo samples that exhibited strong magnetic characteristics [7]. The magnetism of lunar regolith is however different from the terrestrial soils. According to the analysis of regolith samples, Fe^{3+} is non-existent in the lunar soil, so magnetite (Fe_3O_4) which usually exhibits strong ferrimagnetic nature, is scarce in the lunar regolith [56]. There are abundant deposits of ilmenite and pyroxene in the lunar basalts which makes them paramagnetic in nature. However, the strong magnetic properties are a result of native iron (Fe^0) present in the lunar regolith, which is generally found in the agglutinates and glasses. This native iron is considered to be "superparamagnetic" and is the major contributor to magnetism in lunar soil [56]. This motivated the application of magnetic separation methods in the beneficiation of lunar regolith.

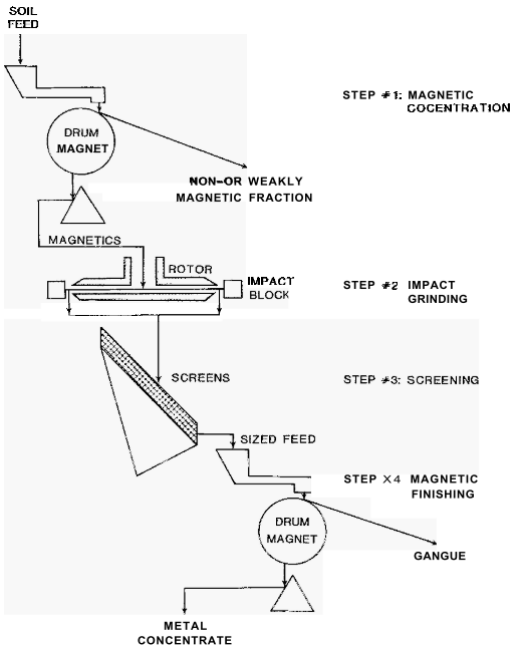

Figure 2.2: Lunar soil beneficiation flow sheet [57]

Some early studies of lunar regolith beneficiation were done right after the Apollo and LUNA missions. In one such study a test bed was developed to examine the separation of metallic minerals using magnetic beneficiation [57, 58]. One of the first studies comprised of a system with an initial magnetic separation stage (using drum magnets) followed by grinding of the magnetic output [57]. This output is screened to get rid of the undersized gangue particles and then it is fed into another magnetic separator. The system schematic is shown in Figure 2.2. The researchers also suggest using electrostatic beneficiation instead of magnetic separation at the later stage after grinding [57]. Overall, the research gave a conclusive feasibility analysis of the magnetic beneficiation system for lunar regolith and the needed resources for its implementation. Furthermore, experiments were also performed for magnetic beneficiation of lunar soil to separate ferrous compounds like ilmenite and pyroxene from the lunar regolith [58]. The experimental results prove that magnetic beneficiation can successfully segregate magnetic compounds present within the lunar regolith. The experiments demonstrated that about $45\ g$ of $30\ wt.\%$ ilmenite can be recovered for every $450\ g$ of lunar mare regolith [58].

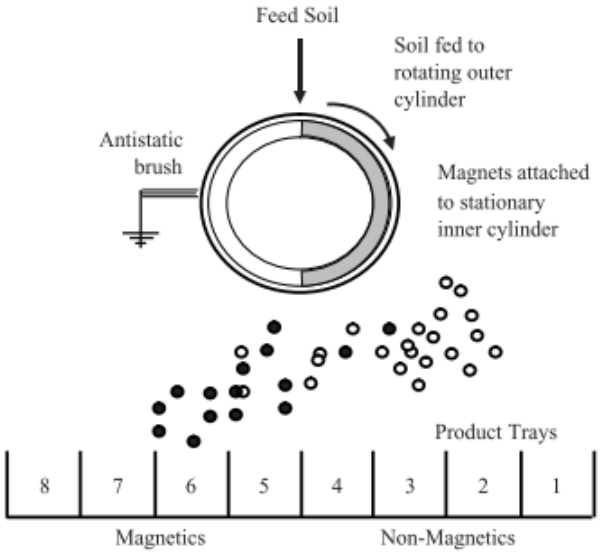

Figure 2.3: Schematic of Magnetic separator used in LSPS [59]

A concept called the Lunar Soil Particle Separator (LSPS) was proposed in a recent study for beneficiation of lunar regolith [59]. It has different stages starting with a particle size separator followed by magnetic and electrostatic separation stages. The magnetic separator used in LSPS is a drum separator that is derived from industrial designs. It has advantages like compact assembly, the possibility to vary operating parameters and good efficiency. Figure 2.3 shows a schematic of the magnetic drum separator used in LSPS. The sieved regolith particles are fed into the magnetic separator from the top. The rotational speed of the drum is changed depending on the magnet positions as well as the feed rate of the input regolith [59]. The magnetic portion of the material is separated in the left bins while the non-magnetic portion is collected in the bins on the right as shown in Figure 2.3.

In conclusion, previous research strongly supports the effectiveness of magnetic separation methods for the segregation of magnetic materials present within the lunar regolith. Therefore, it is one of the primary candidates often considered for the beneficiation of lunar regolith to increase ilmenite concentrations.

Electrostatic beneficiation

Electrostatic beneficiation is the method of beneficiation that uses the differences in electrostatic charges developed on materials for separating them from one another. This method of separation of materials has been a primary commercial solution for the processing of beach sands and alluvial deposits for heavy minerals such as titanium, ilmenite etc. in Australia as well as in the United States [60]. This application helped in the development of this technique further for processing minerals in dry granular mixtures.

Considering the applications of electrostatic beneficiation on Earth for dry granular materials, it has consequently also been studied for lunar regolith beneficiation for a long time. Previous research shows that magnetic beneficiation followed by electrostatic separation can provide better results than just magnetic beneficiation with higher grades of output for beneficiation of lunar regolith [57]. The dry and granular nature of the regolith makes it a good candidate for the implementation of electrostatic separation methods. Some early studies conducted experiments for testing the electrostatic separation of ilmenite from lunar regolith simulants as well as from the original Apollo samples [61]. The lunar regolith fed into electrostatic separators was first treated with hand magnets to get rid of the agglutinates and soil metal. The experiments concluded with the enrichment of ilmenite going from $10\ \%$ (input) to $95\ \%$ (output) and with a recovery of about $68\ \%$ in the collected output [61]. The samples were maintained at approximately $150\ ^{\circ}C$ to keep them dry throughout the experiments and avoid any influence of humidity on the electrostatic separation. The experiments were conducted in three different ambient conditions. The first one was air and normal atmospheric pressure, the second was a nitrogen environment and the third was a vacuum environment.

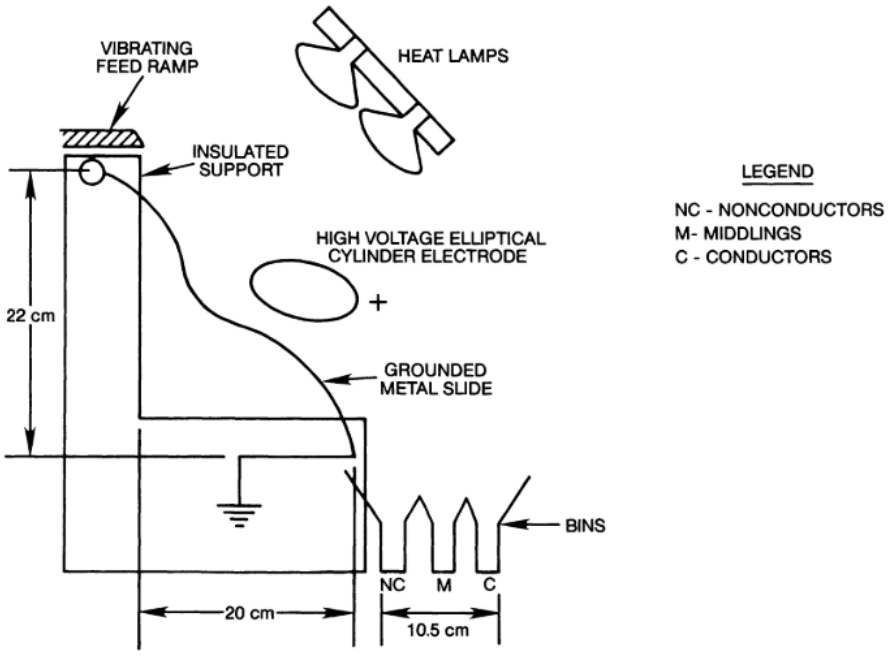

Figure 2.4: Mineral electrostatic separator: Benchtop configuration [62]

The experimental setup of these experiments included a feed ramp which fed the samples in an electrostatic separator with the elliptical electrode and a grounded slide to avoid electrostatic discharge on the surface as shown in Figure 2.4. The vacuum setup, shown in Figure 2.5, was a scaled-down version of the benchtop setup and did not include a feed ramp due to dimensional limitations. These experiments were also conducted in the same three ambient conditions as

mentioned earlier [61]. The experimental results show that there was an average eleven-fold increase in the concentrations of ilmenite going from 7.9 *wt.*% to 90 % after a single pass for the simulant runs in nitrogen [62]. Experiments conducted in vacuum conditions led to a comparatively lower enrichment of ilmenite going from 7 *wt.*% to 29 *wt.*% [62]. Their experiments also observed that the grades of ilmenite in nitrogen and air were significantly better than that in the vacuum environment. One of the reasons for this disparity was that the gas ionization products in the air and nitrogen environments contributed to feed charging which resulted in more electrostatic charges on the regolith particles and thus provided better beneficiation outcomes [62].

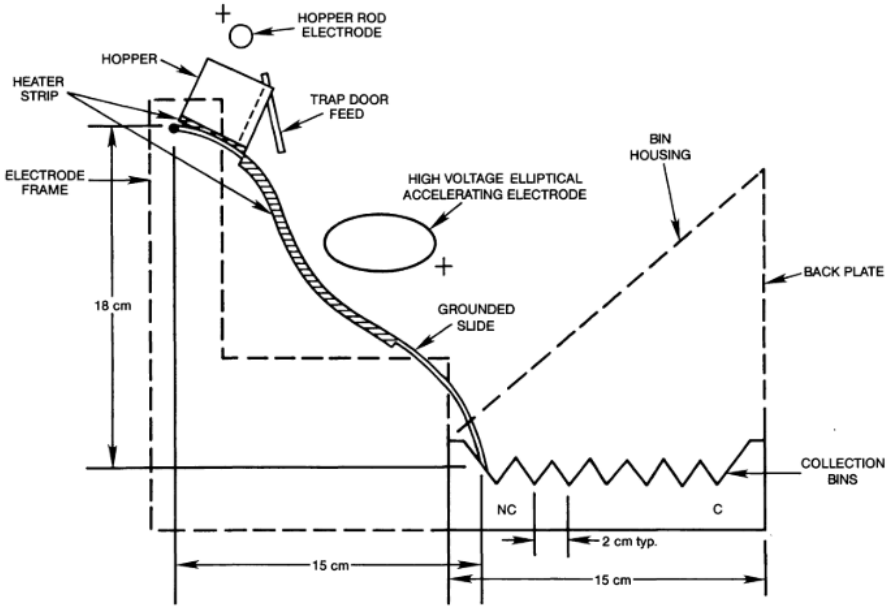

Figure 2.5: Mineral electrostatic separator: Vacuum slide configuration [62]

The commonly considered methods of beneficiation of lunar regolith using the electrostatic forces are conductive induction with slide separators, tribocharging with parallel plate separators and with electrostatic travelling wave [13]. Tribocharging is a promising method for mineral separation, especially for the lunar regolith [63]. When a granular mixture is shaken, there is an accumulation of charge on the mineral particles which is known as the triboelectric effect. This effect is predictable and can be used for controlling the process of separating specific minerals from the mixture [63].

There are multiple parameters involved in the electrostatic beneficiation process and hence the experimental optimisation for such a process requires observation and control over many parameters at the same time, like controlling the material feed rate, electrode system configuration, voltages applied across the electrode plates as well as the ambient environmental conditions [64]. Therefore, the experimental optimisation of a multi-stage beneficiation test bed will have a major portion dependent on the electrostatic beneficiation as it has multiple parameters to optimise and thus holds the key to enabling an efficient beneficiation process.

Parameters for assessment of beneficiation output

One of the most important factors involved in the beneficiation of specific minerals is to quantify the beneficiation. There are some key performance parameters that can be used for quantifying the output results of these beneficiation experiments. These parameters are shown below in eqs. (2.2) to (2.5) [65]:

$$\textbf{Yield} = \frac{\text{Mass of produced product}}{\text{Total mass of feedstock}} \tag{2.2}$$

$$\textbf{Recovery} = \frac{\text{Mass of the produced product}}{\text{Mass of product in raw material}} \tag{2.3}$$

$$\textbf{Grade} = \frac{\text{Mass of produced product}}{\text{Mass of stream}} \tag{2.4}$$

$$\textbf{Enrichment Ratio} = \frac{\text{Grade of given species in the outlet}}{\text{Grade of the given species in inlet}} \tag{2.5}$$

The applications of these equations for quantification of the beneficiation process performed on lunar regolith simulants to produce ilmenite enrichment are as follows:

1. Yield refers to the total mass of ilmenite in the output for every mass unit of feedstock processed.
2. Recovery of ilmenite in the output refers to the mass of ilmenite produced in the output as a fraction of the total mass of ilmenite present in the input.
3. Grade of ilmenite in a specific output is the total mass of ilmenite produced at the selected output for every mass unit of the selected output stream.
4. Enrichment ratio is the ratio of the output grade of ilmenite and the grade of ilmenite in the input. The grade of ilmenite in the input is calculated similarly to the grade of output using the mass of ilmenite present in the input for every mass unit of raw material.

These performance parameters can qualify the output results generated by the beneficiation test bed that will help in the optimisation of process parameters.

This concludes the foundational introduction about the beneficiation of lunar regolith for producing ilmenite-rich feedstock. The next important aspect of research related to ISRU activities on the Moon is the use of regolith simulants for the development of these systems. The next section gives more details about lunar regolith simulants.

2.2.3 Lunar regolith simulants

As discussed earlier, the vast majority of the lunar surface is covered with lunar regolith and it has shown promising results in being used as an alternative source for resources like oxygen, hydrogen and metals as well as a constructional material [43, 66, 67, 68]. However, in order to be able to use a new material, we need to test it thoroughly to find out more about its mechanical as well as chemical properties. The Apollo missions brought back about $381.7\ kg$ of lunar regolith samples to Earth from different locations on the Moon [67, 69]. This quantity is enough to study its chemical composition, general mechanical and thermal properties as well as to understand lunar geology. However, it is not enough to conduct engineering studies on the material like conducting

sintering experiments or studying the effects of different material processing techniques for space mining applications. Such studies require high quantities of material for experimenting and many times have no chance of recovering the raw material after. Hence, there is a need to develop a material similar to the real lunar regolith in terms of physical, chemical and mechanical properties but which can be produced on Earth and used for the development of ISRU technologies.

This discussion brings into focus the discussion about lunar regolith simulants produced on Earth that can be used as lunar soil analogs for hardware development and testing [70]. A lunar regolith simulant is supposed to replicate (or simulate) the lunar regolith as accurately as possible while being made from raw materials found on Earth. This makes it feasible for research institutions and private organisations to access these materials and validate their technologies. It also helps in driving down development costs as testing technologies on regolith can be performed without the need for actual regolith to be collected from the lunar surface. It should also be noted that some characteristics of the real lunar regolith such as the presence of electrostatic charges within the particles as a result of exposure to the cosmic radiations or the presence of native free iron atoms may not be present in the simulants as these are a result of the space environment. However, this can be resolved to an extent by adapting the testing methods to these characteristics and/or adjusting the output results accordingly.

Table 2.4: Comparison of chemical compositions of JSC-1 simulant (Merriam Crater Ash) with Apollo sample 14163 [71]

Mineral Oxide	Merriam Crater Ash Wt.%	Lunar Soil 14163 Wt.%
SiO_2	48.77	47.3
TiO_2	1.49	1.6
Al_2O_3	15.65	17.8
Fe_2O_3	1.71	0.0
FeO	8.88	10.5
MgO	8.48	9.6
CaO	10.44	11.4
Na_2O	2.93	0.7
K_2O	0.81	0.6
MnO	0.19	0.1
Cr_2O_3	-	0.2
P_2O_5	0.66	-
Total	100.01	99.8

One of the first lunar regolith simulants was developed by NASA named the JSC-1 simulant. It was a result of the need for lunar regolith samples in medium to large-scale engineering studies to develop the technologies for future exploration missions to the Moon [71]. It is made up of glass-rich basaltic ash which is comparable to the bulk chemistry of the lunar regolith. The simulant was prepared from a basaltic pyroclastic sheet deposit that was erupted from vents linked to the Merriam Crater located in the San Francisco volcanic field [71]. Upon the completion of production of the simulant, the chemical composition was compared to that of sample 14163 collected during the Apollo 14 mission. The comparison of the chemical composition shown in Table 2.4 concludes that the simulant made using ash collected from the Merriam Crater field deposits, successfully replicates the chemical composition of the real lunar regolith sample (14163). This was the first stepping stone in the development of lunar regolith simulants.

Once results derived from the analysis of Apollo samples were published by NASA in the "Lunar Sourcebook" as well as after the development of JSC-1 Simulant, private companies also started being involved in the production of lunar regolith simulants to keep up with the rising demands [7, 71, 69]. The development of ISRU technologies that support crucial systems/activities like life support systems, rocket fuel production, power generation, construction, etc. need high-fidelity simulants to minimise the effects arising due to deviations in regolith simulants compared to the real lunar regolith [72]. With public as well as private sectors focused on lunar missions, the demand for regolith simulants has increased more than ever before. One of the many private companies producing lunar as well as martian regolith simulants is Exolith Lab [73]. The lunar regolith simulants that they offer are of two main categories: The highlands simulant LHS-1 and the mare simulant LMS-1. They also have dust simulants for both of these which have smaller mean particle sizes but the fundamental differences in the simulants lie in the region of the lunar surface that they resemble. As stated earlier in the section 2.1.2, the lunar mare regions have higher average ilmenite content and are thus of significance for the production of oxygen. The LMS-1 simulant produced by Exolith lab is a general-purpose lunar mare simulant comprised of pyroxene, glass-rich basalt, anorthosite, olivine and ilmenite [74]. The mineralogy and bulk chemistry of the simulant are shown in Table 2.5. As stated here, the ilmenite content in the simulant is at $4.3\ wt.\%$ which is an approximate average as found by Apollo missions in the lunar mare regions [7].

Table 2.5: Mineralogy and bulk chemistry of LMS-1 simulant [74]

Minerology		**Bulk Chemistry**	
Component	Wt.%	Oxide	Wt.%
Pyroxene	32.8	SiO_2	46.9
Glass-rich basalt	32.0	TiO_2	3.6
Anorthosite	19.8	Al_2O_3	12.4
Olivine	11.1	FeO	8.6
Ilmenite	4.3	MnO	0.2
		MgO	16.8
		CaO	7.0
Safety		Na_2O	1.7
See SDS for details.		K_2O	0.7
Primary hazard is dust inhalation.		P_2O_5	0.2
Wear a respirators in dusty conditions.		LOI^*	0.9
		$Total^{**}$	99.0
		*Loss on ignition **Excluding volatiles and trace elements	

An important parameter for deciding the chemical composition of a regolith simulant is the selected region on the lunar surface that it simulates because the composition of regolith is not constant throughout the lunar surface [75]. The simulants available commercially have a fixed composition and generally lack the ability to reproduce variable compositions for different locations on the lunar surface. This creates a challenge in technological efforts where the process outcomes depend on region-specific resources. Therefore a new simulant system was developed by researchers at the University of Technology, Braunschweig but the simulant production is taking

place currently at the Technical University of Berlin. In this system, the simulant composition can be adjusted according to the research requirements [75]. This concept of an adjustable simulant system enables research on different variations of the lunar regolith. This simulant system has two primary categories of base simulants that resemble the highlands and mare lunar regolith. These are named TUBS-T and TUBS-M respectively. The Figure 2.6 shows a schematic process of production of TUBS-M and TUBS-T based modular lunar regolith simulants.

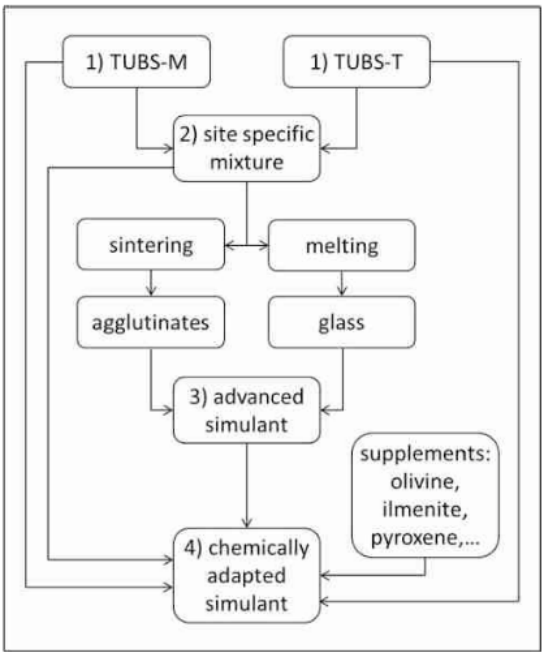

Figure 2.6: Process schematic for production of TUBS-M and TUBS-T based modular regolith simulant [75]

Table 2.6: Bulk rock chemistry of TUBS-M simulant compared to lunar mare samples [75]

Lunar Basalts							TUBS-M	
Mineral	Olivine basalt Apollo 12 [wt%]	Quartz basalt Apollo 15 [wt%]	High-Ti basalt Apollo 17 [wt%]	Aluminous basalt Apollo 12 [wt%]	Average [wt%]	stdev.	Analysis [wt%]	err.
SiO_2	45.00	48.80	37.60	46.60	44.50	4.86	48.61	0.29
TiO_2	2.90	1.46	12.10	3.31	4.94	4.84	2.29	0.02
Al_2O_3	8.59	9.30	8.74	12.50	9.78	1.84	13.28	0.10
FeO	21.00	18.60	21.50	18.00	19.78	1.73	10.14	0.05
MgO	11.60	9.46	8.21	6.71	9.00	2.07	8.73	0.07
CaO	9.42	10.80	10.30	11.82	10.59	1.00	8.31	0.05
Na_2O	0.23	0.26	0.39	0.66	0.39	0.20	3.67	0.07
K_2O	0.06	0.03	0.08	0.07	0.06	0.02	1.71	0.02
MnO	0.28	0.27	0.22	0.27	0.26	0.03	0.18	0.00
Cr_2O_3	0.55	0.66	0.42	0.37	0.50	0.13	0.04	na
P_2O_5	0.07	0.03	0.05	0.14	0.07	0.05	0.51	0.01
LOI	na	na	na	na	-	-	0.63	-
Sum	99.70	99.67	99.61	100.45	99.79	0.35	98.09	-

The chemical analysis of TUBS-M and TUBS-T is shown in tables 2.6 and 2.7 respectively. TUBS-M simulates the basaltic base compounds of the lunar mare regions and TUBS-T is made up of the anorthositic compounds simulating the lunar highlands regions. The system consists of four levels of fidelity for the simulants. The first level consists of only a base simulant. The decision is made between TUBS-M and TUBS-T depending on the requirements. This will form a base simulant with lithic particles and is useful for general applications, geotechnical investigations as well as performing experiments such as sintering. The next type of simulant is the site-specific simulant which is a combination of TUBS-M and TUBS-T for obtaining intermediate regolith simulants containing only lithic particles. These simulants better replicate various lunar surface locations and are generally used for more specific experiments such as optical investigations as well as to develop ISRU technologies.

Table 2.7: Bulk rock chemistry of TUBS-T simulant compared to lunar highlands samples [75]

	Sample no. of lunar ferroan anorthosites								TUBS-T	
Mineral	15363 [wt%]	15415 [wt%]	60015 [wt%]	62236 [wt%]	62237 [wt%]	65315 [wt%]	Average [wt%]	stdev.	Analysis [wt%]	err.
SiO_2	45.30	44.50	43.90	44.20	41.90	44.30	44.02	1.14	48.71	0.29
TiO_2	0.12	0.02	0.02	0.05	0.02	0.01	0.04	0.04	0.12	0.01
Al_2O_3	28.00	35.60	35.00	30.10	29.60	34.90	32.20	3.33	30.33	0.13
FeO	4.76	0.21	0.33	3.67	5.89	0.31	2.53	2.56	1.05	0.04
MgO	3.85	0.26	0.53	3.55	5.11	0.25	2.26	2.16	0.57	0.06
CaO	16.80	20.40	19.00	17.60	16.30	19.10	18.20	1.56	14.57	0.06
Na_2O	0.29	0.36	0.39	0.22	0.21	0.30	0.29	0.08	3.05	0.07
K_2O	0.01	0.01	0.01	0.01	0.01	0.01	0.01	0.00	0.22	0.02
MnO	0.07	0.01	0.01	0.06	0.07	0.01	0.04	0.03	0.015	0.00
Cr_2O_3	0.10	0.00	0.01	0.07	0.06	0.00	0.04	0.04	0.00	0.00
LOI	na	na	na	na	na	na	-	-	0.99	-
Sum	99.29	101.38	99.19	99.52	99.16	99.19	99.62	0.87	99.61	-

The next two types of the simulant are more specialised forms and are important for developing ISRU technologies which are dependent on the mineral composition and chemistry of the lunar regolith. The third type of simulant is called the Advanced simulant. This type of simulant contains agglutinates and glass particles which are produced from a customized composition of TUBS-M and TUBS-T or the site-specific simulant for more special applications. The addition of these thermally-affected regolith components increases the accuracy with which the simulant replicates the real lunar regolith. The next and the highest fidelity simulant in this system is the chemically adapted simulant. This variant of the simulant contains olivine, ilmenite or pyroxenes in the required proportions to replicate the chemical as well as mineralogical composition. It is the last detail that can be added to the simulant giving it a unique identity. This type of simulant is generally very useful in the technological research for extraction of specific chemical compounds or minerals from the lunar regolith and other high-fidelity research [75].

2.3 X-ray Diffraction for sample analysis

The effectiveness of a material processing system can only be determined after the analysis of its output samples. Similarly, in order to quantify the effects of beneficiation experiments conducted, the chemical composition of the output samples needs to be determined which will further help in the optimisation process. This section focuses on the X-Ray Diffraction (XRD) method of analysis used for qualitative and quantitative phase analysis of materials which in this thesis refers to the lunar regolith simulant.

Principle of X-ray diffraction by crystalline materials

XRD is one of the existing scientific techniques used for the analysis of material composition [76]. The research on diffraction of X-rays by crystals was first conducted in 1912 and has since opened up new possibilities in the study of crystalline materials [77]. XRD methods are based on the ability of crystals to diffract X-rays in a characteristic manner which allows one to study their structures with high precision [78]. It can be used for both qualitative as well as quantitative phase analysis of a material. The qualitative phase analysis can be performed by studying the characteristics of the diffraction pattern such as the peak position which gives insight into the crystal parameters such as the lattice parameters, space group, chemical composition, etc. Furthermore, based on the peak intensity information about crystal structure, the texture information can be derived which will enable quantitative phase analysis of the sample. The shape of intensity peaks give information about sample broadening that relates to the crystal size and microstrains [79].

The interaction of X-rays with crystalline materials leads to multiple effects like absorption, various scattering effects, etc. The most significant phenomenon for XRD is a special type of scattering known as Raleigh scattering. This takes place between incident photons and electrons surrounding the atomic nuclei. In Raleigh scattering, energy of the scattered wave remains unchanged and it maintains its phase relationship to the incident wave [80]. This results in the scattering of X-ray photons in all directions [78]. However in the case of crystalline structures, this scattering is not random due to their periodic nature. This results in constructive and destructive scattering of the radiation that leads to a characteristic diffraction phenomenon which can be further investigated to study the crystal structure of a material [78]. This fundamental principle that the diffraction pattern formed by an X-ray incident on a material can be characterised and resolved into useful information is the basis for XRD. Figure 2.7 illustrates the geometrical condition required for creating such a diffraction pattern which was first produced in 1913 [81].

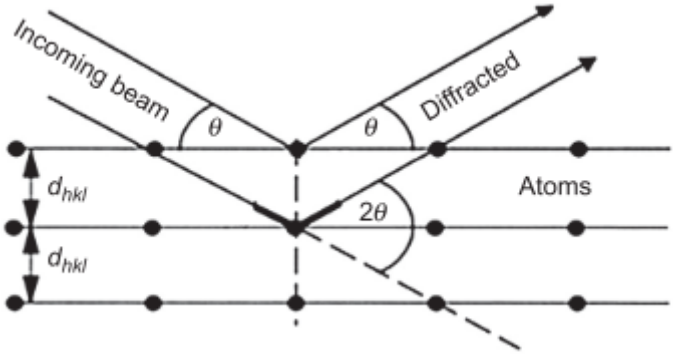

Figure 2.7: Geometrical condition for diffraction from lattice planes [82]

In a perfect poly-crystalline untextured material, diffraction occurs for each plane and direction in the lattice which satisfies Bragg's law for the case of constructive interference. The mathematical representation of Bragg's law is as follows [78]:

$$n\lambda = 2d_{hkl}sin(\theta) \tag{2.6}$$

where, n is the order of diffraction, λ is the wavelength of incident beam in nm, d_{hkl} is the lattice spacing in mm and θ is the angle of diffracted beam in degree. This results in the formation of diffraction cones which if detected on a plane detector produce a pattern called diffraction rings, also known as the Debye rings. Figure 2.8 shows a pictorial representation of the formation of such diffraction cones.

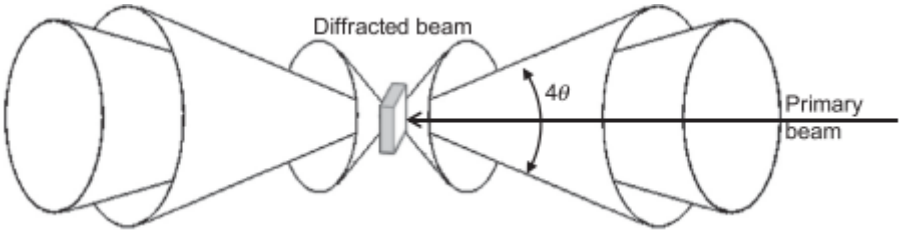

Figure 2.8: Diffraction cones in transmission and reflection occurring for a polycrystalline material [78]

However, the common materials used today are neither completely crystalline nor amorphous but rather a combination of both. Therefore, the intensity distribution produced by the lattice planes differs which also changes the diffraction patterns. This should be considered for all XRD measurements. The shape of the diffraction pattern is a function of many different factors and the resulting signal is their aggregate outcome [78]. The overall diffraction data is generally represented as the distribution of intensity as a function of the diffraction angle (2θ). The developed diffraction pattern can b used to extract information about the phases present in a material and their respective quantities. This is the working principle of XRD analysis. In order to perform both quantitative as well as quantitative phase analysis of a sample using XRD, there are multiple stages involved that lead to a reliable result. This entire process consists of the following major stages:

1. Generation of X-ray
2. Measurement of the generated diffraction pattern
3. Qualitative phase analysis
4. Quantitative phase analysis

These are discussed in detail further in this section.

Generation of X-ray

X-rays are high-energy electromagnetic waves that have a wavelength in the range $10^{-3} - 10^{1}$ nm [83]. A heated tungsten filament kept in a vacuum generates electrons. These electrons are accelerated through high potential fields and made to bombard a target. As a result of this bombardment, X-rays are emitted by the target material [78]. This method is commonly used for generating X-rays in laboratory equipment. There are two primary effects that cause this. The first effect is the emission of X-ray photons with a broad continuous distribution of wavelengths produced by the deceleration of electrons which is also known as Bremsstrahlung [78]. The second effect is the ionisation of the impinged atoms by the ejection of electrons from

their inner shells which results in the electrons from outer shells to jump into these gaps to achieve a more stable state. There exists a difference in the electron energies between different shells and this surplus energy is released in the form of photons when the atom is ionised [78]. Consequently, the effective radiation that is emitted by both of these effects is a superimposition of a continuous spectrum and characteristic radiations.

Measurement of the generated diffraction pattern

The next step of XRD is the measurement of the generated diffraction pattern which will be needed for further analysis [78]. As discussed in earlier sections, there exist different diffraction conditions due to the multiple lattice planes with varying diffracted signals throughout the lattice depending on the crystal structure and phases present. Every phase has a characteristic diffraction pattern that can be used for the identification of the respective phase. When multiple phases exist in a sample, the diffraction pattern produced is a result of the superimposition of the signals from multiple phases. The intensities of the produced diffraction peaks are proportional to the amounts of the respective phases. As a consequence of the absorption and scattering effects, the X-rays lose their energy and attenuate as they travel through a material and thus their intensity decreases. Therefore, a large 2θ range of the diffraction angle needs to be measured to record the maximum possible number of diffraction peaks.

The diffraction pattern usually contains plenty of peaks in the complete 2θ range demonstrating the presence of varying and partially overlapped intensity [78]. The intensities are measured at specific intervals in the given range of diffraction angle. Upon successful measurement of the diffraction pattern, phase analysis of the sample can be performed.

Qualitative phase analysis

The goal of qualitative phase analysis is to identify all the phases present in a given sample. This analysis is done by the comparison of diffraction peaks as seen in the measured XRD data with the database of known values for various materials. The primary database is compiled by the International Center for Diffraction Data (ICDD) [84, 78]. A proper treatment of the measured diffraction data is required to generate reliable results. Fundamentally speaking, the background of XRD measurement data needs to be removed from the measured pattern. Further treatments such as the removal of $K_{\alpha 2}$ radiation or smoothing operations can also be performed [78]. Every intensity peak in the diffraction pattern indicates the presence of a phase that needs to be identified. The search for peak intensities of different phases in the database can be done either manually or by automatic identification methods such as by intensity threshold, peak shape specification and first or second derivatives [82]. This primarily depends on the software being used for analysis.

In order to understand the standard process of qualitative analysis using software tools, a snapshot from the X'pert HighScore software is shown in Figure 2.9. The figure shows measured data on the left along with the potential phases identified in the sample on the right side. The software helps in determining the phases which is used for generating a comprehensive analysis of all phases present.

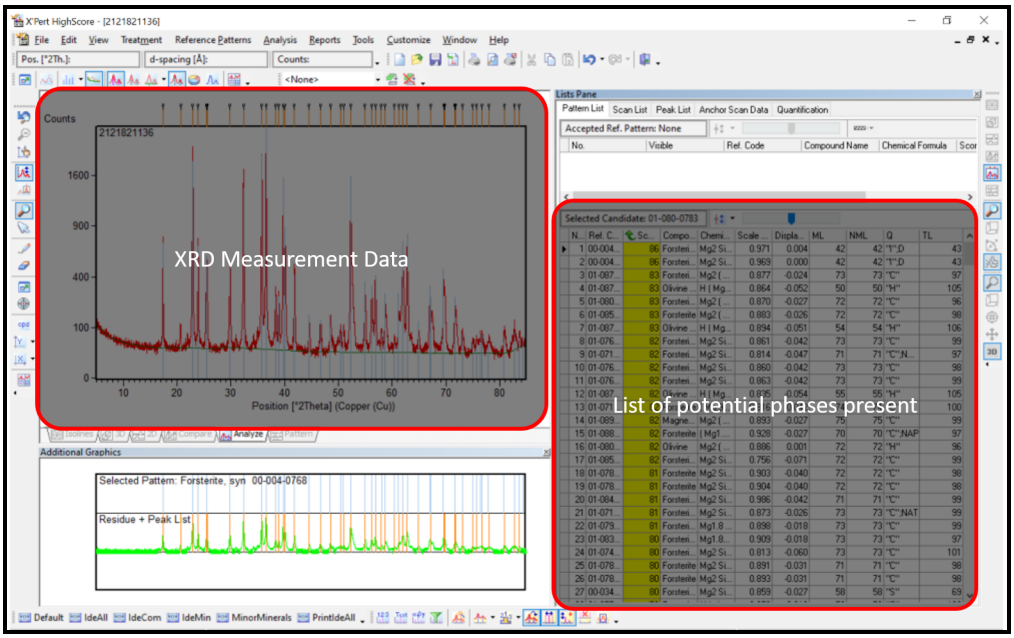

Figure 2.9: Diffraction pattern loaded on X'pert Highscore for qualitative phase analysis

Quantitative phase analysis

Upon the successful identification of phases, the next step involves the quantification of each identified phase. There are different methods for quantitative phase analysis and their use depends on the investigated sample. The different methods used for quantitative phase analysis in XRD are as follows [78]:

1. **Method with external standard:**

   In this method, the intensity of reflection measured in a multi-phase material is compared with that of the pure material measured under the same experimental conditions. The intensities are dependent on the mass absorption coefficients and volume fractions of the pure phase as well as of the phase in the multi-phase material. The formula used for calculations is given in eq. (2.7) [78]:

$$\frac{I_i^S(hkl)}{I_i^P(hkl)} = V_i^S x \frac{\mu^P}{\mu^S} \tag{2.7}$$

   where I_i^S is the intensity peak of the considered phase within the investigated sample, I_i^P is the intensity peak of the pure phase, μ^P is the mass absorption coefficient of the pure phase, μ^S is the mass absorption coefficient of the sample, V_i^S is the volume fraction of the phase in the sample and *(hkl)* represent miller indices of the crystal lattice. The value of μ^S needs to be determined experimentally [82].

2. **Method with internal standard:**

   The method with internal standard is generally used for materials that have more than two phases. It involves the addition of a standard phase with known parameters like mass or volume in the given sample. This method is however limited to powder samples. The calculation of mass concentration of the phase of interest can be calculated by using the

eq. (2.8) [80]:

$$W_i = K_{ij} \text{ x } W_j \frac{I_i(hkl)}{I_j(hkl)} \tag{2.8}$$

where W_i is the mass concentration of the phase of interest, W_j is the mass concentration of the standard phase, $I_i(hkl)$ is the considered incident intensity, $I_j(hkl)$ is the intensity of added phase and K_{ij} is the proportionality factor. This factor can be experimentally determined by using known mixtures. In order for the method to work it should be ensured that the intensity peak of the added phase does not overlap with that of the phase to be measured.

3. **Method of intensity ratio:**

   As the name suggests, the method of intensity ratios involves the direct calculation of ratios of the reflexions of every phase present in the material. As there is no need for additional phases to be added to the material it is generally used for solid materials. The total amount of phases present in the sample need to be known to calculate their individual quantities. The volume fraction of the phase in the material can be calculated using the eq. (2.9) [82]:

$$V_i = \left(\sum_j \frac{I_j(hkl)}{I_i(hkl)} \text{ x } \frac{R_i(hkl)}{R_j(hkl)} \right)^{-1} \tag{2.9}$$

   where V_i is the volume fraction of the phase to be measured, $I_i(hkl)$ is the intensity peak of the phase to be measured, $I_j(hkl)$ is the intensity peak of other phases present, $R_i(hkl)$ and $R_j(hkl)$ are phase- and peak-specific factors respectively which can be calculated or determined experimentally.

4. **Rietveld method:**

   The previous methods dealt with specific intensity peaks and their corresponding phases. However, the Rietveld method also known as Rietveld refinement considers the entire pattern at once. It involves the simultaneous analysis of multiple peaks. The measured pattern is refined with a calculated pattern that takes into account many structural, experimental as well as micro-structural parameters [85]. The refinement is performed by minimisation of function S in the eq. (2.10):

$$S = \sum_i u_i |y_{iobs} - y_{icalc}|^2 \tag{2.10}$$

   where y_{iobs} and y_{icalc} are the observed and calculated intensities at each 2θ position respectively and u_i is the weight factor derived from experimental error margins [85]. Multiple factors are taken into account that depend on each phase present in the analysed sample as well as the measurement instrument used [82].

   There are two different strategies available for profile refinements. The first strategy includes development of a mathematical function such as Gaussian, Lorentzian, Voigt, Pseudo-Voigt, etc. in a way that the calculated pattern most closely describes the peak shapes [85, 78]. This method is useful in scenarios where the instrumental details are unknown. As this method is a pure mathematical fitting process it allows the user to extract micro-structural information from the analysed diffraction patterns [78]. The second strategy is known as the fundamental parameters approach. In this method, the profile (Y)

calculation is achieved by convolution of the Emission profile (W), all instrument contributions (G) and the sample contribution (P) and can be calculated using the eq. (2.11) [82, 78]:

$$Y(2\theta) = (W \circledast G) \circledast P \tag{2.11}$$

Upon successful refinement, it is important to qualify the results as reliable and suitable according to standard measurement criteria. One of the best criteria for analysing the refinements is to compare the calculated plots with the observed data. Any large differences represent inaccuracies of the calculated plot. A criterion called the Residuals weighted profile (R_{wp}) is calculated which gives information about the quality of fit. The smaller the R_{wp}, the better is the quality of fit. Another parameter denoted as R_{exp} is calculated which represents the minimum expected R_{wp} for a given number of experiments (N) and the number of refined parameters (Q). A ratio of both these parameters gives the goodness of fit (GOF) which is also a refinement quality parameter. These parameters together give a better insight into the reliability and accuracy of the refinements. The formulae for calculation of these parameters are given in eqs. (2.12) to (2.14):

$$R_{wp} = \sqrt{\frac{\sum_i u_i (y_i obs - y_i calc)^2}{\sum_i u_i (y_i obs)^2}} \tag{2.12}$$

$$R_{exp} = \sqrt{\frac{N - Q}{\sum_i u_i (y_i obs)^2}} \tag{2.13}$$

$$GOF = \left(\frac{R_{wp}}{R_{exp}}\right)^2 \tag{2.14}$$

$$\tag{2.15}$$

The Rietveld refinement can be used for quantitative analysis of complex multi-phase materials. Moreover, it can also be used for the evaluation of parameters such as crystallographic texture, crystallite size, strains and micro-strains [78]. Figure 2.10 shows an example of Rietveld refinements with the difference plots that show the variance between the measured and calculated data. The difference plot below the calculated pattern shows a very good fit quality in Figure 2.10.

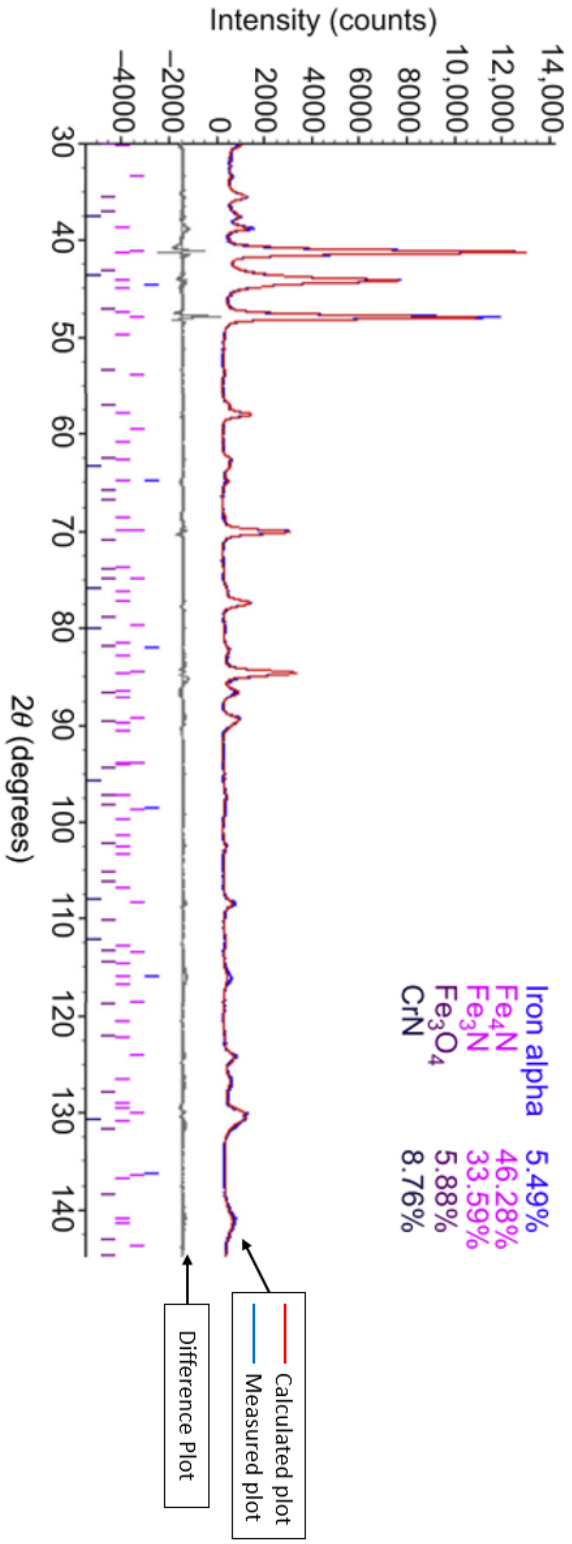

Figure 2.10: Quantitative phase analysis of nitrided tool steel by the Rietveld method [78]

Chapter 3

Methodology

This chapter discusses in detail the processes involved in the beneficiation experiments conducted within the scope of this thesis. The reader will be introduced to the lunar regolith beneficiation testbed developed at Deutsches Zentrum für Luft- und Raumfahrt (DLR) Bremen along with details about its components. Further, the chapter also gives more information about the parameters of the beneficiation process to be optimised, simulants used for conducting the experiments, procedures followed and the process of sample phase analysis using XRD.

3.1 Experimental setup and instrumentation

A lunar regolith beneficiation testbed called the Lunar Ilmenite Enrichment Demonstrator (LIED), was developed at DLR for the beneficiation of lunar regolith focusing on the enrichment of ilmenite to produce a feedstock that can be used for extraction of oxygen from ilmenite. It is comprised of multiple stages that achieve controlled beneficiation of lunar regolith simulants and represents TRL-4 level fidelity of the technology [86, 14]. The three stages of LIED are gravitational, magnetic and electrostatic beneficiation. Figure 3.1a illustrates the system schematic design that shows the three major stages of beneficiation along with individual components involved at each stage. The regolith particles follow a top-down trajectory which begins with a vibratory feeder at the top that transfers the simulant to a horizontal vibratory sifter. Upon being processed by the sifter, the sieved material is taken further for magnetic separation. The non-magnetic particle stream is conveyed further to the electrostatic beneficiation stages of tribocharger and electrostatic plate separator that produce the final output of LIED in the bins at the bottom. The final assembled LIED system is shown in Figure 3.1b.

This section will discuss the specific components and techniques used in LIED at every stage that provides the reader with an understanding of the processes and parameters involved in the optimisation experiments.

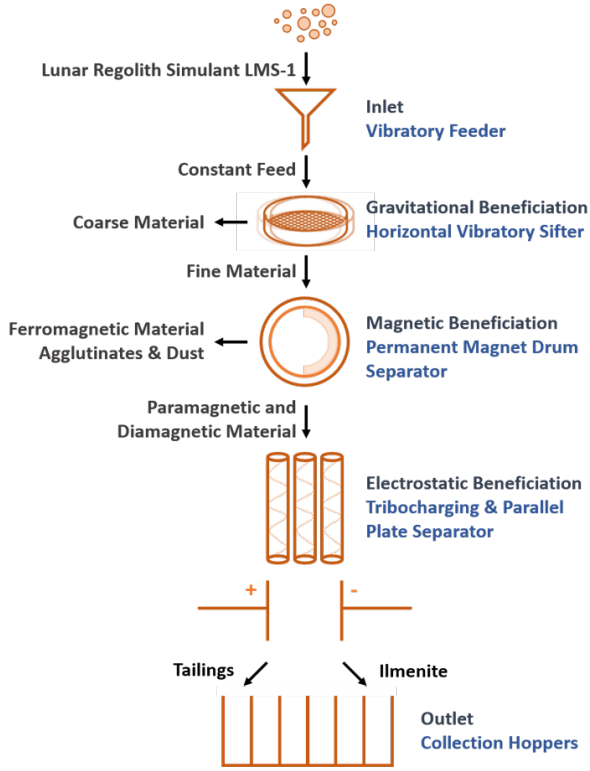

(a)

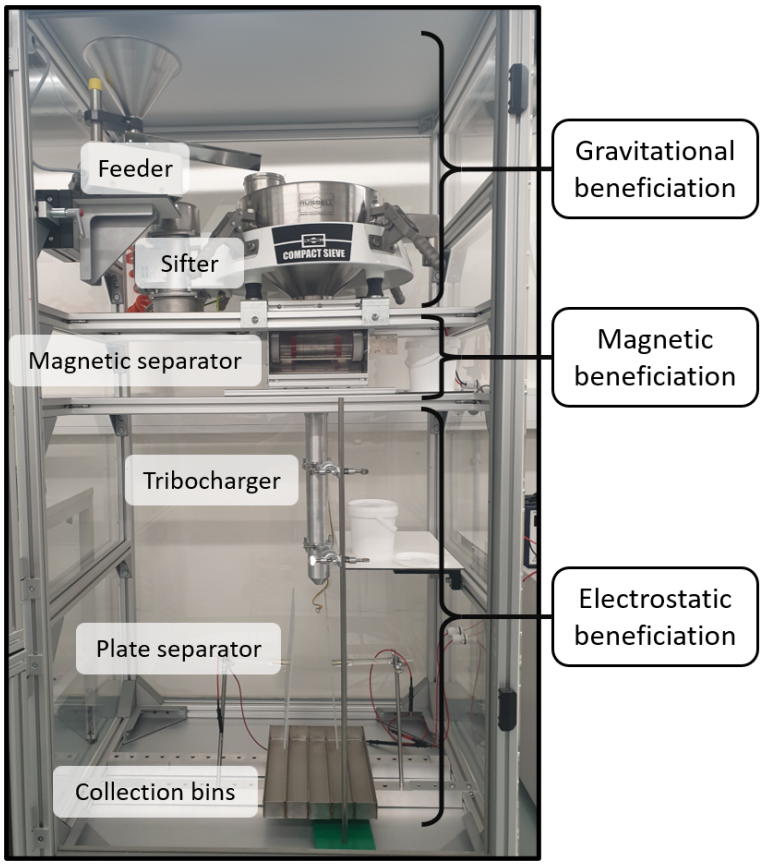

(b)

Figure 3.1: Beneficiation process schematic [14] (a); Lunar Ilmenite Enrichment Demonstrator (b)

Gravitational beneficiation

The gravitational beneficiation stage consists of two major components: a vibratory feeder and a horizontal vibratory sifter. The vibratory feeder *Laborette 24* produced by *Fritsch GmbH*, a German manufacturer of laboratory equipment is used to control the input feed rate of the regolith simulant. It has a funnel on top which is the inlet for unprocessed regolith simulant. The feed rate can be set to any integer value between 0 and 100 using its control panel shown in Figure 3.2. This range is in percentage scale and corresponds to the frequency of vibrations provided by the feeder. With increasing vibration frequency, the feed rate also increases. The control panel also allows the operator to set a timer for feeding the test sample. However, this function is not used for the experiments performed within the scope of this thesis. The output of the feeder comes out on an extended V-shaped rail on the side as shown in Figure 3.2 which transfers the simulant to the next step of beneficiation at the preset feed rate.

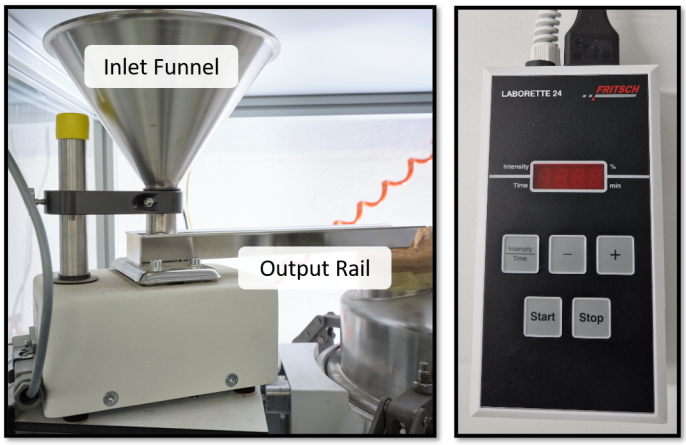

Figure 3.2: Vibratory feeder [L]; Feeder control panel [R]

The *Russell Compact Sieve*, a horizontal vibratory sifter manufactured by the British enterprise *Russell Finex* (as depicted in Figure 3.3), serves as the second stage of processing in LIED. It is used for the segregation of particles based on their size. The sifter inlet is located at the top and positioned close to the feeder output rail to allow easy transfer of material from the feeder. Upon successful processing of the simulant, particles larger than the sieve size (coarse particles) are collected on the right side while those smaller than the sieve size have an axial output at the bottom of the sifter. This makes it easier in connecting the output to further processing stages.

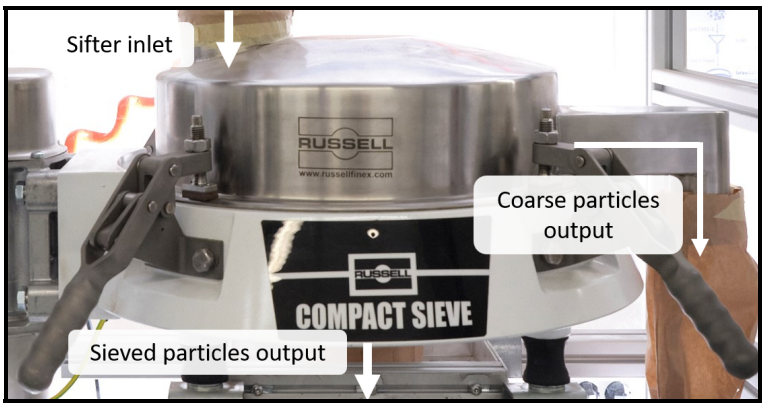

Figure 3.3: Russel vibratory sifter

The beneficiation experiments discussed in this thesis are performed with a 200 μm sieve. Apart from the sieve size, the sifter parameters such as the vibration amplitude, frequency, etc. cannot be changed. The experiment results will determine if the sieve size can be used as an additional parameter that can be manipulated to further improve the enrichment process. The vibratory sifter and feeder together complete the gravitational beneficiation stage of LIED.

Magnetic Beneficiation

The sieved material is transferred to the next step of magnetic beneficiation which consists of a permanent magnet drum separator [14]. It has a rectangular funnel-shaped inlet at the top for directing simulant particles towards the rotating drum. There are two cylinders within the rotating drum: an outer rotating cylinder and an inner stationary cylinder. The inner cylinder has permanent magnets attached to it in an arc shape. The outer rotating cylinder is driven by a brushed DC motor which is controlled by adjusting the voltage on its power supply. In this way, the rotational speed of the drum is kept adjustable as it can influence the output results of the magnetic beneficiation and will be important for the optimisation process [59].The drum assembly with stationary and rotating cylinders is shown in Figure 3.4.

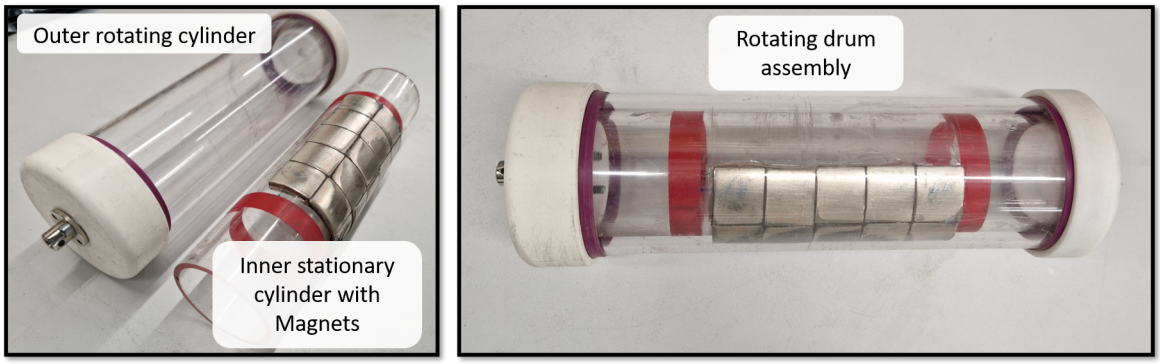

Figure 3.4: Rotating magnetic drum components [L]; Assembled magnetic drum [R]

There are two outlets for the magnetic separator: one for magnetic particles and the other one for non-magnetic ones. The fed simulant lands on the outer rotating cylinder and gets propelled in the direction of rotations. As the outer cylinder rotates, the non-magnetic particles fall off the cylinder surface sooner than the magnetic ones as these remain attracted towards the magnets and travel further. Once they pass the last set of magnets they get separated from the cylinder surface and fall on the other end of the separator. According to the system design, the magnetic stream consists of the agglutinates and metallic dust particles while the paramagnetic ilmenite and other para-, dia- and non-magnetic particles should be in the non-magnetic stream [14]. As the focus mineral is ilmenite, the non-magnetic outlet is connected further to the electrostatic beneficiation stage while the magnetic particles are redirected towards a separate bin **via paper bags**. Figure 3.5 shows the complete magnetic separator assembly in LIED.

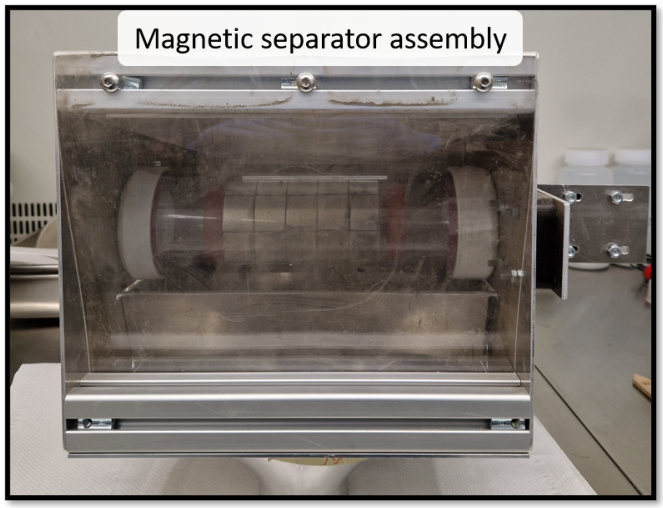

Figure 3.5: Magnetic separator assembly

Electrostatic Beneficiation

The last stage of LIED is electrostatic beneficiation. Upon successful gravitational and magnetic beneficiation, the non-magnetic particles are processed at this stage. The electrostatic beneficiation process consists of two major components: a tribocharger and an electrostatic plate separator. The tribocharger consists of an aluminium cylinder with a spiral electrode inside. As the particles travel through the electrode a charge known as the triboelectric charge is developed on the particles. The level of triboelectric charge developed on a particle depends on multiple factors such as particle size, shape, molecular content, gravitational acceleration etc. [14]. The bottom of the cylinder has a nozzle-like shape to focus the output particle stream towards the next step of beneficiation. The tribocharger outer cylinder and the spiral electrode are shown in Figure 3.6.

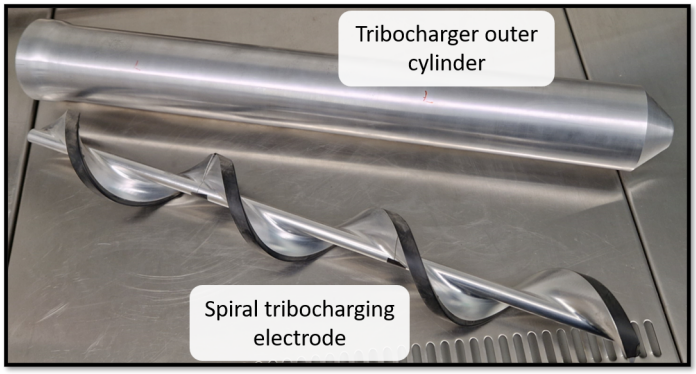

Figure 3.6: Tribocharger components

The tribocharged particles are further passed through an electrostatic plate separator. The plate separator produces a high-voltage electrostatic field across two aluminium plates. These plates are connected to a high-voltage power supply that is capable of producing up to 25 kV. Depending on the levels of tribocharging of the particles, the electrostatic field creates different forces on them as they pass through it and deflects their trajectories segregating them into different collection bins. There are 5 collection bins placed at the bottom where the particles are collected upon successful beneficiation. Ilmenite usually develops a positive charge while

minerals like olivine, plagioclase and pyroxene develop a negative charge upon tribocharging and hence end up in different collection bins. In this way, the electrostatic beneficiation process filters out ilmenite from the tailings. The complete electrostatic beneficiation assembly is shown in Figure 3.7.

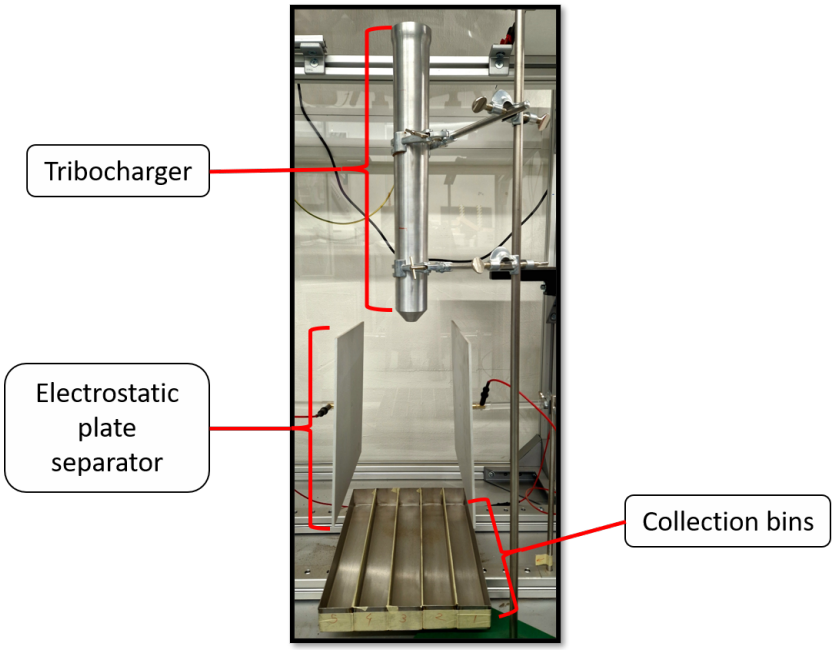

Figure 3.7: Electrostatic beneficiation assembly with tribocharger at the top, followed by plate separator and collection bins at the bottom

The material obtained in the collection bins is the final output produced by LIED which will be analysed for quantifying the effects of the selected process parameters. This concludes the entire process of beneficiation in LIED.

Process parameters of the LIED system

The complete list of process parameters that can be manipulated in LIED is given in Table 3.1. These are important to consider in the planning of the optimisation experiments.

Table 3.1: List of adjustable process parameters of LIED

Beneficiation Stage	**Parameters**	**Range**
Gravitational beneficiation	Feed rate (F)	$0 - 100$ %
	Sieve size	Adjustable
Magnetic beneficiation	Motor rpm (ω_m)	$0 - 1324^*$ *rpm*
Electrostatic beneficiation	Electrostatic field voltage (V)	$0 - 25$ *kV*
	Plate separator distance (d)	20 *cm***
** There is no rpm measurement device and hence the motor rpm is changed according to the datasheet values of rpm that correspond to the respective voltages as shown in Table 3.2*		
*** The plate separator distance can be changed at regular intervals of approximately* 10 *cm*		

Table 3.2: Rotational speed corresponding to voltage for magnetic separator motor (refer Appendix B.1)

Voltage (V)	Rotational speed (rpm)
4.5	397
6	530
9	794
12	1059
15	1324

According to the system design, the minimum necessary rotational speed for the magnetic separator is 715 rpm and therefore, only the rotational speeds corresponding to 9, 12 and 15 V are considered for the optimisation experiments [14].

The parameters selected for initial optimisation are the feed rate (f), motor rpm (ω_m) and electrostatic field voltage (V). This selection was made to allow the optimisation of at least one parameter in each of the beneficiation methods employed. The remaining parameters will be fixed during the optimisation experiments.

3.2 Lunar regolith simulants

The optimisation experiments for LIED involve the use of two simulant systems. The first one is LMS-1, a commercial lunar mare simulant from *Exolith Lab* [74]. The second simulant system used is the TUBS-M-based modular lunar regolith simulant developed at the *Technische Universität Braunschweig* and currently produced by the research group at the *Technische Universität Berlin* [75]. The details about these simulants are already discussed in the earlier chapter, however, a comparative analysis of the most relevant characteristics of the simulants is shown in Table 3.3. This analysis will be used to examine any simulant dependent outcomes that the LIED system may exhibit.

Table 3.3: LMS-1 and TUBS-M based modular regolith simulant [75, 74]

Parameter	LMS-1	TUBS-M
Grain density (g/cc)	2.92	2.96
Angle of repose (°)	38.3	41.9 - 45.8
Ilmenite content ($wt.\%$)	4.03	Adjustable
Mean particle size (μm)	91	87
Particle size distribution (μm)	0.04 - 1000	0 - 2000

3.3 Sample identification system

To effectively manage and analyse the output samples generated during the experimental optimisation of LIED, a nomenclature system is developed. This system ensures the unique identification of each sample along with their corresponding process parameter values, facilitating organised and comprehensive result analysis. The sample identification system and the list of legends for the respective identifiers are shown in Figures 3.8 and 3.9 respectively. For example, an experiment sample collected from the collection bin 5 in the first trial produced with LMS-1 simulant at 70 % feeder intensity, $\omega_m = 794\ rpm$, $V = 1\ kV$ will be identified as LMS-EB-4102E-01. Every sample is labelled according to this identifier to maintain records of experiments.

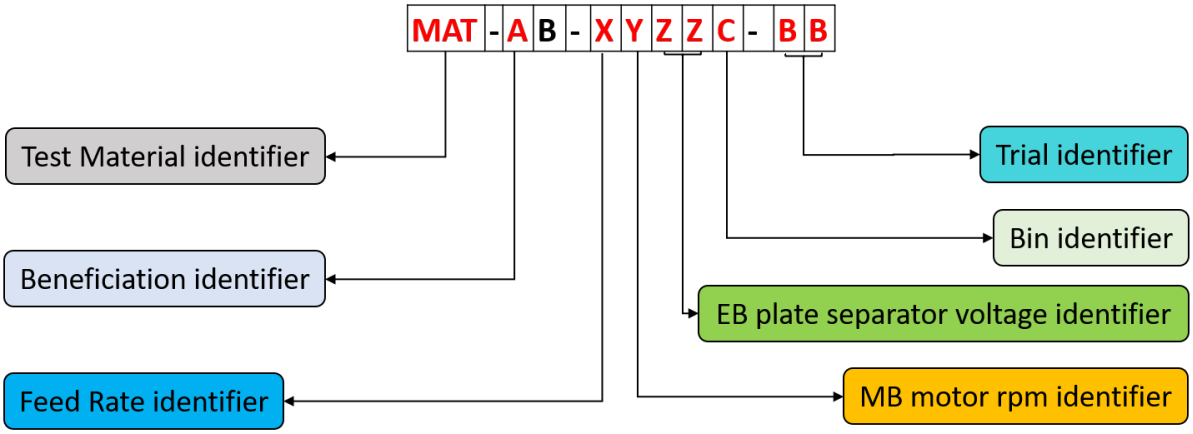

Figure 3.8: Sample identification system

Test Material Identifier	
Identifier	Sample Name
LMS	LMS-1
TUB	TMIAX
LHS	LHS-1
ILM	Ilmenite CR50

Beneficiation Identifier	
Identifier	Beneficiation stage
M	Magnetic and Gravitational beneficiation
E	Electrostatic , Magnetic and Gravitational beneficiation

Feed Rate Identifier	
Identifier	Feed rate
0	0%
1	40%
2	50%
3	60%
4	70%
5	80%
6	90%
7	100%

MB** motor rpm identifier		
Identifier	rpm	Motor voltage
0	0	0 V
1	794	9 V
2	1051	12 V
3	1324	15 V

EB* plate separator voltage identifier	
Identifier #	EB voltage kV
0	0
1	0.5
2	1
3	1.5
...	...
50	25

Trial Identifier	
Identifier	Trial #
01	Trial 1
02	Trial 2
03	Trial 3
04	Trial 4
05	Trial 5

Bin Identifier	
Identifier	Bin Nr.
A	1
B	2
C	3
D	4
E	5
F	Sieve (>200)
G	Non-magnetic
H	Magnetic

**EB stands for electrostatic beneficiation*

***MB stands for magnetic beneficiation*

Figure 3.9: Sample identification system: Legend

3.4 Sample phase analysis

As mentioned previously, the chemical phase analysis of output samples generated from the optimisation experiments is conducted using X-ray Diffraction (XRD). A standardised procedure is followed for the analysis of each sample to minimise measurement discrepancies. The XRD measurements are carried out at the *Department of Solid State Chemical Crystallography* in *Universität Bremen*. The author did not have access to this laboratory, so the experiments were kindly carried out by Muhammad Izzuddin Hanafi under the guidance of Prof. Dr. Thorsten Gesing, from the *Department of Solid State Chemical Crystallography*. They also granted access to the TOPAS and X'pert Highscore software tools for phase analysis, as well as provided the author with templates for phase analysis designed specifically for LMS-1 and TMIA4 regolith simulants. The author acknowledges their support in providing these resources. The rietveld refinements for the measured samples are performed by the author using these templates. This section delves into a comprehensive explanation of the XRD analysis procedure conducted for the samples.

Sample Preparation for XRD Measurements

In order to produce and measure diffraction patterns, a fine and uniform particle size distribution is necessary for XRD. Therefore, the measurement samples are crushed down to a fine dust-like consistency using a hand grinder for about 10 *min*. The crushed sample is then transferred to a sample holder (Figure 3.10: A-B). The sample powder is compacted within the sample holder cavity using a solid metallic cylinder that ensures uniform volumetric distribution of the sample powder (Figure 3.10: C - D). This process is done multiple times until no more sample powder can fit into the holder. Then the sample holder is removed from the support block by attaching it to a support plate and labelled with the allocated identification number provided by the laboratory (Figure 3.10: E). The sample is now ready and will be placed on the diffractometer for measurements.

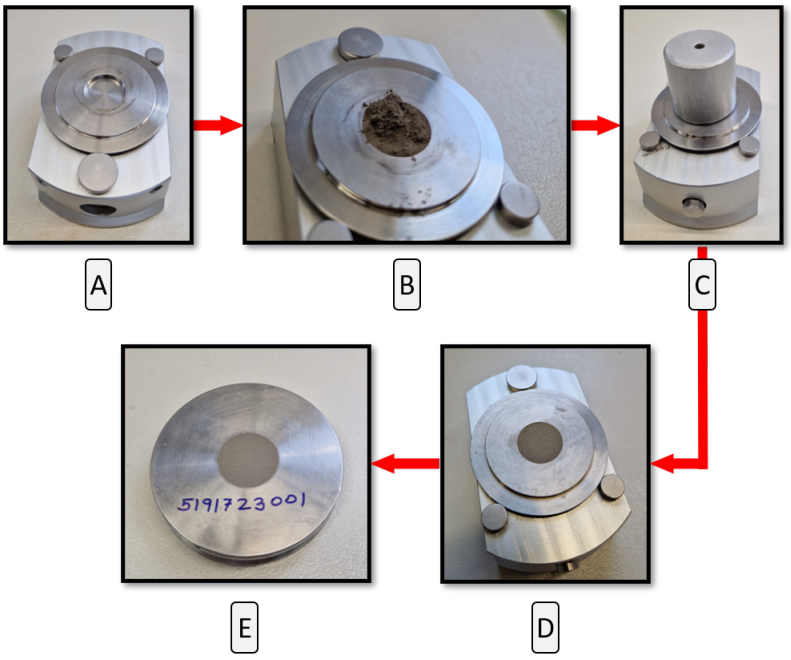

Figure 3.10: Sample preparation steps for XRD measurements

Qualitative and quantitative phase analysis

The XRD measurements generate a plot of the diffraction intensities of X-rays which is analysed for qualitative and quantitative phase analysis of the samples. This is done using software tools provided by the laboratory. X'pert Highscore uses a pre-selected database as a reference for identifying different phases in the sample and provides a list of all the phases present. The quantification of identified phases is accomplished on TOPAS which uses the rietveld refinement method of quantitative phase analysis [85]. The analysis was conducted based on the templates provided by the laboratory to avoid inaccuracies. Once refinements are successfully completed, conclusive results are obtained regarding the presence of phases and their corresponding quantities within a sample. These results serve as the basis for evaluating the effectiveness of the chosen beneficiation process parameters.

3.5 Experiment procedure

A standardised experimental procedure is established for all experiments to mitigate any variations in the output results caused by changes in the experimental process. The optimisation experiment consists of four stages: sample preparation, experiment setup, experimental run and results analysis. During the sample preparation stage, the regolith simulant undergoes a drying process prior to each experiment to eliminate any moisture content. The simulant samples are dried in batches of $1.5\ kg$ at a temperature of $80°C$ for a duration of two days. Once dried, the simulant is carefully stored in air-tight containers until it is ready for use in the experiments. For each experiment, a quantity of $300\ g$ from the dried simulant will be used. The next step is the experiment setup, which entails configuring the process parameter values. Attention is given to ensuring that all machine components are properly prepared for the experiments. Following this, $300\ g$ of the dried simulant sample will be loaded into the feeder inlet funnel. Finally, the machine doors will be securely closed, finalising the setup process.

The subsequent step is the experimental run, which involves activating the different stages of beneficiation in a predetermined sequence to ensure successful processing of the entire sample material. The power is initially turned on for the electrostatic and magnetic beneficiation stages, followed by the activation of the sifter and the feeder. Once the simulant has been successfully fed, the feeder is turned off, followed by the sifter, magnetic separator, and then the electrostatic plate separator, while ensuring that each stage has thoroughly processed the simulant sample. Subsequently, in the last stage of results analysis, the samples collected in different bins are extracted, their weights are measured, and they are labeled according to the sample nomenclature system discussed in section 3.3. The samples are sent further for XRD measurements and their phase analysis is performed as discussed earlier in section 3.4. The complete procedure for conducting experiments is illustrated in Figure 3.11. This procedure is implemented for all experiments conducted within the scope of this thesis. The adoption of a standardised workflow mitigates the impact of variations in experimental methods, ensuring reliable and reproducible outcomes.

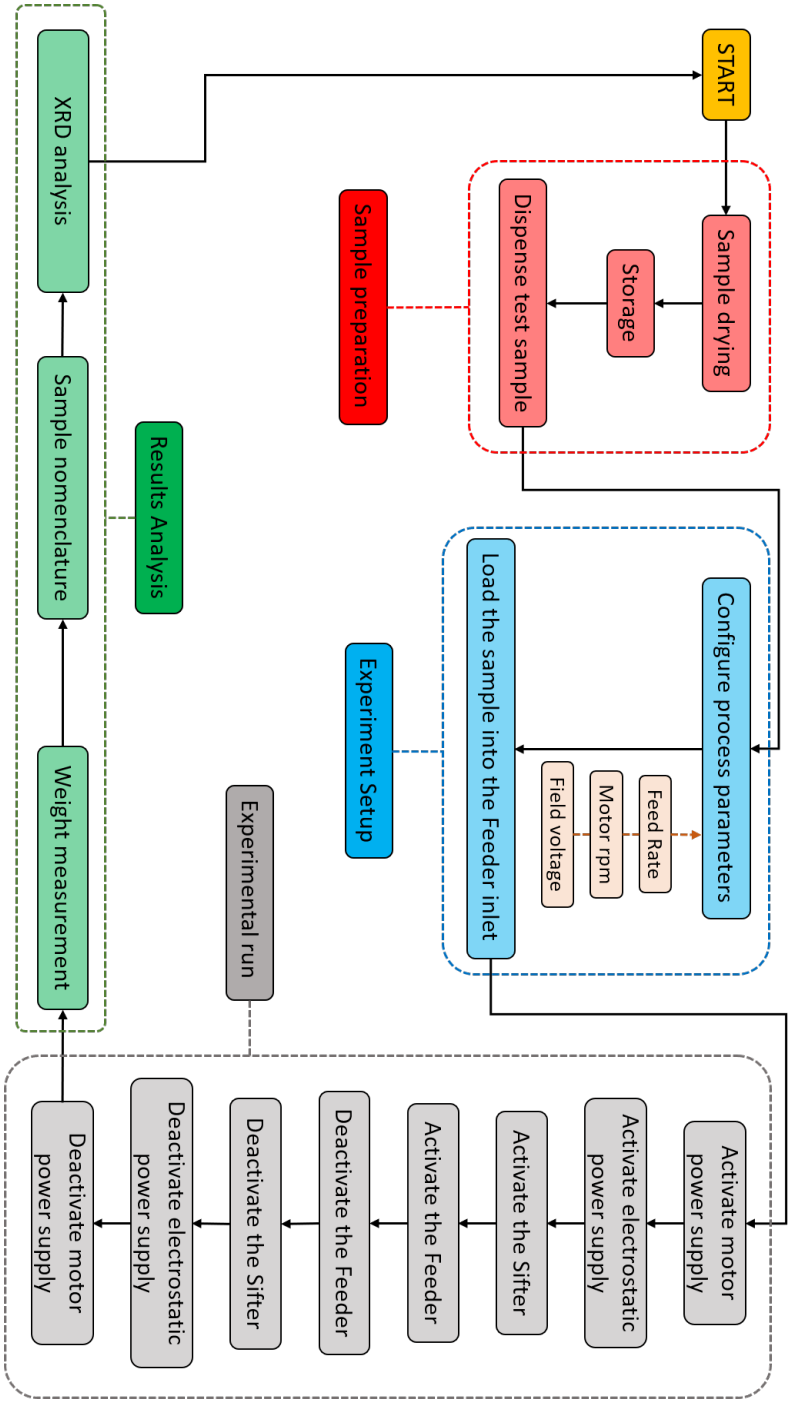

Figure 3.11: Optimisation experiment procedure

In conclusion, the methodologies outlined in this chapter provide a solid foundation for conducting the experimental investigations and analysis required to address the objectives of this study. By employing rigorous and replicable procedures, the reliability and validity of the results obtained can be ensured . The comprehensive understanding gained through these methodologies will serve as a crucial basis for the next chapter, where the experimental findings and their implications will be thoroughly examined and discussed.

Chapter 4

Experimental optimisation of Lunar Ilmenite Enrichment Demonstrator

The experimental optimisation of LIED is carried out using a conventional experimental analysis approach, encompassing experimental assumptions, objectives, apparatus, and procedures. The LIED system, which has been previously described in Chapter 3, serves as the experimental apparatus. This chapter provides a comprehensive discussion of the experimental assumptions, beneficiation objectives, and the procedures implemented for optimisation. Moreover, it delves into the strategy employed to optimise the output of the LIED system, while presenting a detailed examination of the experimental phases and their corresponding results.

4.1 Experimental approach for optimisation

This section aims to establish the foundation for the experimental analysis of LIED. Since this is the initial experimental run of the system, certain assumptions are made to simplify the dynamic parameters and concentrate on optimising the process parameters. Once these parameters are optimised, the remaining influencing factors can be taken into account for further enhancements. The experimental assumptions and goals provide a reference point for readers to grasp the context of the optimisation experiments.

Assumptions

In the process of optimising LIED, it is necessary to establish certain assumptions to streamline the experimental analysis. These assumptions help in narrowing down the focus on the key parameters that directly influence the beneficiation output. While there are numerous factors that can indirectly affect the results, this section primarily emphasises the machine parameters for the initial round of optimisation. By ensuring the accuracy of these assumptions, the aim is to identify the optimal machine parameter configuration. Once this configuration is determined, further considerations can be made regarding the remaining influencing parameters and their respective contributions to the overall beneficiation output. The following section outlines the specific assumptions made for the experimental analysis, providing a foundation for the subsequent optimisation experiments.

1. The ambient conditions of the laboratory remain constant at 25 $^{\circ}C$ and a maximum relative humidity of 60 % throughout the experiments.
2. The mineral composition of the regolith simulant used for experiments is homogeneous and constant throughout all experiments.
3. The regolith simulant is 100 % devoid of moisture upon being dried in the oven.
4. The rotational speed of the magnetic separator drum corresponds accurately to the specified voltage as indicated in the motor datasheet.
5. The error in the relative position of the electrostatic beneficiation collection bins and the plate separators is negligible across all experiments.
6. The system material residuals remain constant for every experiment.
7. The contribution of material residuals in the connecting paper tubes to the total system residual is negligible.
8. The errors in weight measurements are negligible.
9. The errors in XRD measurement remain constant for all measurements leading to useful and reliable relative analyses.

Goals for experimental optimisation of LIED

The primary objective of the LIED optimisation experiments is to produce an ilmenite-rich feedstock. The system-level requirements, as defined in the theoretical design goals outlined by the LIED system design, serve as the benchmarks to be achieved through these optimisation experiments [14]. The specific experimental output requirements derived from these goals are given in Table 4.1.

Table 4.1: Goals for experimental optimisation of LIED [14]

System requirement Identifier	Description
SMU_BEN_009	The grade of ore mineral within the produced feedstock shall be at least 40 $wt.\%$
SMU_BEN_010	The recovery of ore mineral within the produced feedstock shall be at least 50 $wt.\%$
SMU_BEN_011	The enrichment ratio of ore mineral within the produced feedstock shall be at least 4.5

4.2 Experimental optimisation strategy

As discussed in section 3.1, the process parameters selected for optimisation of LIED are the feed rate of the vibratory feeder (f), the rotational speed of the magnetic separator (ω_m) and the voltage of the electrostatic plate separator (V). To optimise the beneficiation process and attain an optimal configuration of these process parameters, it is necessary to conduct multiple experiments, systematically varying and combining these parameters.

An effective optimisation for any experimental setup involves testing the effects of different process parameter values on the system output. For instance, the feed rate ranges from $0 - 100$ %, the motor rpm has 5-speed settings corresponding to voltage inputs, and the electrostatic field voltage can be adjusted in the range of $0 - 25$ kV. To address potential result deviations, multiple experiment trials should be conducted for each parameter configuration, and the average output results should then be considered. Assuming intervals of 10 % for feeder intensities, 1 kV for the field voltage and the 5 values of rotational speeds possible, a total of 1200 experiments need to be performed ideally to test every possible parameter configuration. However, conducting such a high number of experiments within the available time and resources is impractical and time-consuming. Therefore, an alternative strategy has been developed to overcome these challenges.

The aim of this strategy is to minimise the number of experiments required while still achieving the optimisation goals. Initially, the focus was shifted to identifying processes that can be studied independently within the LIED system. The gravitational and magnetic beneficiation processes are interconnected, as variations in the feed rate directly impact the material throughput of the magnetic separator. Due to dimensional and design constraints, the magnetic separator has a limited processing capacity, setting an upper limit on the amount of material it can effectively process at any given time. Moreover, the rotational speed of the magnetic separator affects the magnetic beneficiation output. Consequently, experiments for different combinations of f and ω_m need to be conducted simultaneously. On the other hand, altering the value of f does not directly influence the feed rate for particles entering the tribocharger and plate separators. As a result, the optimisation of electrostatic beneficiation can be isolated from the rest of the system, significantly reducing the necessary permutations of parameter configurations. However, electrostatic beneficiation is sensitive to particle size and magnetic properties (see Section 2.2.2). Therefore, electrostatic beneficiation experiments can only be performed on samples that have undergone gravitational and magnetic beneficiation. Furthermore, to compensate for experimental deviations, each experiment is repeated three times, and the average output result is considered for further improvement. Although extreme deviations could introduce some inaccuracies, the likelihood of such deviations is minimal. Thus, conducting three trials for each parameter configuration is deemed sufficient.

Following the aforementioned guidelines and constraints, a multi-phase strategy was developed for efficient optimisation of LIED. Since the system has not been tested before, the first phase of experiments focuses on conducting individual tests for each of the beneficiation stages. This allows for the evaluation and refinement of their operational designs. In addition, the feed rate of the vibratory feeder can only be adjusted on a percentage scale by default. To enable comparison with future beneficiation systems and serve as a reference, it is crucial to convert this percentage scale to a more conventional feed rate unit of kg/h. This is an integral part of the first phase of experiments. By conducting stage-specific experiments and establishing a conventional feed rate scale, the first phase of optimisation ensures a comprehensive assessment of each beneficiation stage's performance and sets the foundation for further improvements.

Upon validation of the system's operational design, the next phase of experiments focuses on

optimising the gravitational and magnetic beneficiation stages. Through a series of experiments, the goal is to identify the optimised values for parameters f (feed rate) and ω_m (rotational speed of the magnetic separator) that yield the most favourable beneficiation results. These optimised values serve as key references for achieving enhanced performance in the subsequent phases of optimisation.

Once the optimised configuration of f and ω_m is determined, it remains unchanged for the subsequent phase, which focuses on optimising the electrostatic beneficiation process. The parameter under consideration for optimisation in this phase is the electrostatic field voltage (V). Given its paramount importance in the beneficiation process, it is crucial to conduct experiments encompassing a wide range of values for V. To accomplish this, the optimisation of the electrostatic beneficiation stage is divided into two phases. The initial optimisation involves performing experiments across the complete range of possible V values with larger intervals between them.

Following a thorough analysis of the results, a more refined and narrower range of voltages will be selected for the second iteration of optimising the electrostatic beneficiation process. This deliberate selection allows for obtaining results encompassing the entire spectrum of possible voltages, facilitating a comprehensive understanding of their effect on the beneficiation output. Subsequently, this approach will yield a final configuration of the values for f, ω_m, and V that collectively provide the most optimised and efficient beneficiation outcome within the given system.

In the final phase of optimisation experiments, the selected combination of process parameters will be tested on a different simulant system. This phase aims to investigate potential dependencies of LIED on the specific simulant employed for the experiments. By conducting these tests, the entire LIED system will undergo comprehensive examination and optimisation, ultimately yielding the best achievable beneficiation results. The different phases of the optimisation strategy and their respective goals are listed below for more details :

1. Phase 0: Preliminary experiments
    - Calibrate the units of the feed rate from a percentage scale to kilograms per hour (kg/h).
    - Operational design validation of the magnetic separator.
    - Operational design validation of tribocharger and electrostatic plate separator.
2. Phase A: Optimisation of gravitational and magnetic beneficiation
    - Investigate magnetic beneficiation output across different feed rates (f) and rotational speeds (ω_m).
    - Determine the combination of f and ω_m that provides the most desirable beneficiation output.
3. Phase B: Optimisation of electrostatic beneficiation (Iteration 1)
    - Investigate electrostatic beneficiation output across the entire range of possible field voltages.
    - Determine the value of field voltage that provides the best beneficiation results (V_i).
4. Phase C: Optimisation of electrostatic beneficiation (Iteration 2)
    - Investigate electrostatic beneficiation output across a field voltage range of $\pm 2\ kV$ relative to the previously determined optimum voltage (V_i).

- Determine the final combination of f, ω_m and V_f (selected voltage upon optimisation) that provides the most desirable beneficiation output.

5. Phase D: Validation of selected process parameter configuration with the TMIA4 simulant system
   - Validate the beneficiation results produced from the selected combination of f, ω_m and V_f on using TMIA4 simulant.
   - Compare the results and determine simulant-dependent changes in the beneficiation output (if any).

In this way, the final strategy for the optimisation experiments has reduced the total number of experiments by a large margin while still maintaining the level of possible optimisation. Upon the completion of all the experimental phases, the entire list of results will be analysed to study the distribution of beneficiation results across different variables and the interdependencies of the different process parameters. A flow chart of the optimisation strategy is shown in Figure 4.1.

f	Feed rate
ω_m	Magnetic separator rotational speed
V_i	Optimal voltage of electrostatic plate separator (Iteration 1)
V_f	Optimal voltage of electrostatic plate separator (Iteration 2)

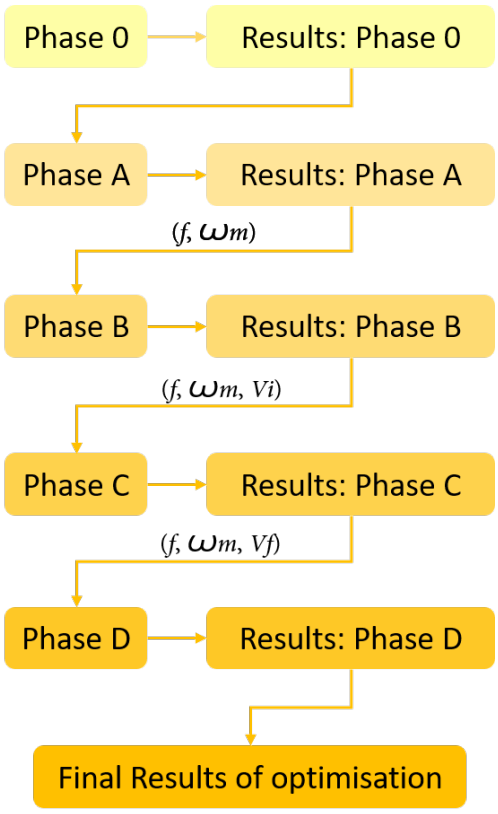

Figure 4.1: Experimental optimisation strategy

4.3 Experimental Analysis

This section comprehensively examines the experimental procedures and findings of this study. It delves into the systematic analysis and evaluation of the collected data, aiming to uncover meaningful insights and draw scientifically sound conclusions. By conducting optimisation experiments and analysing their results, this section aims to shed light on the relationships, trends, and correlations within the different variables that contribute to the beneficiation output. Through a detailed exploration of the experimental results, the analysis aims to validate the experimental hypotheses, identify key patterns, and gain a deeper understanding of the parameters under investigation. The calculation of the beneficiation parameters within this section is conducted in accordance with eqs. (2.2) to (2.5).

4.3.1 Phase 0: Preliminary experiments

Conversion of feed rate units

The feed rate, currently expressed on a percentage scale, requires conversion to conventional units such as kg/h for accurate reference and control. This will make the beneficiation results independent of the equipment used as long as the feed rate is maintained at the same values. The conversion process involves measuring the time needed to dispense a predetermined mass of regolith simulant using the designated feeder intensity. By performing experiments across the entire range of available feeding intensities and measuring their corresponding feeding times, it is possible to compute the effective mass flow rate in kg/h. A sample weight of $500\ g$ is used for these experiments. To account for potential variations, every experiment is repeated five times using identical settings, and their average value is taken into consideration.

The experimental procedure starts by setting the feed intensity to $100\ \%$ and measuring the respective feeding times. The procedure is repeated for all values of feeder intensities at regular intervals of $10\ \%$. However, at the feeder intensity of $40\ \%$, the feeding time increased to nearly $40\ min$, which is deemed excessively slow for a $500\ g$ sample. Therefore, the feed rate corresponding to $40\ \%$ is considered the minimum feed rate for the optimisation experiments. Figure 4.2 shows the variation of feed rate, measured in kg/h, with increasing feeder intensity (%). The conversion for feed rate from % to kg/h is shown in Table 4.2. For a complete list of results from the feeder experiments see Table A.1 of the Appendix A.

Table 4.2: Feed rate [kg/h] corresponding to feeder intensity [%]

Feeder Intensity [%]	Feed rate [kg/h]
40	0.84
50	1.77
60	3.65
70	6.14
80	9.96
90	16.29
100	28.82

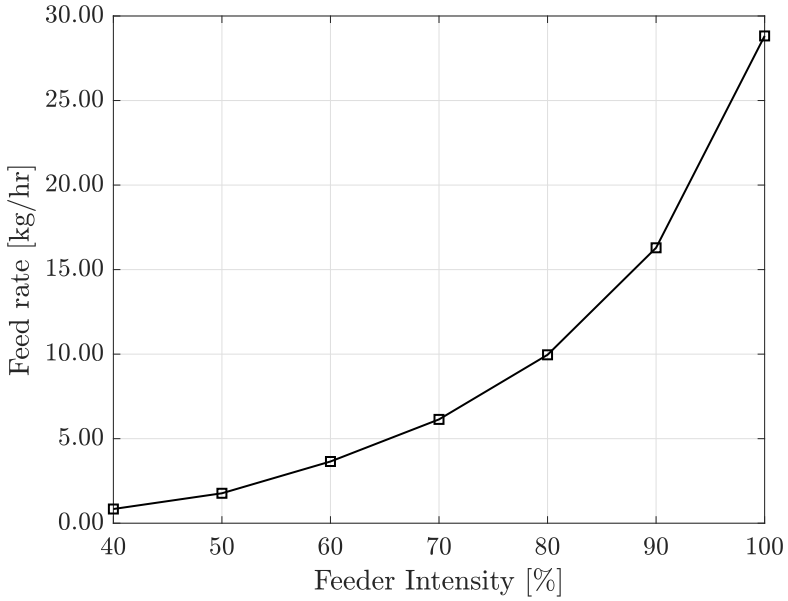

Figure 4.2: Feed rate vs Feeder intensity

Operational validation of magnetic separator

The magnetic separator of LIED uses a permanent magnet rotating drum design that is developed at the DLR Bremen facility. However, the assembled system was not previously tested for validation of the operational design. Therefore, the focus of these preliminary experiments is to examine the assembled components of the separator and test its functionality. For the purpose of these experiments, the magnetic separator was removed from the LIED system and tested independently.

After a preliminary inspection of the assembly, it became apparent that one of the magnets on the stationary cylinder was protruding more than the others. The intended gap between the outer surface of the magnets and the inner surface of the rotating cylinder is 1 mm. To assess the impact of the protruding magnet on the rotating drum, the entire system was assembled, and the motor was powered ON. Through multiple trials, it became evident that the magnet hindered the rotations of the outer cylinder. Multiple solutions were considered to address this issue, such as increasing the inner diameter of the rotating drum, replacing the stationary cylinder with another one that has properly assembled magnets, repositioning or replacing the protruding magnet or filing down the surface of the protruding magnet to reduce its thickness and eliminate the obstruction. However, altering the drum dimensions was not possible due to the selected bearings and other attachments, obtaining a new inner cylinder assembly was not feasible due to a lack of availability of the specially selected magnets, and removing or reassembling the old magnets proved difficult due to the epoxy adhesive used for bonding. As a result, the protruding magnet was filed down using a series of flat and curved metal files. Throughout the process, the assembly was tested by manually rotating it to ensure no further obstructions remained in the rotating drum. It is worth noting that this modification may cause a slight change in the magnetic field generated by the filed magnet, although this effect is assumed to be insignificant.

After the successful removal of obstructions, the drum was assembled inside the separator assembly and tested again. However, it was observed that after a few seconds of rotation, the motor shaft got disengaged from the drum and started spinning freely. The method of coupling

used for the motor shaft and the rotating drum lacked a secure locking mechanism. The motor shaft has a D-cut on it and a D-cut hole was present on the side of the rotating drum as shown in Figure 4.3a. The only method of locking used was a transition fit between the motor shaft and the rotating drum mount. The drum mount was made from ABS while the motor shaft is aluminium. The aluminium shaft wore out the ABS attachment, enlarging the hole made in the ABS attachment. To solve this issue, a new attachment was manufactured using PLA and a steel coupling was attached to it as shown in Figure 4.3b. In this solution, the motor shaft is mechanically attached to the drum with a bolted joint which is not as influenced by the material wear over time as with the previous design. Certain adjustments were necessary for the separator side plates to accommodate the passage and connection of the new attachment to the motor. Nevertheless, this arrangement significantly enhanced the operational reliability of the entire system.

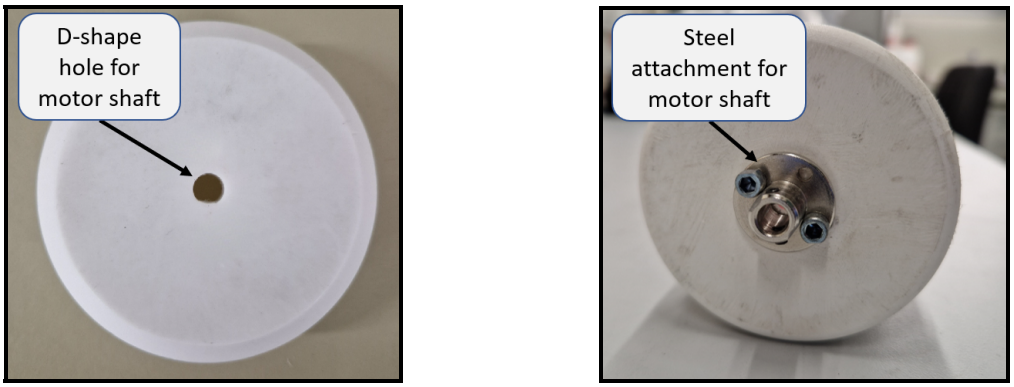

(a) *(b)*

Figure 4.3: Original drum mount (a); New drum mount with steel coupling (b)

After conducting a thorough assessment of the new attachment, the separator was reassembled and subjected to testing. However, it was observed that the drum failed to rotate despite the absence of any visible obstructions in the system. Further investigation revealed that the selected DC motor lacked sufficient torque. Analysis of the DC power supply revealed a reduction in motor voltage requirements to compensate for the high current demand, thus preventing excess power draw. Specifically, when set to $9\ V$ with a current limit of $0.9\ A$, the motor drew $0.9\ A$ but experienced a voltage drop to $2.5\ V$. The motor reached its maximum current draw from the power supply in an effort to cope with the elevated loads. Unfortunately, the magnetic separator assembly and all the attachments are designed to accommodate the selected brushed DC motor and hence, using a different motor was difficult due to its changed dimensions. To evaluate the capability of the selected motor for magnetic separation, it was decided to test it at higher current limits. Accordingly, the current limit on the DC power supply was gradually increased to ascertain drum rotation. Beginning from the initial limit of $0.9\ A$, determined based on the motor datasheet, the current was raised in increments of $0.05\ A$. Eventually, the drum began rotating at $1.6\ A$, albeit at very low rotational speeds. To achieve higher rotational speeds, the current was gradually increased to $1.8\ A$ which resulted in overheating and damage to the motor winding. Consequently, the motor was replaced with a new one of the same model. As increasing the current limit further resulted in damage to the motor, the limit was capped at $1.67\ A$ which is considered the optimal point for continuous operation between the very low rotational speed at $1.6\ A$ and the damaging point at $1.8\ A$. Multiple tests were conducted to validate this solution, ensuring that no overheating of the motor has occurred. Therefore, a decision was made to proceed with the optimisation experiments using fixed rotational speed for the magnetic separator.

Operational validation of electrostatic beneficiation

The electrostatic beneficiation stage comprises three components: Tribocharger, electrostatic plate separator and the collection bins. In this phase of experiments, each of these components is tested and assembled inside the LIED system.

As shown in Figure 3.6, the tribocharger has an outer cylinder with an aluminium spiral electrode inside. The electrode, manufactured in three parts due to its complex geometry, is assembled using dowel pins. Subsequently, the assembled electrode was inserted into the tribocharger cylinder for examination. A noticeable gap was observed between the outer surface of the electrode and the walls of the tribocharger cylinder. This gap could lead to a loss of material that would bypass the electrode and fall into the plate separator without undergoing the tribocharging process. To mitigate this issue, multiple layers of insulation tape were applied to the outer surface of the electrode until the gap was effectively filled. The decision to use electrical tape was made to ensure no direct influence of the added material on the tribocharging of regolith particles. The tribocharger position was then adjusted to establish a direct connection with the non-magnetic output of the magnetic separator, while the magnetic output was collected in a separate output bin to ensure the isolation of magnetic particles from the tribocharger. Subsequently, the tribocharger assembly underwent testing by passing regolith simulant samples through it and carefully examining the process. The evaluation revealed the presence of a notable amount of residual material remaining on the spiral electrode. It can be, however, fairly assumed that the quantity of residual material will remain constant for every experiment and this can be adapted to the experimental analysis. Aside from the residuals, no other issues were observed during these tests.

The position of the electrostatic plate separator was adjusted to keep the tribocharger output in the centre. The plates are mounted on the structural members at the bottom using steel rods. However, there is no locking mechanism to stop the mounting rods from rotating. Consequently, the orientation of the plates must be assessed prior to each experiment to verify their parallel alignment with each other. The collection bins located at the bottom were intentionally not fixed in place to provide flexibility in their positioning relative to the tribocharger. As the bins were not originally designed to be attached to each other, achieving a synchronized position can be challenging. To address this, the bins are secured together using masking tape to maintain their relative positions. As there is no specific attachment mechanism to fix the collection bins onto the structural members, their position was adjusted and marked on the underlying structure to ensure consistency throughout the experiments. Although there may be some minor variations in positioning the bins precisely for each experiment, this error is deemed negligible for the purposes of the optimisation experiments.

Results: Phase 0

The preliminary experiments effectively validated the operational functionality of each component within the LIED systems. Furthermore, significant modifications were made to the experiment plans based on the outcomes and insights gained from these initial tests. The results for these preliminary experiments for each beneficiation stage are listed below:

1. Gravitational beneficiation:
    - It was observed that after every $10 - 12$ experiments, the build-up of dust on the feeder output rail caused an increase in feeding time. This effect was particularly pronounced at feed rates below $70\ \%$ intensity. Therefore, it is recommended to utilise feed rates equal to or higher than $70\ \%$ to minimise the need for maintenance interventions. Also, at feeder intensities more than $90\ \%$, the feeder becomes unstable as the vibration frequency increases and starts moving on the mounting platform. Therefore, if further experiments require these high feeder intensities, an attachment should be designed for improved feeder stability.
    - The functionality of the vibratory sifter was initially assessed upon its delivery as a quality control measure and hence, no operational tests were performed on the sifter at this stage.
2. Magnetic beneficiation:
    - The rotational speed of the magnetic separator cannot be increased with the selected motor configuration. As a new motor would affect the entire separator outer assembly, it is decided to conduct the beneficiation experiments with a fixed rotational speed corresponding to $9\ V$ and a current limit of $1.67\ A$.
    - It has also been noted that some magnetic material remains attached to the rotating cylinder and does not dislodge into either of the outlets. However, this occurs uniformly throughout each experiment, leading to the assumption that the residual amount remains constant across all experiments.
3. Electrostatic beneficiation:
    - The tribocharger exhibits a significant accumulation of residuals following each experiment. While the residual amount remains consistent across all experiments, it is imperative to clean the tribocharger between the tests for different beneficiation parameter configurations to prevent the mixing of results from these experiments.
    - The aluminium plates of the plate separator need to be parallel to each other but their positions cannot be mechanically fixed in the current design. Therefore, prior to each experiment, it is essential to verify and ensure that the plates are positioned as intended. Any deviations or errors in their positioning during the experiments are neglected.
    - The collection bins are not fixed in place and hence, their positions are marked on the support structure in accordance with the selected positions of the tribocharger and plate separator. Any deviations or errors in the placement of the collection bins are neglected during the experimental optimisation process.

4.3.2 Phase A: Optimisation of gravitational and magnetic beneficiation

Phase A of the experimental analysis involves the investigation and optimisation of gravitational and magnetic beneficiation. The process parameters targeted for optimisation in this phase include the feed rate (f) and the rotational speed of the magnetic separator (ω_m). However, based on conclusions drawn from the preliminary experiments (Phase 0), ω_m cannot be changed and will remain fixed at 794 rpm. Additionally, based on the findings of the preliminary experiments, it was observed that the feed rate corresponding to 40 % feeder intensity is deemed as too slow for the beneficiation process. To focus solely on the relevant range of feed rates for beneficiation, the feed rates of 1.77 kg/hr, 6.14 kg/hr and 28.82 kg/hr corresponding to feeder intensities of 50 %, 70 % and 100 % respectively are selected for the phase A experiments.

Another important aim of this phase is to quantify the ilmenite distribution across the magnetic and non-magnetic outputs of the magnetic separator, thereby validating its design. Figure 4.4 provides a visual representation in the form of a flowchart, outlining the different combinations of parameters employed for conducting the optimisation experiments during this phase. A total of nine experiments are conducted, resulting in the production of 18 samples for subsequent analysis. Specifically, nine samples are obtained from the magnetic output, while the remaining nine samples are obtained from the non-magnetic output.

A complete list of samples tested in phase A of the optimisation experiments is shown in Table A.2 and their respective experimental measurements are shown in Table A.3 of the Appendix A. These measurements are used for the analysis discussed further in this section.

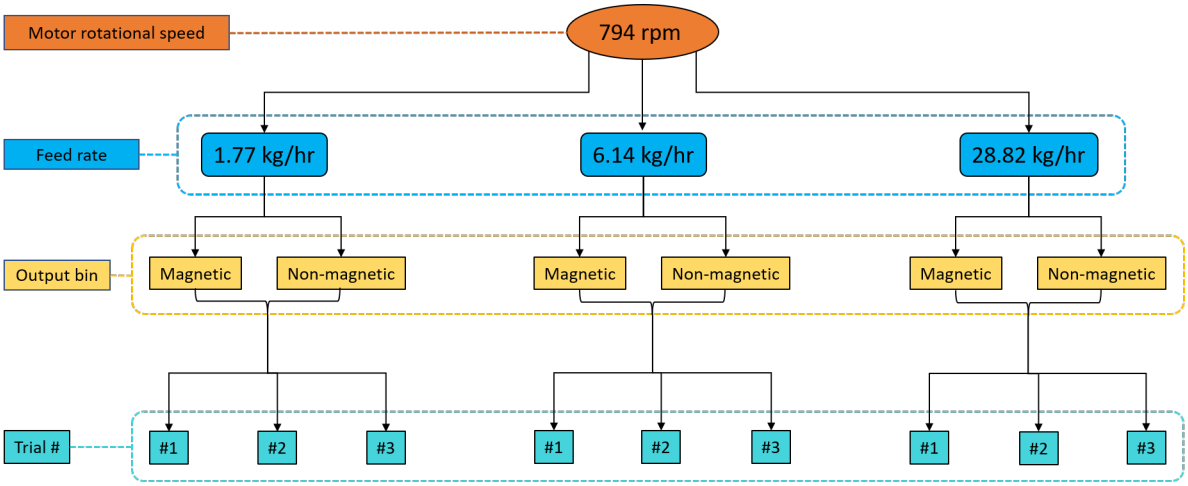

Figure 4.4: Process parameter configurations for optimisation experiments: Phase A

Results: Phase A

Ilmenite detection in simulant samples

The phase A optimisation experiments constitute the first optimisation campaign for the LIED system, as well as the first implementation of the designated procedures. Therefore, apart from the experiments, all the procedures decided previously were also validated and updated as per need. As ilmenite detection and quantification were not tested before, it was important to first analyse and characterise the tested samples to set the frame of reference for further phase analysis. During the XRD analysis of tested samples, the presence of ilmenite could not be detected in any of them. Initially, this was attributed to the possibility of extremely low concentrations of ilmenite, which could fall below the detection threshold. To validate this claim, a sample of 100 % ilmenite Cr50 was analysed to understand its chemical composition. Further testing and a detailed phase analysis of the sample was performed by Md. Izzuddin Hanafi from the *Department of Solid State Chemical Crystallography* in *Universität Bremen*. It was concluded from this analysis, that the inability to detect ilmenite stemmed from its complex multi-phase composition. The phase analysis concluded that the ilmenite Cr50 is composed of four phases. These are rutile (TiO_2), moganite (SiO_2), hematite (Fe_2O_3) and a solid solution of ilmenite and hematite ($(FeTi0_3)_x -_x (Fe_2O_3)_x$). Their respective quantities within the ilmenite Cr50 sample are shown in Table 4.3.

Table 4.3: Ilmenite Cr50 phase composition according to XRD measurements

Sample material	Rutile	Moganite	Hematite	$(FeTi0_3)_x -_x (Fe_2O_3)_x$
Ilmenite Cr50	31.76	7.98	23.74	36.52

A comparison between the measured diffraction patterns of ilmenite Cr50 and LMS-1 is shown in Figure 4.5, revealing that the peak intensities generated by the ilmenite samples are significantly lower than those of the LMS-1 samples. The Y-axis shows the intensities of diffraction and the X-axis shows the diffraction angles. This illustrates the lower peak intensities of ilmenite (green) being superimposed by the LMS-1 diffraction peaks (blue), thereby leading to a misleading result.

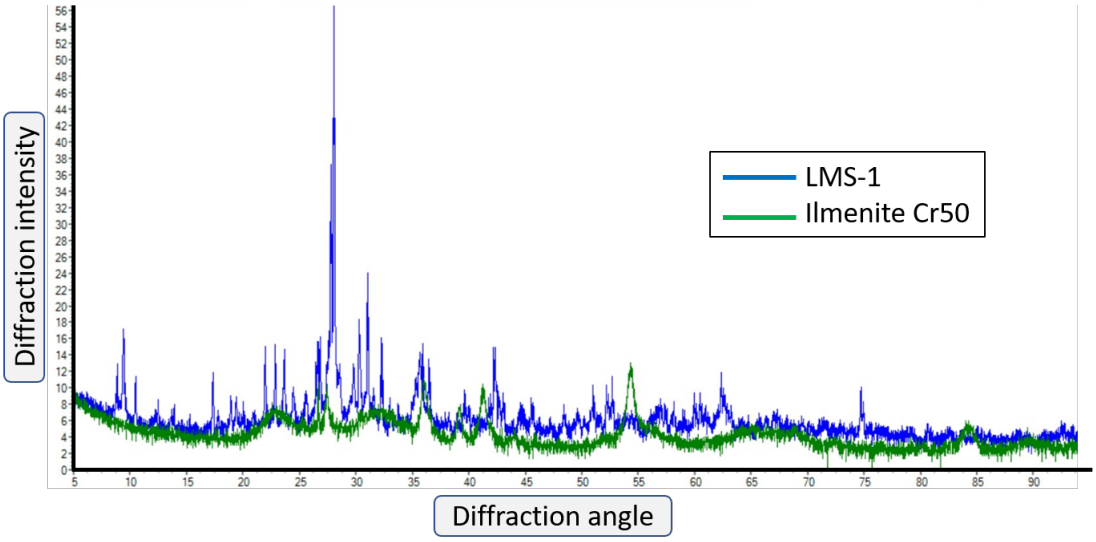

Figure 4.5: Ilmenite Cr50 and LMS-1 diffraction patterns generated in TOPAS software

Upon the completion of this analysis, a template for conducting phase analysis on the TOPAS software was provided which is used for all further XRD analyses of the experiment samples. This template quantifies the different phases of ilmenite and therefore, the total ilmenite content used in results analysis is a sum of the quantities of the different phases of ilmenite.

Quantitative analysis of ilmenite distribution in magnetic and non-magnetic outputs

According to the magnetic separator design implemented in LIED, the primary objective is to achieve effective separation of ferromagnetic agglutinates and dust particles from the ilmenite and the remaining weakly magnetic particles. Consequently, it is expected that the ilmenite concentrations in the magnetic output will be lower compared to the non-magnetic output. The validation of this separation method is supported by the analysis of results obtained from the phase A experiments. Figure 4.6 illustrates the average ilmenite concentrations in the magnetic and non-magnetic outputs across different feed rates. These values represent the averages obtained from three independent trials conducted for each feed rate setting. The noticeably higher ilmenite concentration in the non-magnetic output validates the effectiveness of the magnetic beneficiation process.

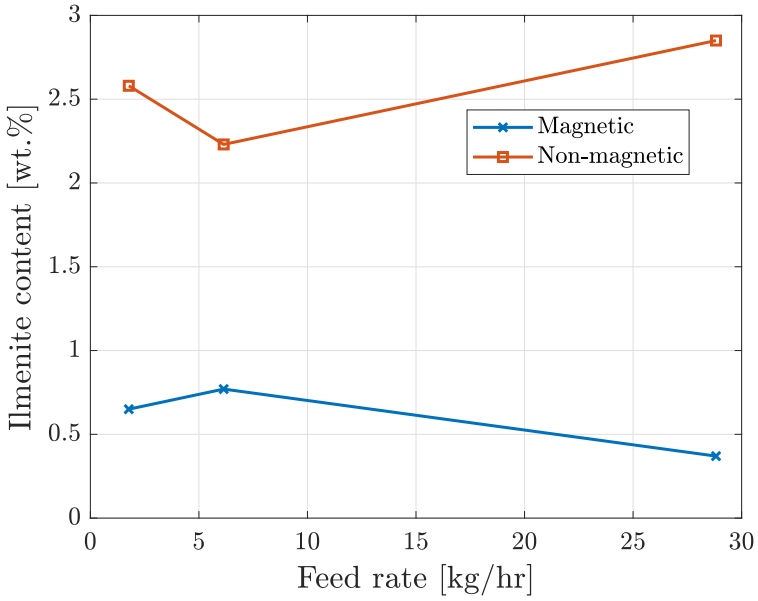

Figure 4.6: Average ilmenite content in magnetic and non-magnetic output

In conclusion, the analysis of phase A experiments has revealed that the non-magnetic output consistently exhibits higher average ilmenite content compared to the magnetic output. This finding reinforces the significance of the beneficiation process in effectively separating ilmenite from the other components. Moving forward, a detailed investigation of the beneficiation parameters is performed to provide valuable insights into the underlying mechanisms and dynamics of the process.

Quantitative analysis of beneficiation parameters in phase A experiments

The following section presents a quantitative analysis of the beneficiation parameters conducted after the phase A experiments. The primary objective of this analysis is to systematically evaluate the effects of feed rate and rotational speed of the magnetic separator on the beneficiation process and identify their optimal configuration that produces the desired results. The obtained results will be used as a starting point for the optimisation of electrostatic beneficiation in the further experimental phases. The calculated beneficiation parameters from these analyses are shown in Figures 4.7 to 4.10.

Yield of ilmenite in the output

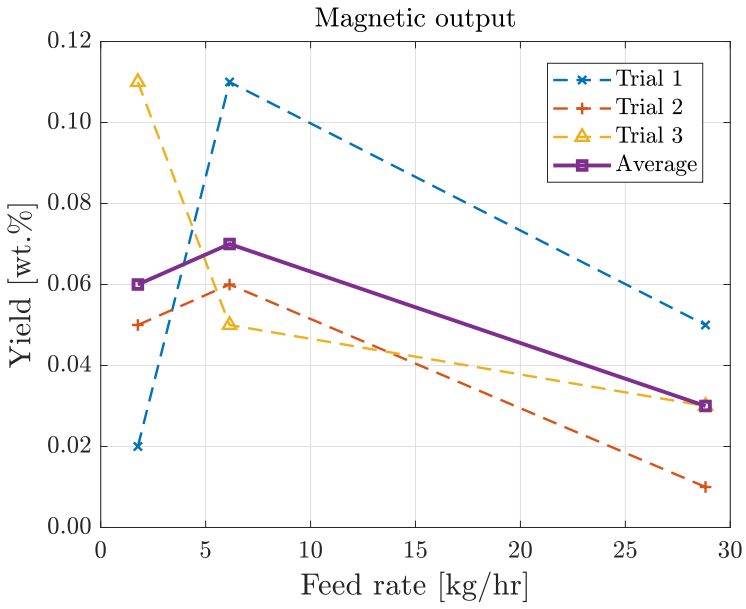

(a)

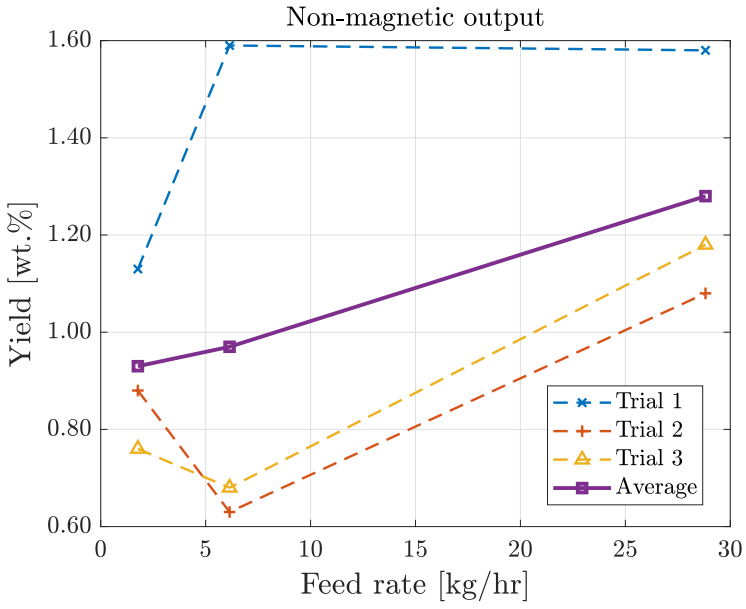

(b)

Figure 4.7: Yield of ilmenite in the magnetic output (a); Yield of ilmenite in the non-magnetic output (b)

Recovery of ilmenite in the output

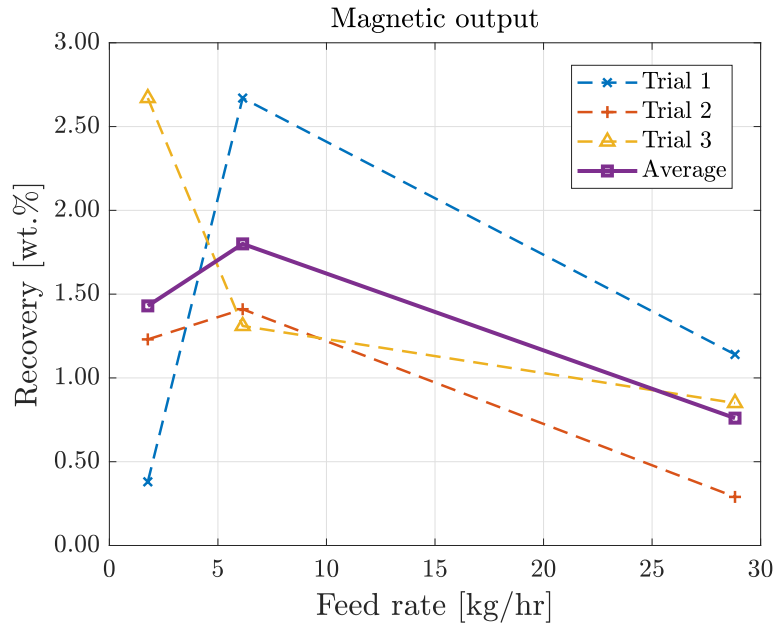

(a)

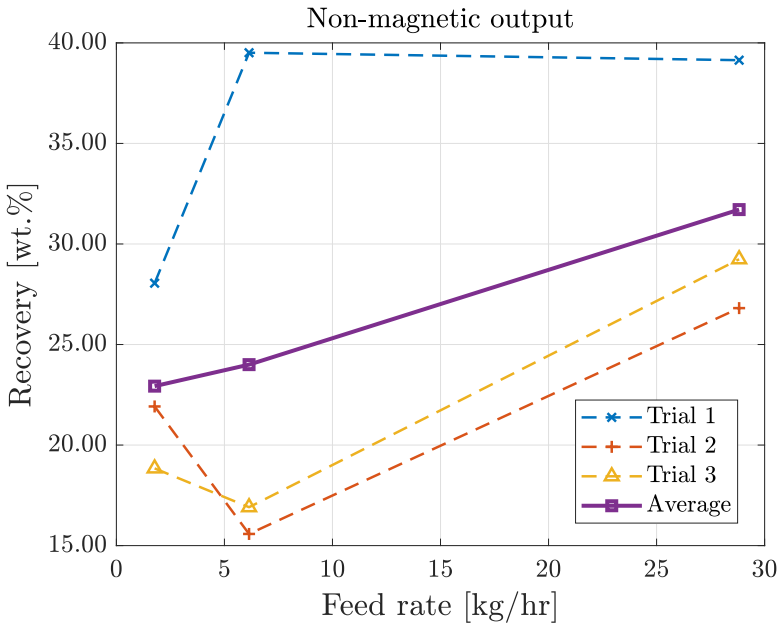

(b)

Figure 4.8: Recovery of ilmenite in the magnetic output (a); Recovery of ilmenite in the non-magnetic output (b)

Grade of ilmenite in the output

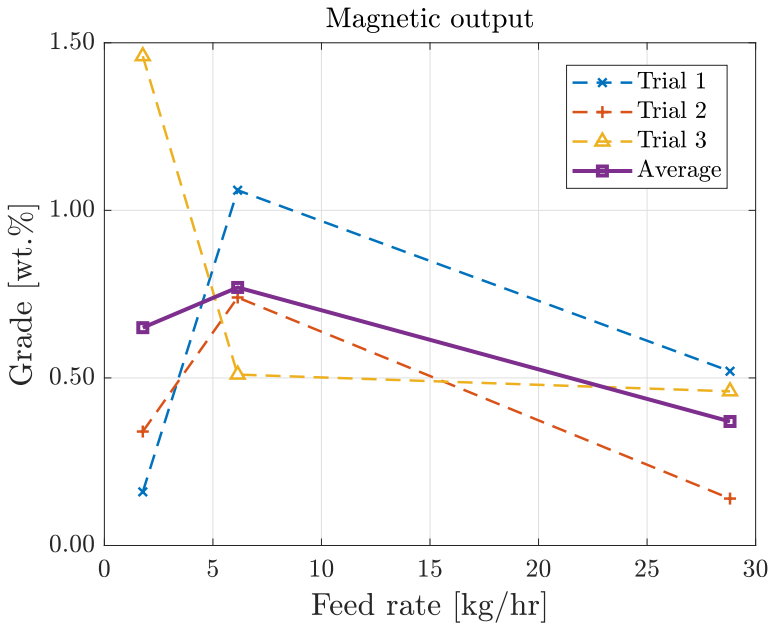

(a)

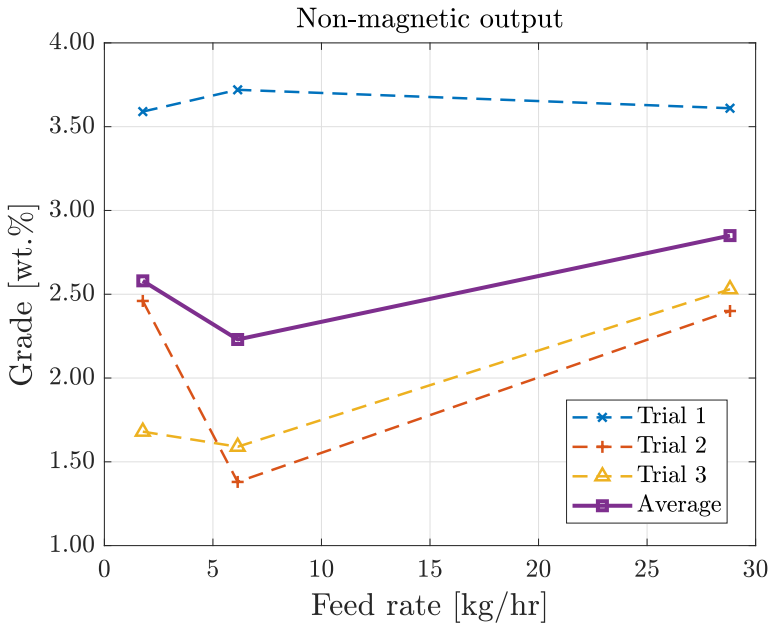

(b)

Figure 4.9: Grade of ilmenite in the magnetic output (a); Grade of ilmenite in the non-magnetic output (b)

Enrichment ratio for ilmenite upon beneficiation

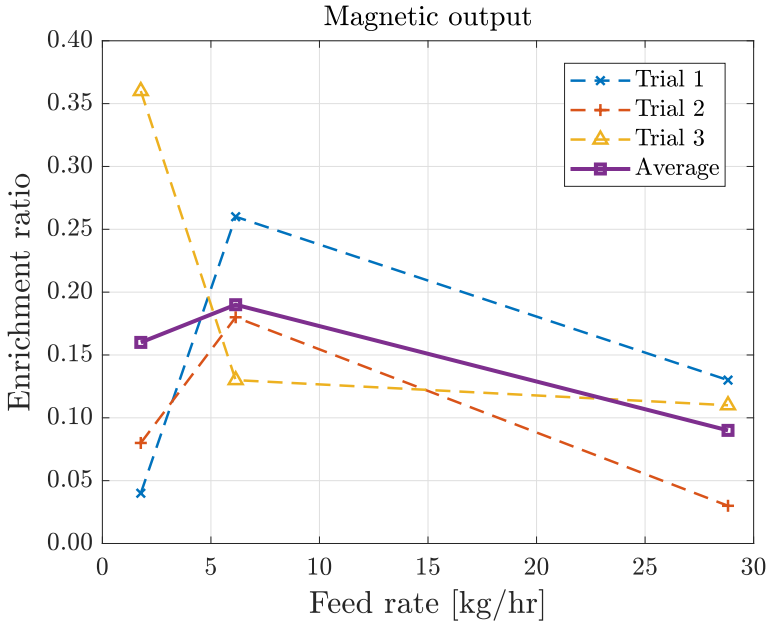

(a)

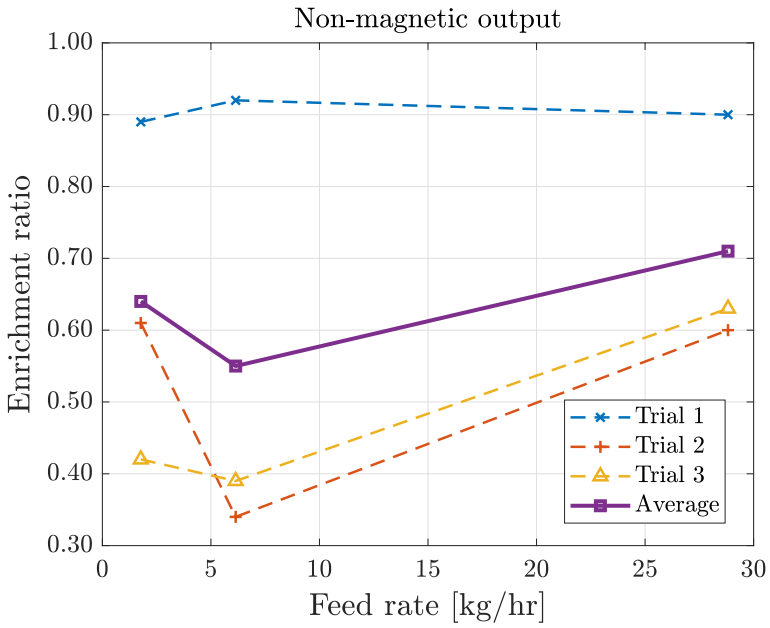

(b)

Figure 4.10: Enrichment ratio of ilmenite in the magnetic output (a); Enrichment ratio of ilmenite in the non-magnetic output (b)

It can be observed from these results that the non-magnetic output of the magnetic separator has on average higher yield, recovery and grade of ilmenite leading to an overall higher enrichment ratio for ilmenite. In conclusion, the non-magnetic output of the magnetic separator has higher ilmenite concentrations compared to the magnetic output. This successfully validates the operational design of the magnetic separator. Upon analysing the experimental results obtained from varying feed rates, it is clear that the small standard deviations of the measured data as shown in Table 4.4, provide evidence that the feed rate has no significant effect on the beneficiation output.

Furthermore, these standard deviations can also be attributed to experimental or measurement errors which can further reduce the existing variance in the beneficiation results.

Table 4.4: Standard deviation in beneficiation results of the non-magnetic output

Parameter	Yield [$wt.\%$]	Recovery [$wt.\%$]	Grade [$wt.\%$]	Enrichment ratio
Mean	1.06	26.22	2.55	0.63
Standard deviation	0.36	0.89	0.91	0.23

This analysis of the experimental data leads to the conclusion that the variation of feed rate has minimal impact on the beneficiation outcomes of the LIED system. Consequently, for further optimisation experiments, a feed rate of $6.14\ kg/hr$ that corresponds to $70\ \%$ feeder intensity is selected as the preferred operational configuration. This selection is motivated by the observed instability of the feeder on the mounting platform at feed rates exceeding $90\ \%$. Furthermore, the phase 0 experiments also demonstrate that the frequency of cleaning needed to maintain the desired feed rate decreases significantly at a feeder intensity of $70\ \%$ compared to intensities below $70\ \%$. Hence, in order to maintain efficient feeding operations with minimal maintenance requirements, it is decided that all subsequent optimisation experiments will be conducted at $f = 6.14\ kg/hr$ and $\omega_m = 794\ rpm$. This approach ensures a reduced feeding time along with enhanced system stability, resulting in improved overall performance.

4.3.3 Phase B: Optimisation of electrostatic beneficiation (Iteration 1)

The phase B optimisation experiments mark the first iteration in optimising the electrostatic beneficiation stage of LIED. The process parameter under consideration for optimisation is the field voltage (V) of the electrostatic plate separator. The feasible range of values for V spans from $0 - 25\ kV$ which is defined by the selected high-voltage power supply. During each electrostatic beneficiation experiment, up to five samples can be generated and collected in the designated bins at the bottom. Consequently, for every parameter configuration, a maximum of 15 samples are produced, that need subsequent XRD analysis. To ensure experimental feasibility while covering the entire voltage range, the experiments are conducted at field voltage values of $5\ kV$, $15\ kV$ and $25\ kV$, respectively. The values for f and ω_m remain fixed at $6.14\ kg/hr$ and $794\ rpm$ respectively as defined by the phase A experiments.

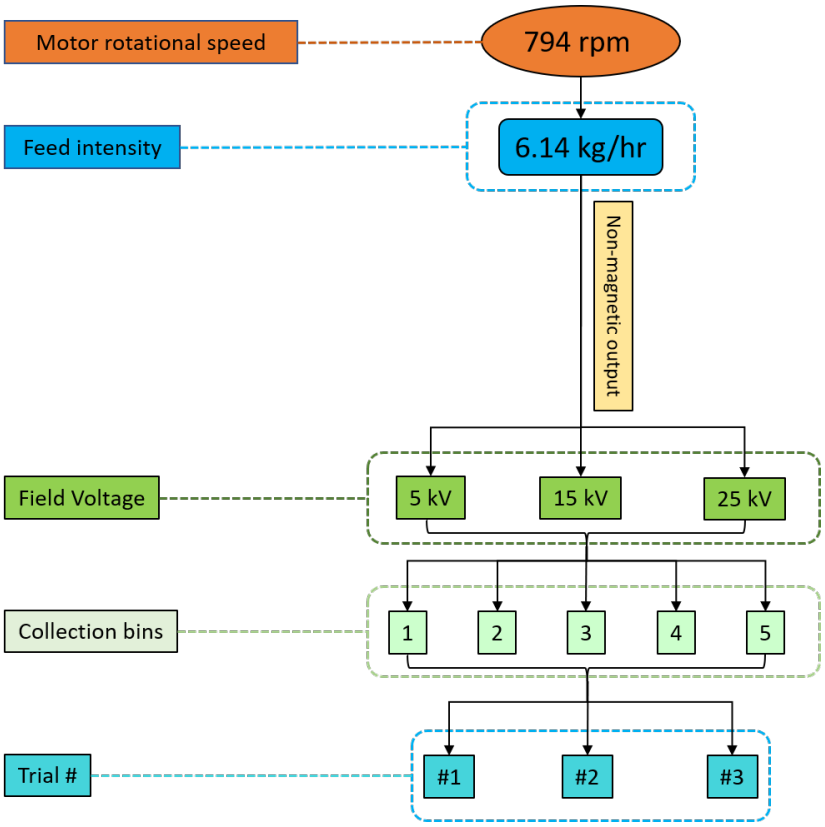

Figure 4.11: Process parameter configurations for optimisation experiments: Phase B

Figure 4.11 provides a visual representation in the form of a flowchart, outlining the various combinations of parameters employed for conducting the optimisation experiments during this phase. A total of nine experiments are conducted, resulting in the production of 40 samples. Specifically, 24 samples are obtained from the different collection bins that are analysed with XRD. A list of all tested samples in phase B of the optimisation experiments is shown in Table A.4 and their respective experimental measurements are shown in Table A.5 of the Appendix A. The measurements obtained are utilised for the quantitative analysis of the beneficiation outcomes in the phase B optimisation experiments, which are further discussed in detail in this section.

Results: Phase B

Distribution of ilmenite across the collection bins (Phase B)

The initial step in validating the effectiveness of electrostatic beneficiation involves identifying the collection bin that exhibits the highest concentrations of ilmenite. This section focuses on the distribution of ilmenite across the collection bins. By determining the bin with the highest ilmenite content, we can assess the ability of the electrostatic separation process to effectively concentrate and collect ilmenite particles. This analysis allows for the assessment of system performance and determines if adjustments are required to achieve the desired distribution of ilmenite in the collection bins.

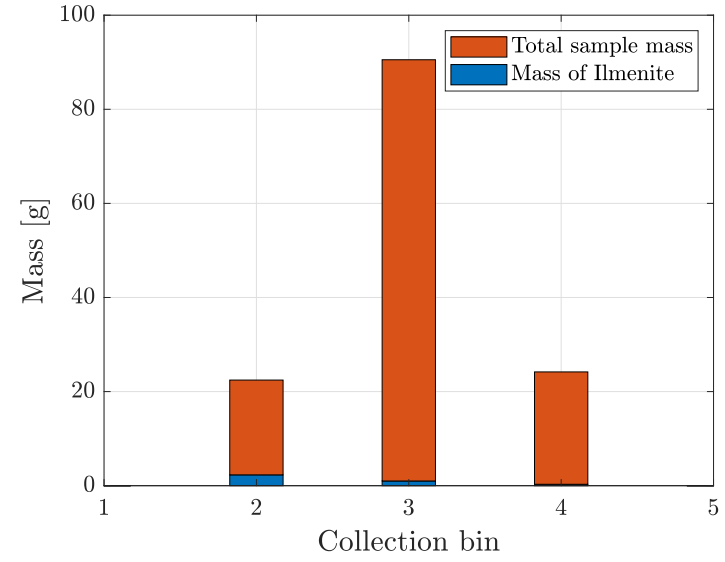

(a)

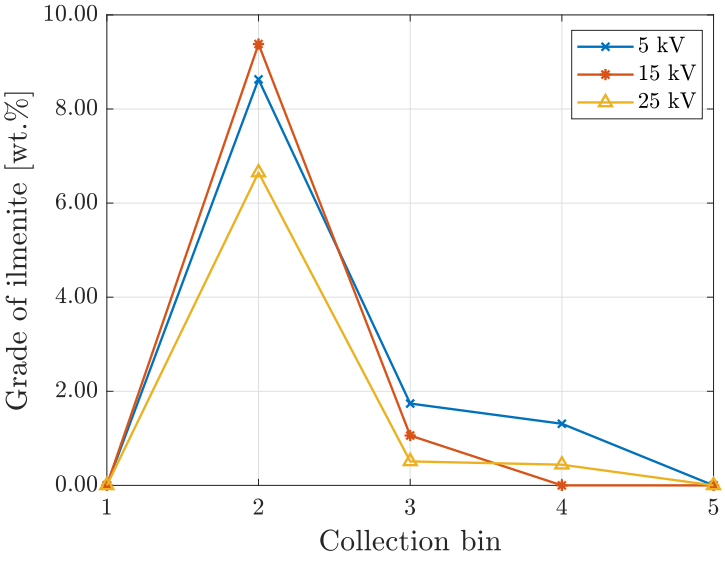

(b)

Figure 4.12: Mass distribution of samples across collection bins (Phase B) (a); Grade of ilmenite across collection bins (Phase B) (b)

The results shown in Figure 4.12 reveal that the bins situated on the extreme ends do not accumulate any sample material. Most samples are collected in bins 2 and 3, with a few deposits observed in bin 4 during certain experiments. Figure 4.12a shows the mass distribution of ilmenite and the total sample mass across the collection bins which demonstrates the average higher ilmenite content of the collection bin 2. This results in the higher grade of ilmenite in the produced sample from the collection bin 2 as shown in Figure 4.12b. It is clear from these observations, that the high-grade ilmenite-rich feedstock is present in bin 2. Therefore, further analysis for quantification of the beneficiation parameters is performed specifically for output samples from collection bin 2. The detailed results from the remaining collection bins are illustrated in Table A.5.

Quantitative analysis of beneficiation parameters in phase B experiments

The following section presents a quantitative analysis of the beneficiation parameters conducted during the phase B experiments which is used to evaluate the effect of field voltage on the beneficiation output from LIED. The aim of this analysis is to identify the value of field voltage that provides the best beneficiation results within this iteration. The beneficiation parameters as a function of the field voltage are shown in Figures 4.13 to 4.16.

Yield of ilmenite in output

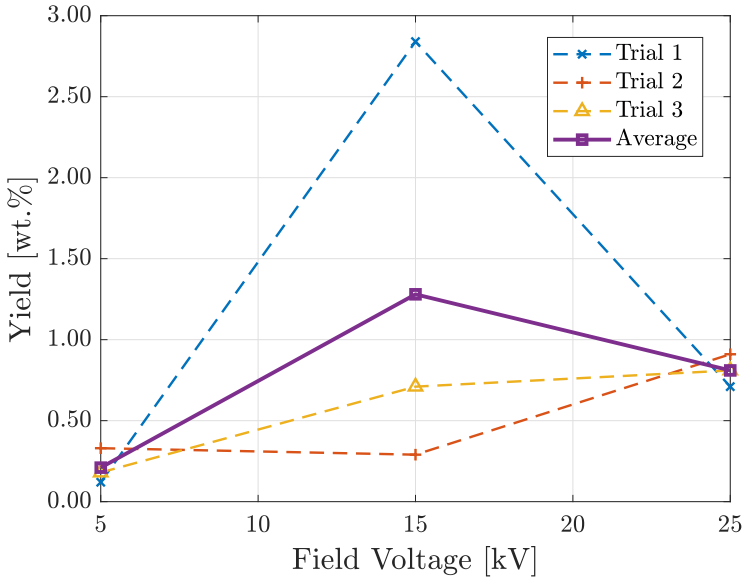

Figure 4.13: Yield of ilmenite in output from collection bin 2 (Phase B)

Recovery of ilmenite in output

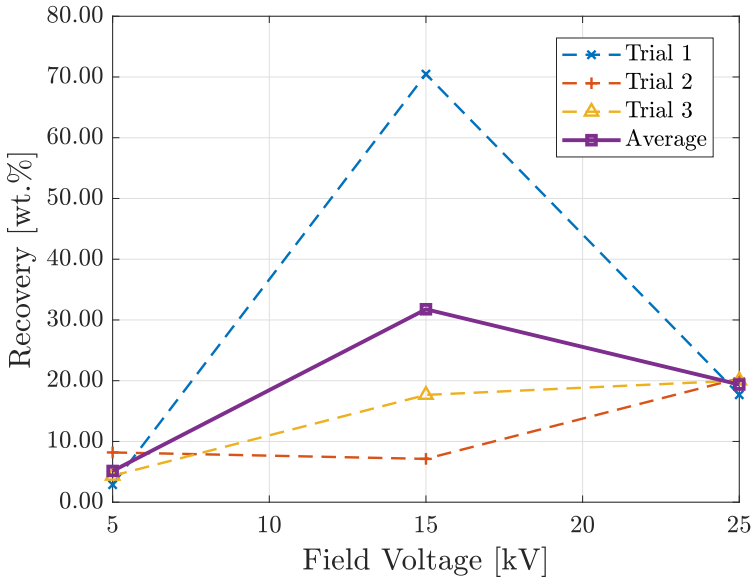

Figure 4.14: Recovery of ilmenite in output from collection bin 2 (Phase B)

Grade of ilmenite in output

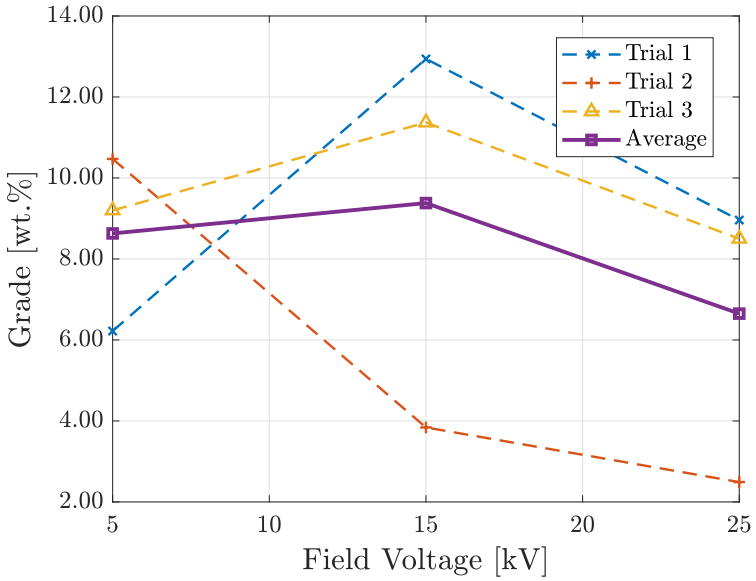

Figure 4.15: Grade of ilmenite in output from collection bin 2 (Phase B)

Enrichment ratio for ilmenite upon beneficiation

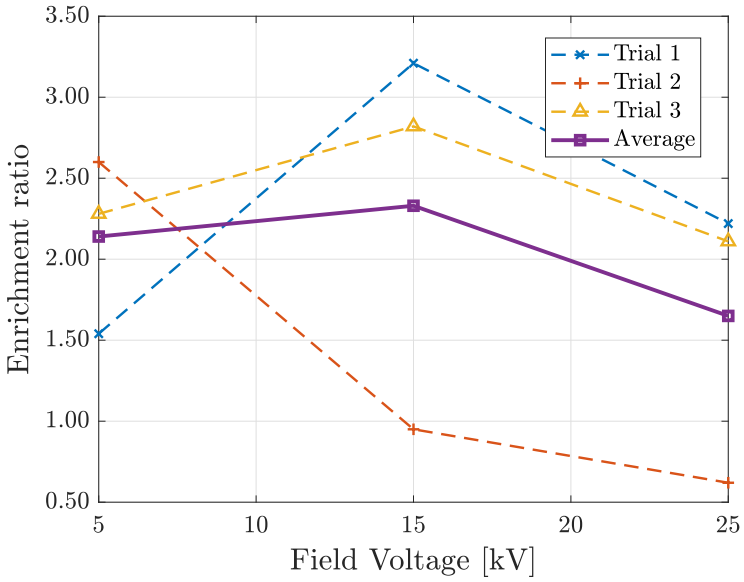

Figure 4.16: Enrichment ratio of ilmenite from collection bin 2 (Phase B)

These results demonstrate that, among all the beneficiation parameters, the most favourable outcomes in terms of ilmenite beneficiation are consistently observed in collection bin 2 at a field voltage of $15\ kV$. The corresponding output from bin 2 exhibits a yield of $1.28\ wt.\%$, recovery of $31.76\ wt.\%$, grade of $9.38\ wt.\%$. and an enrichment ratio of 2.33 for ilmenite. Another important observation from these results is the extreme deviations of results in some experimental trials. This can be attributed to multiple factors such as variations in the mass of the collected output in collection bins, primarily influenced by changing quantities of residual materials in the tribocharger and errors in positioning of the collection bins relative to the tribocharger. These fluctuations contribute to errors in the calculations, thereby impacting the accuracy of these measurements. By examining the average values and assuming consistent measurement errors across all experiments, a discernible trend can be observed in the beneficiation results. It can be concluded that a field voltage of $15\ kV$ yields the most favourable output for ilmenite enrichment.

Consequently, the next phase of optimisation for electrostatic beneficiation focuses on exploring field voltage values in proximity to $15\ kV$. This will allow for a comprehensive assessment of the system's behaviour within this specific range, providing valuable insights for further refinement of the beneficiation process. Therefore the input parameters for the next phase will be $f = 6.14\ kg/hr$, $\omega_m = 794\ rpm$ and the optimised field voltage (first iteration) $V_i = 15\ kV$. The range of field voltage to be tested and its impact on beneficiation outcomes is discussed in the next phase of optimisation.

4.3.4 Phase C: Optimisation of electrostatic beneficiation (Iteration 2)

This phase of optimisation involves the analysis of beneficiation outputs across a smaller range of field voltages for the electrostatic beneficiation process. Based on the optimised parameter configuration obtained from phase B, where 15 kV yielded promising results, the focus now shifts to conducting experiments within a narrower range. According to the optimisation strategy, a range of 15 ± 2 kV is selected for this phase of optimisation. Therefore, experiments are conducted for field voltages in the range of $13 - 17$ kV at 1 kV intervals. By examining the outcomes of these experiments, it is possible to study trends in the behaviour of the beneficiation parameters within this smaller range of field voltages. Ultimately, this analysis aims to identify an optimised configuration for the process parameters, ensuring enhanced performance and efficiency of LIED.

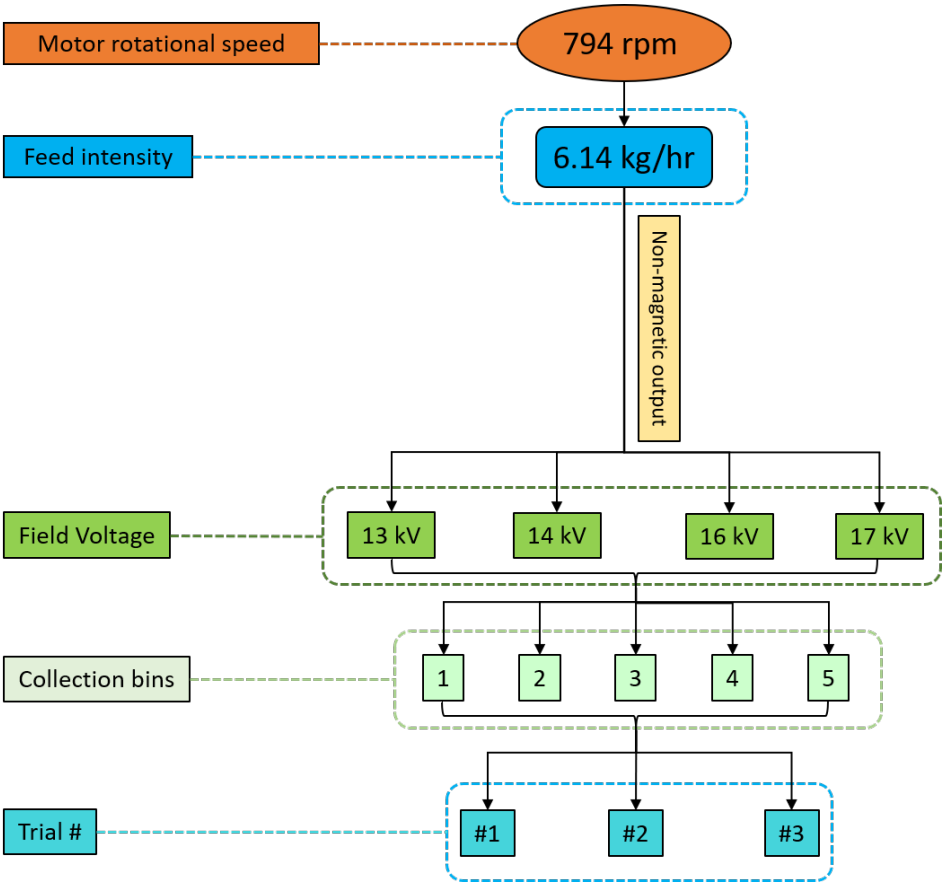

Figure 4.17: Process parameter configurations for optimisation experiments: Phase C

Figure 4.17 shows the different combinations of parameters employed for conducting the optimisation experiments during this phase. A total of twelve experiments are conducted within this phase of experiments and the produced samples are analysed with XRD. The complete list of tested samples is shown in Table A.7 and their respective experimental measurements are shown in Table A.8 of the Appendix A. These measurements are used for the quantitative analysis of beneficiation output discussed further in this section.

Results: Phase C

Distribution of ilmenite across the collection bins (Phase C)

Similar to phase B, the first step in validating effective beneficiation in this phase is to identify the collection bin that exhibits the highest concentrations of ilmenite. A quantitative analysis is performed for results obtained from phase C experiments to study the distribution of ilmenite across the collection bins as shown in Figure 4.18.

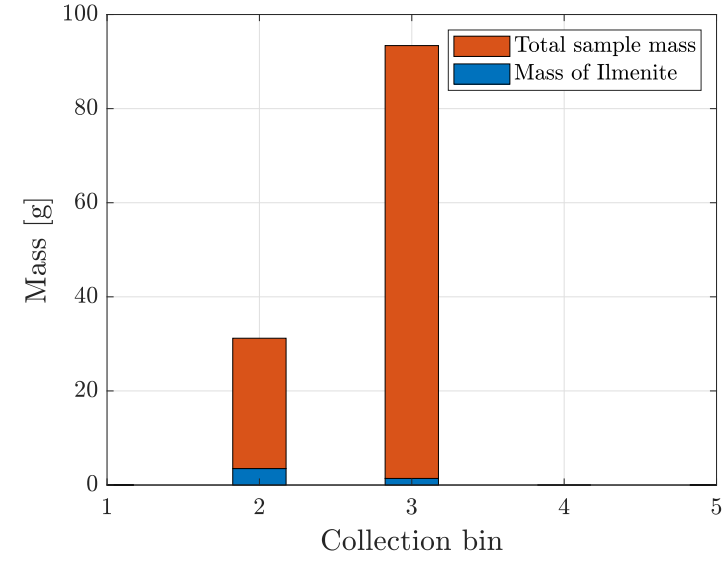

(a)

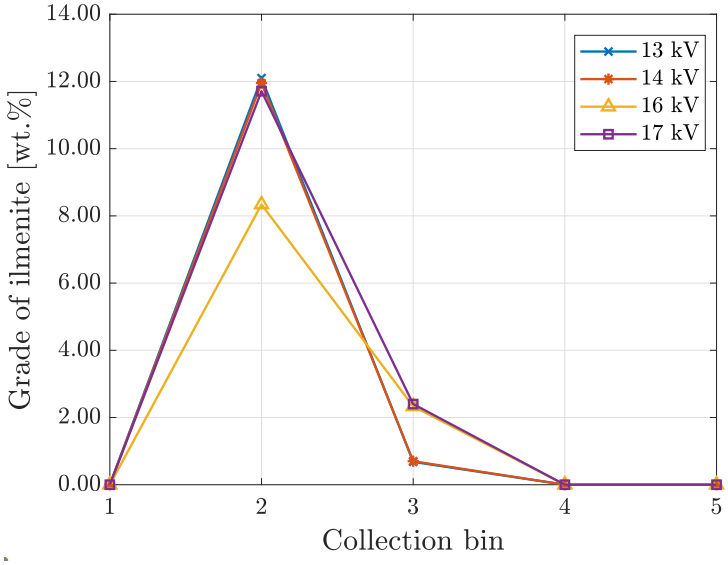

(b)

Figure 4.18: Mass distribution of samples across collection bins (Phase C) (a); Grade of ilmenite across collection bins (Phase C) (b)

The analysis of ilmenite distribution shown in Figure 4.18 concludes similar results as that of phase B. The mass distribution of ilmenite within the sample material shown in Figure 4.18a demonstrates the higher amount of ilmenite in collection bin 2. The overall less mass of the sample along with higher ilmenite content leads to a higher grade of ilmenite in the collection bin 2 as shown in Figure 4.18b. Bins 1, 4 and 5 did not collect any sample materials in this phase of experiments. Collection bin 2 has the highest average ilmenite concentration across different field voltages. It is observed again as in the previous phase that the desired higher-grade ilmenite-rich feedstock is collected in bin 2. Therefore, further analysis for quantification of the beneficiation output is performed for samples from collection bin 2. The detailed list of results for the remaining collection bins is shown in Table A.8.

Quantitative analysis of beneficiation parameters in phase C experiments

The following section presents a quantitative analysis of beneficiation parameters conducted during phase C of optimisation. The aim of this phase is to identify an optimised configuration of process parameters for the entire LIED system. The results from 15 kV field voltage experiments are also used for comparative analysis. The beneficiation parameters as a function of the field voltage are shown in Figures 4.19 to 4.22.

Yield of ilmenite in output

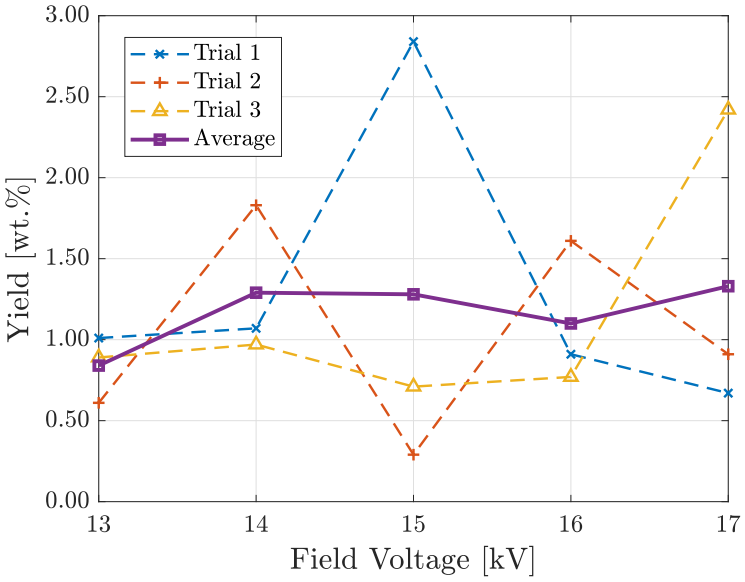

Figure 4.19: Yield of ilmenite in output from collection bin 2 (Phase C)

Recovery of ilmenite in output

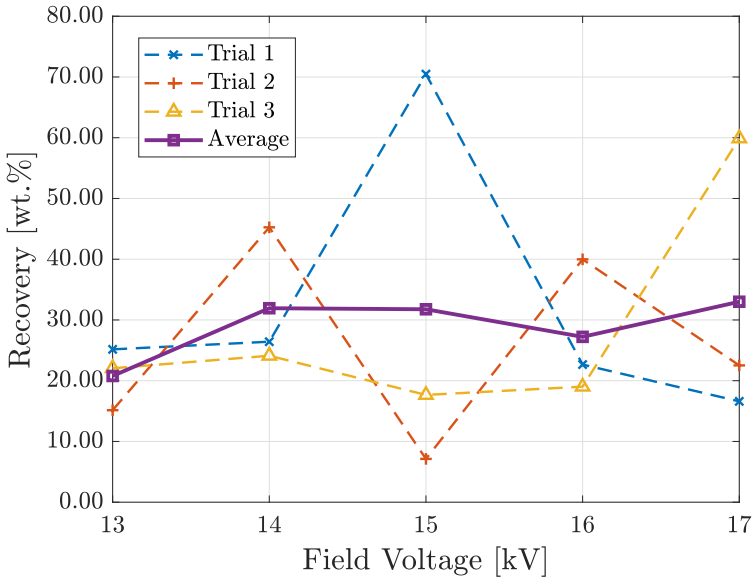

Figure 4.20: Recovery of ilmenite in output from collection bin 2 (Phase C)

Grade of ilmenite in output

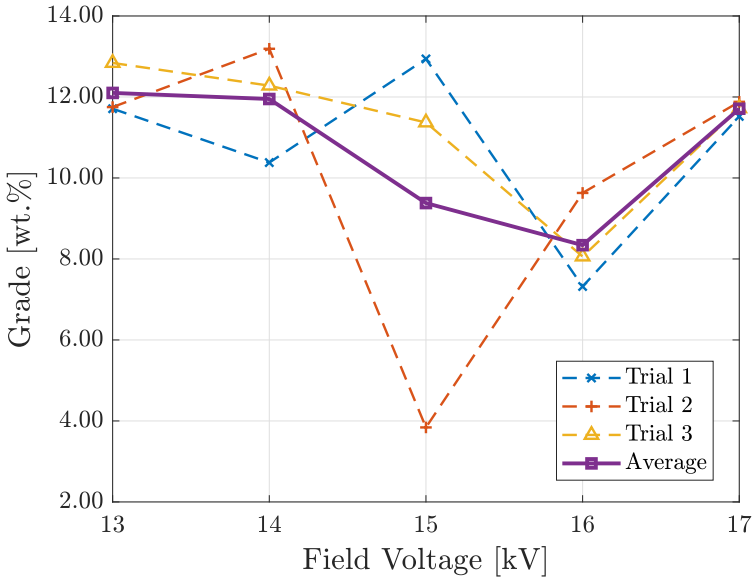

Figure 4.21: Grade of ilmenite in output from collection bin 2 (Phase C)

Enrichment ratio of ilmenite upon beneficiation

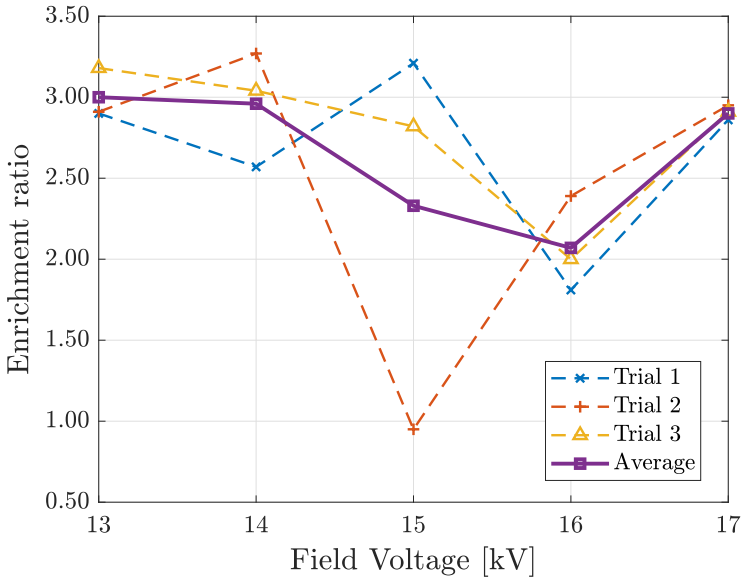

Figure 4.22: Enrichment ratio of ilmenite from collection bin 2 (Phase C)

In order to get a better overview and understanding of these results as well as to conduct an effective trade-off analysis and identify the optimal value of field voltage, the beneficiation parameters as a function of the field voltage values are shown in the form of a table in Table 4.5. At 13 kV, a high-grade ilmenite output with the highest enrichment ratio is observed. However, the yield and recovery of ilmenite are comparatively low, indicating a loss of material during the beneficiation process. In contrast, at 17 kV, the yield and recovery increase, suggesting a higher recovery of input material. However, the grade and enrichment ratio of ilmenite decrease, indicating the presence of more unwanted material in the output. However, the beneficiation output at 14 kV has higher yield and recovery of ilmenite compared to 13 kV as well as higher ilmenite-grade and enrichment ratio than at 17 kV. Therefore, the final optimised field voltage is selected as $V_f = 14$ kV from the phase C experiments. This voltage setting strikes a balance between achieving desirable ilmenite concentration while maintaining an acceptable level of yield and recovery, making it an optimal choice for the electrostatic beneficiation process.

Table 4.5: Beneficiation parameters for ilmenite as a function of the field voltage (Phase C)

Field Voltage [kV]	Yield [$wt.\%$]	Recovery [$wt.\%$]	Grade [$wt.\%$]	Enrichment ratio
13	0.84	20.78	12.10	3.00
14	1.29	31.93	11.95	2.96
15	1.28	31.76	9.38	2.33
16	1.10	27.22	8.34	2.07
17	1.33	33.00	11.71	2.90

Lowest — Highest

In summary, the parameter configuration of $f = 6.14\ kg/hr$, $\omega_m = 794\ rpm$ and $V = 14\ kV$ produces the most optimised beneficiation results from LIED as tested within the scope of these optimisation experiments. This concludes the optimisation process for the LMS-1 simulant system. The next step of optimisation is to validate these results by implementing them on the TMIA4 simulant which is achieved in the next phase of experiments.

4.3.5 Phase D: Validation of selected process parameters with a different simulant system

In this phase of optimisation, the focus shifts to validating the optimised process parameter configuration ($f = 6.14\ kg/hr$, $\omega_m = 794\ rpm$, $V = 14\ kV$) achieved in phase C using the TMIA4 simulant. The objective is to examine the impact of simulant properties on the beneficiation process. A thorough cleaning of the entire LIED system is conducted to remove any debris remaining from the previous LMS-1 experiments, thus eliminating any potential influence on the beneficiation process with the TMIA4 simulant. To ensure consistency and minimise experimental deviations, all procedures for this phase of the experiments remain unchanged from the previous phases.

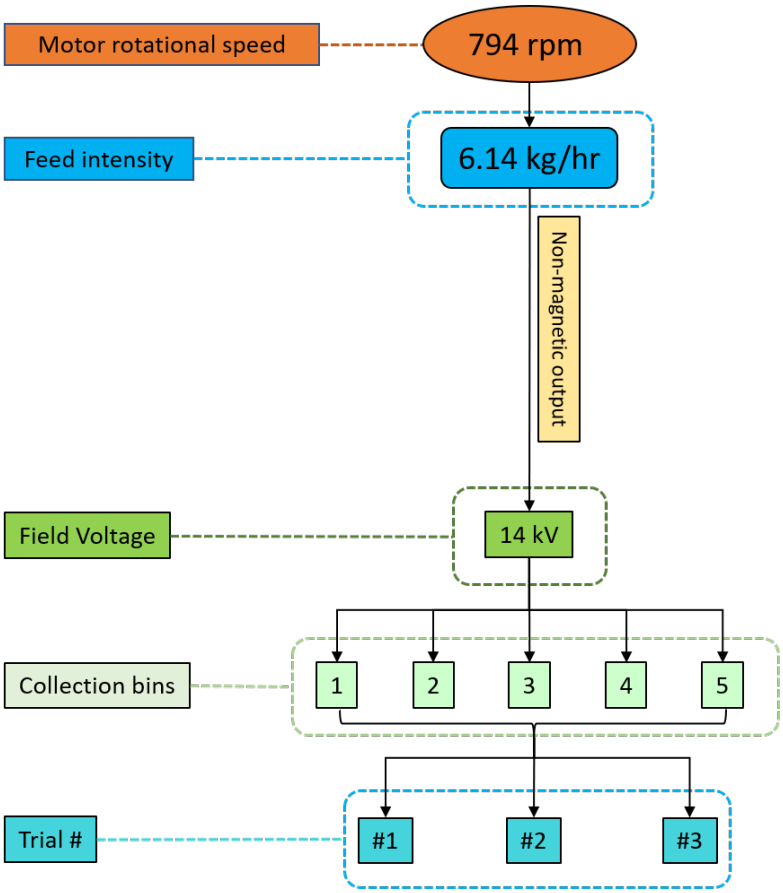

Figure 4.23: Process parameter configurations for optimisation experiments: Phase D

Figure 4.23 provides an illustration that shows the parameter configuration employed and samples produced from phase D. A total of three experiments are conducted within this phase of experiments and the produced samples are analysed with XRD. The complete list of tested samples is shown in Table A.9 and their respective experimental measurements are shown in Table A.10. These measurements are used for the quantitative analysis of beneficiation outcomes discussed further in this section.

Results: Phase D

An important observation from the TMIA4 experiments is that the sample material required a longer feeding time compared to the LMS-1 simulant. At a feed rate setting of $f = 6.14\ kg/hr$ on average the LMS-1 simulant required approximately $5\ min$ for feeding, whereas TMIA4 required nearly $10\ min$. This is observed across 3 trials with the same settings for the feed rate. Another peculiarity of the TMIA4 experiments is that the material residuals inside the sifter were visibly more. Also, the sieve got clogged up after the third trial and needed to be cleaned for any further experiments to be performed. These observations indicate definitively that the simulant properties do in fact influence the beneficiation process. A primary contributor to this variance is the higher aspect ratio of TMIA4 compared to the LMS-1. However, it is more important to understand if these discrepancies are also transferred to the beneficiation results of the experiments. The next section discusses in detail the beneficiation results from phase D experiments.

Distribution of ilmenite across the collection bins (Phase D)

The first step in validating the effects of the selected process parameters on the beneficiation results for TMIA4 is to analyse ilmenite concentrations across all collection bins and compare them with the LMS-1 experiments. This analysis can demonstrate the separation efficiency of the LIED system for TMIA4. Figure 4.24 shows the distribution of ilmenite across the collection bins for all experimental trials and their average observed at $14\ kV$ field voltage.

Similar to the findings in phase C, it is seen from Figure 4.24 that the system output is only collected in bins 2 and 3. However, as shown in fig. 4.24a, the mass of ilmenite present in bins 2 and 3 is almost equal. The higher total mass of the sample in bin 3 leads to a lower grade of ilmenite in bin 3 compared to that of bin 2 which is observed in Figure 4.24b. Nevertheless, the difference in the grade of ilmenite between bins 2 and 3 is not as large as that observed with the LMS-1 simulant. The difference in average grade of ilmenite from samples in bins 2 and 3 with the same process parameters using the LMS-1 simulant is $11.25\ wt.\%$, whereas, that with the TMIA4 simulant is only $2.90\ wt.\%$. This indicates that although the beneficiation process successfully enriches ilmenite in the TMIA4 simulant, the separation of ilmenite from the tailings is relatively less efficient compared to the LMS-1 simulant. These observations will be used to further understand the results of phase D experiments. And although collection bin 3 also has significant ilmenite content for TMIA4, to have a fair comparison with LMS-1 results, the analysis in this section is isolated to the results from collection bin 2. The measurements from the rest of the collection bins are shown in Table A.10.

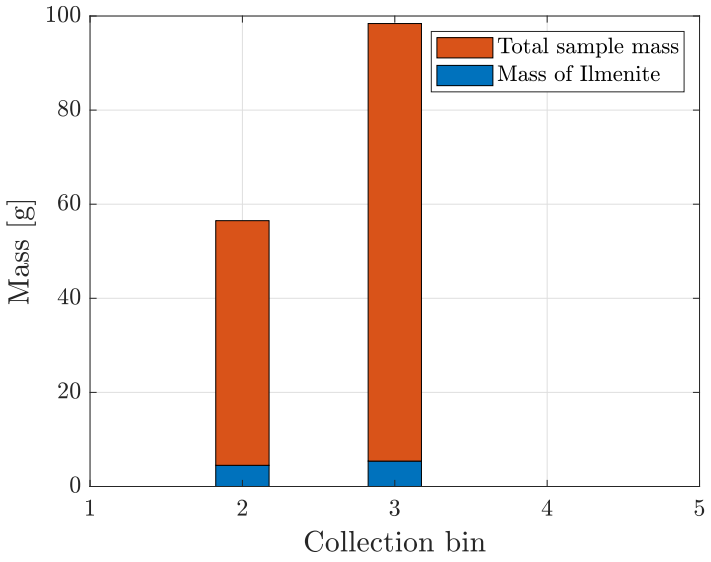

(a)

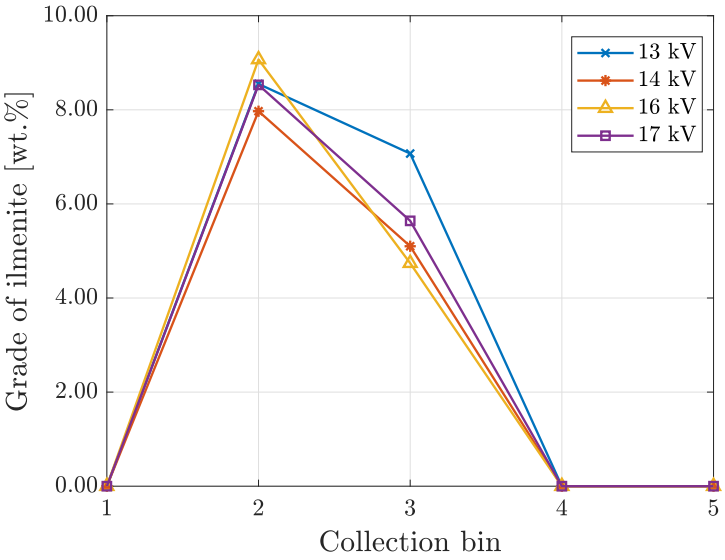

(b)

Figure 4.24: Mass distribution of samples across collection bins (Phase D) (a); Grade of ilmenite across collection bins (Phase D) (b)

Quantitative analysis of beneficiation parameters in phase C experiments

The following section presents a quantitative analysis of the beneficiation parameters conducted on the output from phase D experiments. The aim of this analysis is to test the reliability and repeatability of the optimised beneficiation results obtained in the previous experimental phases using a different simulant system. The beneficiation parameters calculated for the phase D experiments are shown in Tables 4.6 to 4.9.

1. Yield of ilmenite in output

Table 4.6: Yield of ilmenite in output from collection bin 2 (Phase D)

Field Voltage [kV]	Yield of ilmenite in output [$wt.\%$] (Phase D)			
	Trial 1	Trial 2	Trial 3	Average
14	0.36	1.83	2.29	1.49

2. Recovery of ilmenite in output

Table 4.7: Recovery of ilmenite in output from collection bin 2 (Phase D)

Field Voltage [kV]	Recovery of ilmenite in output [$wt.\%$] (Phase D)			
	Trial 1	Trial 2	Trial 3	Average
14	8.88	45.28	56.89	37.02

3. Grade of ilmenite in output

Table 4.8: Grade of ilmenite in output from collection bin 2 (Phase D)

Field Voltage [kV]	Grade of ilmenite in output [$wt.\%$] (Phase D)			
	Trial 1	Trial 2	Trial 3	Average
14	8.55	7.97	9.07	8.53

4. Enrichment ratio of ilmenite upon beneficiation

Table 4.9: Enrichment ratio of ilmenite from collection bin 2 (Phase D)

Field Voltage [kV]	Enrichment ratio of ilmenite (Phase D)			
	Trial 1	Trial 2	Trial 3	Average
14	2.12	1.98	2.25	2.11

The optimisation experiments conducted with TMIA4 revealed measurable differences in how the system responds to changes in simulant properties. This is evident from the increased feeding time at the same feed rate setting and the increase in residuals. One of the reasons for this disparity is the higher aspect ratio of TMIA4 particles compared to LMS-1. Also, the recovery of ilmenite with TMIA4 shows large deviations which are specifically observed for the trial 1 compared to trials 2 and 3. Similar disparities are seen with the yield of ilmenite in trial 1 compared to trials 2 and 3. This is attributed to the potentially higher amount of residuals for every first trial as seen with previous experiments.

However, it should be noted that only one parameter configuration was tested with TMIA4 simulant in this phase. The main objective of this phase was to assess the repeatability of beneficiation with a different simulant system, which was successfully achieved. Analysis of the data presented in Tables 4.6 to 4.9 demonstrates that the LIED system effectively produces an ilmenite-rich feedstock for the TMIA4 simulant. However, further testing of the system using TMIA4 simulant

is necessary to draw reliable conclusions regarding material residuals under different parameter configurations, changes in maintenance requirements, and other factors that may impact overall system performance. Nevertheless, a comparative study between the outcomes of TMIA4 and LMS-1 simulants is conducted and discussed further in this section.

Comparative Study: Phase C and Phase D beneficiation results

The following section presents a comparative study of the beneficiation results obtained from the phase C and phase D experiments. These phases focused on optimising the beneficiation process and evaluating the performance of the system using different simulant materials. By analysing and comparing the outcomes of these experiments, valuable insights can be gained regarding the effectiveness of the system across different simulants. The beneficiation results for ilmenite in the collection bin 2 from phase C with LMS-1 and phase D with TMIA4 obtained at $f = 6.14\ kg/hr$, $\omega_m = 794\ rpm$ and $V = 14\ kV$ are shown in Figure 4.25.

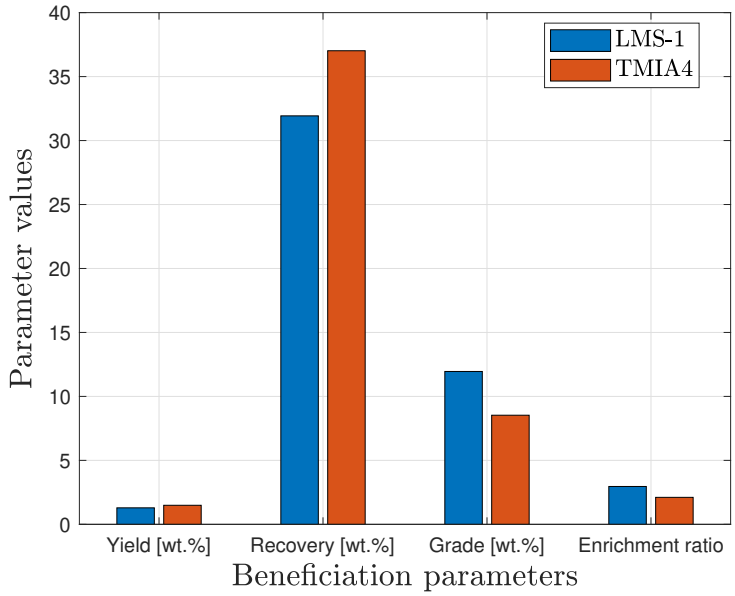

Figure 4.25: Comparison of beneficiation results with LMS-1 and TMIA4 respectively

The results obtained from the phase C and phase D experiments reveal comparable outcomes of beneficiation for the same set of process parameters. This highlights the validity, reliability, and repeatability of the beneficiation process across different simulant systems. The differences that exist between the phase C and D experiments have the potential to change depending on the experimental errors. Once the errors are accounted for, these differences might increase or even disappear, but within the available scope of data, it can be concluded that the optimised parameter configuration can also produce similar beneficiation results with TMIA4 as it does with LMS-1.

However, there are notable differences observed in the degree to which ilmenite can be separated from the tailings, as evidenced by the analysis of ilmenite distribution across the collection bins in both phases. Additionally, the increased feeding time required for the TMIA4 simulant should be taken into consideration for further optimisation efforts. In conclusion, while the behaviour of the LIED system may vary with different simulants, the beneficiation of the simulant can still be achieved to a similar extent.

Analysis of residuals across experimental phases

In this section, a comprehensive analysis of residuals across different experimental phases is conducted. Residuals, which refer to the remaining material in the system after beneficiation, play a critical role in assessing the overall system efficiency. The findings from this analysis contribute to optimising the system and help in improving the overall material recovery of LIED.

A quantitative investigation is undertaken to analyse the distribution of residual material quantities across the experimental trials. The mass measurements for all collected material at different outlets are known for all experiments. The residuals are calculated as the difference between the total sample material at the inlet (300 g) and the total material collected in the outlets and expressed as a percentage of the total input sample weight. This calculation is performed for every experimental trial. The tribocharger has the highest frequency of cleaning which is after every three experiments to avoid contamination of results from different parameter configurations. Hence, in order to investigate the influence of continuous experiments on residuals, the fluctuations in residual quantities are monitored for each parameter configuration throughout the experimental trials in all phases of optimisation. The collected data is presented in Figure 4.25, revealing a constant trend.

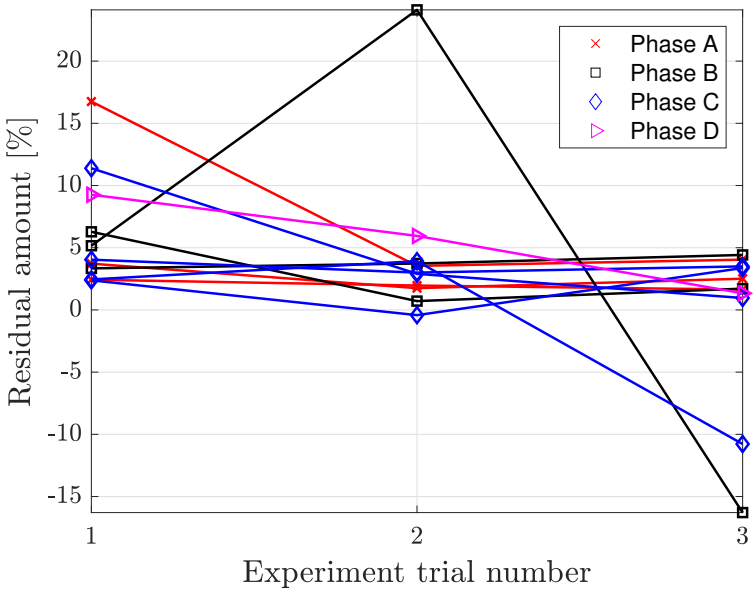

Figure 4.26: Material residuals across experimental phases

Notably, the first trial consistently exhibits a higher average residual amount, which gradually decreases and reaches a minimum by the third trial for all experiments. The negative residuals indicate the presence of excess residual materials from previous experiments that remain in the system. These errors can result in inaccuracies in measurements for the respective experiments. These findings are of significant importance, as they impact the accuracy of the analyses conducted for quantification of the beneficiation results and warrant consideration for future optimisation efforts.

Energy consumption of LIED across experimental phases

As the beneficiation system is developed with future aspirations of deploying it in space missions, energy consumption is a key point to consider. The energy produced in space comes at a very high cost and therefore, every system designed for space should be studied and developed with the highest possible energy efficiency. Also, space missions can last for extended periods, ranging from months to years. Efficient energy consumption is vital to ensure the longevity of the mission by conserving energy resources and preventing premature depletion. This contributes to the overall sustainability of the system deployed.

This section provides a comprehensive analysis of the energy consumption of LIED and its correlation with varying process parameters across the different experimental phases. The goal of this analysis is to evaluate and compare the energy requirements of the beneficiation process at different phases of optimisation. By examining the energy consumption across different phases, valuable insights can be gained regarding the potential for energy savings and process optimisation. The detailed energy calculations are shown in Table A.11 of the Appendix A. The total energy consumption of LIED as a function of different process parameters is shown in Figure 4.27.

The results obtained from the phase A experiments demonstrate a notable decrease in the energy consumption of the LIED system with an increase in feed rate as shown in Figure 4.27a. This reduction can be attributed to the decreased feeding times, leading to reduced utilisation of the vibratory feeder. However, in phases B and C which are involved in the optimisation of the electrostatic beneficiation process, as illustrated in Figures 4.27b and 4.27c, do not exhibit a significant impact on the overall energy consumption with varying field voltages. Even with increased feeding time for the phase D experiments, the energy consumption is $61\ Watt - hr$ which is similar to that of the phase C experiments. Consequently, it can be inferred that upon successful optimisation and selection of a fixed parameter configuration, the energy consumption of the LIED system remains nearly constant throughout the beneficiation trials. Also, the maximum possible energy consumption of LIED with the optimised parameter configuration comes out to $61\ Watt - hr$ which is equivalent to a normal light bulb used for household purposes. This finding is crucial as it alleviates the need for extensive high-energy storage and supply systems in deploying such beneficiation systems in space.

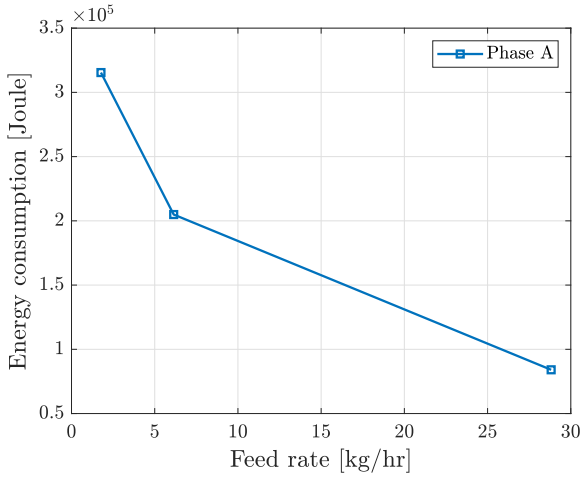

(a)

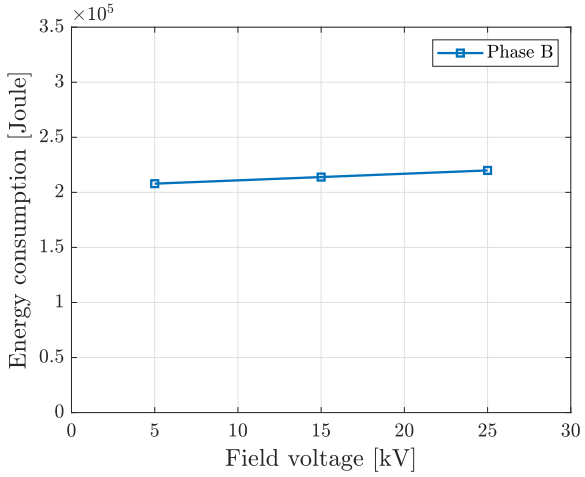

(b)

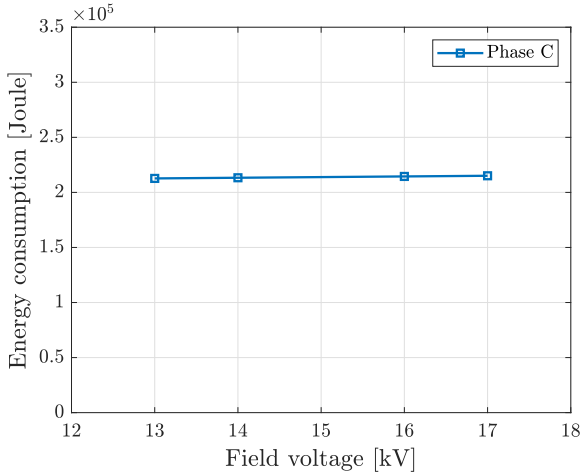

(c)

Figure 4.27: Energy consumption in phase A experiments (a); Energy consumption in phase B experiments (b); Energy consumption in phase C experiments (c)

Discrepancy Analysis: Expected vs. Actual experimental results

Discrepancy analysis is a critical component of experimental research, aimed at evaluating the disparities between expected and actual results. This section delves into the examination of such discrepancies in the beneficiation outcomes from LIED, exploring potential factors that may have influenced the observed variations. Figure 4.28 shows the expected and actual results obtained from the experimental analysis of LIED. The detailed list of results is shown in Table A.12 of the Appendix A. The results for LMS-1 and TMIA4 simulants are listed individually to demonstrate any simulant-specific deviations.

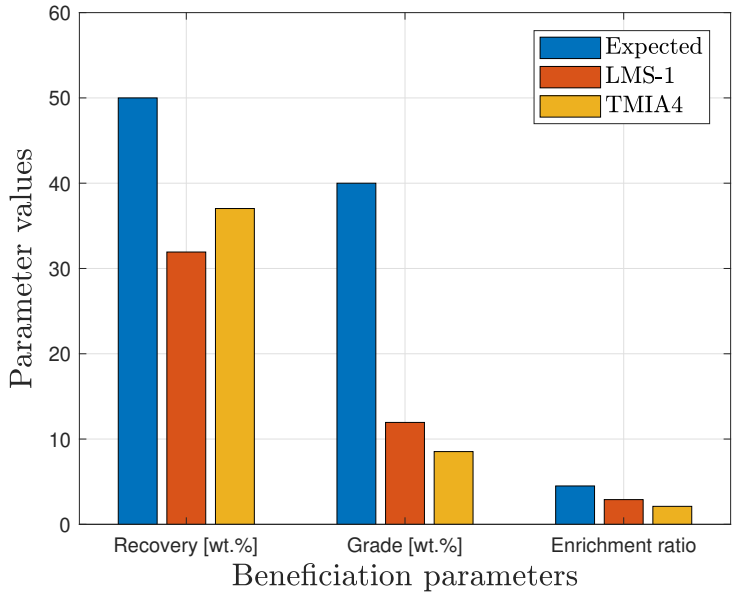

Figure 4.28: Discrepancy analysis: Expected vs. Actual experimental results

The recovery of ilmenite in the output is lower than the design expectations which indicates a higher loss of ilmenite in the beneficiation process. There are multiple explanations for this discrepancy. The results illustrated for LMS-1 and TMIA4 in Figure 4.28 are only from the output in collection bin 2. However, as seen earlier from the distribution of ilmenite across the collection bins, it is clear that some of the ilmenite is deposited in collection bins 3 or 4 which might have the remaining ilmenite. Another possibility for the loss of ilmenite is the loss in the magnetic separator. The rotational speed of the separator could not be increased beyond the minimum required limit. Therefore, it can be assumed that further optimisation with an updated design for the magnetic separator might help in reducing the loss of ilmenite at this stage.

It can also be seen that a lower grade of ilmenite is produced from LIED compared to the expected outcomes. The lower grade of ilmenite and therefore lower enrichment ratios produced in the feedstock during experiments can be a cumulative effect of many factors. One of the possible factors is the need for higher field voltages for the effective separation of ilmenite from the tailings. Another reason might be the inadequacy of the tribocharger to effectively charge all simulant particles with the high amounts of residuals from previous experiments still present within. Overall, there are many indirect parameters that can have an influence on the beneficiation results and these need to be studied for further optimisation of LIED. However, these are not the final results for LIED as there is a potential for further optimisation and they provide encouraging validation for the fundamental principles behind the system design. This discrepancy analysis is the beginning of further optimisation of LIED to achieve the expected goals of

beneficiation.

Therefore, the optimisation experiments have successfully validated the capability of LIED to produce an ilmenite-rich feedstock through the beneficiation of lunar regolith simulant. This marks the completion of the experimental analysis and optimisation of LIED within the defined scope of this thesis. The next chapter delves into the conclusions derived from this analysis and provides important insights into potential avenues for further optimisation of the beneficiation processes.

Chapter 5

Conclusion and Outlook

The experimental analysis of the Lunar Ilmenite Enrichment Demonstrator (LIED), specifically designed for the beneficiation of lunar regolith, has yielded promising results. The series of optimisation experiments conducted within the defined scope of this study have successfully identified an optimal parameter configuration for the production of an ilmenite-rich feedstock. This achievement highlights the significant progress made in developing a robust and efficient system for extracting valuable resources from the lunar regolith. Furthermore, the optimisation experiments have provided valuable insights into the operational design of LIED and have also highlighted certain limitations of the system. The successful testing of LIED has allowed for a comprehensive analysis of the system output, laying the foundation for future enhancements and advancements in the beneficiation process. These findings contribute to the ongoing efforts in refining and optimising the process of lunar regolith beneficiation for improved performance and efficiency.

It is evident from the experimental analysis that the improvement in beneficiation parameters of the produced feedstock takes place gradually with every optimisation phase. The grade of ilmenite in the output went from 3.63 *wt.%* in phase A to 9.00 *wt.%* in phase B and 12.00 *wt.%* in phase C. A similar increase of enrichment ratio from 0.71 in phase A, to 2.33 in phase B and 2.96 in phase C is observed. This demonstrates the effectiveness of the developed optimisation strategy in improving the overall beneficiation performance of LIED. The final results show that up to 32 % of the total ilmenite from the input regolith simulant is recovered in the produced feedstock with the optimised parameter configuration. The total time for processing 300 *g* of simulant is about 30 *min* resulting in an average energy consumption of about 61 *Wh*.

These results, while promising, exhibit variations when compared to the expected outcomes for the beneficiation process. The discrepancy analysis shown in section 4.3.5 demonstrates a significant deviation of the experimental outcomes from the target values for both the simulants. Specifically, the grade of ilmenite achieved with LMS-1 is only 30 % of the target value and TMIA4 exhibits an even lower grade, achieving only 21 % of the target value. A similar behaviour is observed in the enrichment ratio, with LMS-1 achieving an output equivalent to about 65 % of the target value, while TMIA4 falls short at approximately 47 % of the target value. This trend is however reversed when considering the ilmenite recovery, as LMS-1 achieves roughly 64 % of the target value, whereas TMIA4 performs comparatively better, reaching nearly 75 % of the target value. These findings underline the effectiveness of the beneficiation process for both simulants while emphasising the nuanced differences in their responses to the different processes. The experimental results suggest that while substantial progress has been made in the optimisation of the beneficiation process, there is room for improvement to reduce the discrepancy between

the expected and achieved results.

There are several factors contributing to these disparities. One such factor is the difference between the implemented experimental procedures and the originally planned strategies. Adjustments had to be made to the experiment procedures due to the experimental challenges as well as limitations in the system design. A key limitation was the insufficient torque from the motor used for the magnetic separator. As a result, the rotational speed of the magnetic separator could not be changed and thus, the optimisation of the magnetic beneficiation was incomplete. Another challenge encountered during the experiments was the presence of excessive residuals within the sieve, which required additional steps for their removal during the experiments, impacting the experiment duration and overall energy consumption of the system. The tribocharger assembly also exhibited high residuals throughout the experiments. Although these were assumed to remain constant for every experiment and the assembly was cleaned for every new parameter configuration, the deviations in weights of obtained samples suggest otherwise.

In addition to the experimental obstacles, a further challenge emerged during the phase analysis of initial experimental samples, wherein the presence of ilmenite content could not be detected. Upon further analysis of the available ilmenite Cr50 samples used in TMIA4, it was discovered that the ilmenite is a multi-phase mixture and each individual phase of ilmenite needs to be analysed separately. The assumption of identical phase compositions between ilmenite Cr50 and ilmenite within LMS-1 was made due to the unavailability of the ilmenite used in LMS-1 for analysis. However, it is important to acknowledge that the phase composition can vary depending on their respective sources, consequently affecting the XRD measurements for all experiments. Conducting a comprehensive phase analysis of the ilmenite used in LMS-1 and incorporating it into the analysis of LMS-1 experiment samples would help mitigate this error.

In order to improve the experimental results and achieve the desired beneficiation goals, future optimisation efforts should focus on more experimental analysis as well as design changes to LIED. Previous research has shown that multiple pass experiments improve the efficiency and effectiveness of regolith beneficiation which should be used as a starting point for further optimisation with the existing configuration [62]. The output samples from the collection bins should be passed through the entire system again and the samples from each pass should be separately analysed. The beneficiation results should change gradually with each pass showing signs of improvement. This analysis aims to achieve a saturation point for beneficiation parameters beyond which any further passes would show little or no improvement in the beneficiation results. This can help to improve the overall efficiency and performance of LIED.

A major portion of the further optimisation experiments should focus on electrostatic beneficiation as it has the highest sensitivity to experimental deviations and changes in process parameters. Previous research has demonstrated that an optimised tribocharger has a significant influence on the beneficiation outcomes for electrostatic plate separation [87]. Hence, in order to validate and enhance the design of the tribocharger, it is necessary to conduct experiments with and without the tribocharger. Their comparative analysis will quantify the variations in beneficiation outcomes and offer valuable insights for refining the tribocharger design. The next important parameter of electrostatic beneficiation is the field voltage applied across the electrostatic plate separator. The final optimisation experiments concluded $14\ kV$ to be the most optimal value for producing desirable beneficiation outcomes. However, previous research claims better beneficiation performance at higher field voltages [14]. This claim must be validated by testing the remaining range of available field voltages between $17 - 25\ kV$. Also, the process of electrostatic separation is not directly affected by the field voltage but by the effective electrostatic field strength which depends on the field voltage as well as the distance between the electrodes [14]. In the case of LIED, the plate separation distance will influence the electrostatic field intensity

for the given field voltage. This should be tested by conducting experiments for different plate separation distances at the same field voltage to study its influence on the beneficiation output. With higher field intensity, potentially better beneficiation results can be achieved at the same field voltage. This can help to further improve the electrostatic beneficiation process. It is clear from these discussions that multiple avenues remain to be explored in the experimental optimisation of LIED with the available configuration of components which can help in decreasing the existing disparity in results.

In addition to the improvements in the experimental process, certain limitations and challenges in the optimisation process can be attributed to the inherent design of LIED. These design constraints are a limiting factor for further improvement of the beneficiation results. The most evident design limitations for the optimisation of LIED are observed with the magnetic beneficiation stage. The rectangular funnel at the inlet of the magnetic separator lacks sufficient slope, resulting in a high amount of residuals in each experiment. Additionally, the motor power cables use crocodile clamps for connection, which impede access to the sifter attachments and get easily disconnected during the removal of sifter residuals. They should therefore be replaced with a more durable and reliable solution. To resolve the problem of insufficient torque from the selected motor of the magnetic separator, an updated configuration capable of providing higher torques should be implemented along with appropriate modifications to the existing assembly to effectively accommodate this change. In conclusion, a comprehensive study and enhancement of the magnetic separator's design are necessary to facilitate its optimisation in future beneficiation experiments.

Another drawback of LIED is the lack of mechanical attachments for some of the components in order to fix their positions. The vibratory feeder, for instance, is simply placed on the mounting platform, requiring frequent adjustments to align the output rail with the sieve output for each experiment. This lack of mechanical attachment leads to instability at higher feeder intensities and imposes limitations on usable feed rates. Similarly, the magnetic separator and other components such as the tribocharger, plate separator, and collection bins are not securely fixed in their positions. It is recommended to employ mechanical supports and attachments to secure all components in place, mitigating experimental deviations and preventing damage to adjoining components.

Furthermore, the feedstock produced by LIED will be the input raw material for an oxygen extraction plant. In order to be able to produce enough feedstock to support the continuous operation of a full scale oxygen production plant, tonnes of regolith needs to be processed every hour [11]. The current design of LIED can process a $300\ g$ sample in about $30\ min$. While increasing the sample size will help in processing more regolith in the same time, it is nowhere near the expected mass flow rates. The scalability of the current design is also quite limited due to the selected component configurations and therefore, future designs should take this into consideration and develop systems that can accommodate these demands.

The motivation behind the development and optimisation of LIED stemmed from the existing knowledge gaps in beneficiation technologies and the necessity to conduct research in this field due to its significant potential for enhancing oxygen extraction plant efficiencies. These knowledge gaps were identified through the ISRU Gap Assessment Report 2021, which highlighted the need for demonstrating mineral beneficiation along with the analysis of energy consumption, assessing the possible degree of separation, and drawing conclusions regarding system reliability and durability [5]. In the case of LIED, the degree of separation of ilmenite is evident from the analysis of ilmenite distribution across the collection bins. The comprehensive analysis of energy expenditure performed for LIED not only demonstrates its efficiency but also provides insights into the infrastructure necessary to support such systems in space. The optimisation

experiments shed light on maintenance and cleaning requirements for different stages as well as create opportunity to study the system reliability and durability across multiple experiments. Through these findings, the optimisation of LIED has generated valuable results that contribute to the advancement of knowledge in regolith beneficiation, while also outlining avenues for future research and development.

While the focus of LIED lies in the enrichment of ilmenite, its underlying principles can be extended to the beneficiation of other minerals in the lunar regolith. The XRD analysis of experiment samples plays a crucial role in identifying all the phases present in each output sample, enabling a study of how various minerals can be collected at different stages of the LIED process. This valuable information opens avenues for exploring the potential utilisation of the remaining outputs, such as the magnetic output or the coarse output, for other purposes such as in-situ construction activities or the extraction of metals and other minerals. Moreover, this knowledge also provides insights into the behavior of different mineral phases present within the regolith simulant during the beneficiation processes, laying the groundwork for the development of future beneficiation systems for other minerals.

In summary, this work has successfully explored and optimised the Lunar Ilmenite Enrichment Demonstrator (LIED) for the beneficiation of lunar regolith simulants. Through a systematic approach, the process parameters of the system have been investigated and refined to achieve improved beneficiation outcomes. The experimental results have demonstrated the effectiveness of LIED in producing ilmenite-rich feedstock, with significant advancements observed in the grade, recovery, and enrichment ratio of ilmenite. The comparative analysis of different simulant systems has highlighted the adaptability and repeatability of the LIED process. Furthermore, the evaluation of energy consumption has provided valuable insights into the feasibility and sustainability of implementing the LIED system for space applications. Overall, the author is hopeful that this research has contributed to the understanding and optimisation of the beneficiation processes in LIED, while also outlining avenues for future research and potential applications in the field of space exploration and resource utilisation.

Bibliography

[1] Annette Froehlich. *Space resource utilization: A view from an emerging space faring nation, Annette Froehlich, editor*. Vol. volume 12. Studies in space policy. Cham, Switzerland: Springer, 2018. ISBN: 978-3-319-66968-7.

[2] Cmwarner. *Artemis Base Camp – artemis*. Oct. 2020. URL: https://blogs.nasa.gov/artemis/tag/artemis-base-camp/.

[3] NASA. *NASA Artemis*. URL: https://www.nasa.gov/specials/artemis/.

[4] Christie Bertels. "Crew Maintenance Lessons Learned from ISS and Considerations for Future Manned Missions". In: *SpaceOps 2006 Conference*. Reston, Virigina: American Institute of Aeronautics and Astronautics, 2006. ISBN: 978-1-62410-051-2. DOI: 10.2514/6.2006-5952.

[5] TWG ISRU GAP. "In-Situ Resource Utilization Gap Assessment Report". In: (2021).

[6] H.M. Sargeant et al. "Hydrogen reduction of ilmenite: Towards an in situ resource utilization demonstration on the surface of the Moon". In: *Planetary and Space Science* 180 (2020), p. 104751. ISSN: 0032-0633. DOI: https://doi.org/10.1016/j.pss.2019.104751. URL: https://www.sciencedirect.com/science/article/pii/S0032063319301813.

[7] G. H. Heiken, D. T. Vaniman, and B. M. French. "Lunar sourcebook : a user's guide to the Moon". In: (1991).

[8] Lunar Sample Preliminary Examination Team. "Preliminary Examination of Lunar Samples from Apollo 11". In: *Science (New York, N.Y.)* 165.3899 (1969), pp. 1211–1227. ISSN: 0036-8075. DOI: 10.1126/science.165.3899.1211.

[9] Lukas Schlüter and Aidan Cowley. "Review of techniques for In-Situ oxygen extraction on the moon". In: *Planetary and Space Science* 181 (2020), p. 104753. ISSN: 00320633. DOI: 10.1016/j.pss.2019.104753.

[10] Lawrence A. Taylor and W. David Carrier. "Production of Oxygen on the Moon: Which Processes Are Best and Why". In: *AIAA Journal* 30.12 (1992), pp. 2858–2863. ISSN: 0001-1452. DOI: 10.2514/3.48974.

[11] J. A. Colozza. "Small Lunar Base Camp and In Situ Resource Utilization Oxygen Production Facility Power System Comparison". In: (2020).

[12] J. J. Cilliers, J. N. Rasera, and K. Hadler. "Estimating the scale of space resource utilisation (SRU) operations to satisfy lunar oxygen demand". In: ().

[13] J. N. Rasera et al. "The beneficiation of lunar regolith for space resource utilisation: A review". In: *Planetary and Space Science* 186 (2020), p. 104879. ISSN: 00320633. DOI: 10.1016/j.pss.2020.104879.

[14] Michel Franke. "Development of a Testbed for the Beneficiation of Lunar Regolith". In: (2022).

[15] Shuanggen Jin, Sundaram Arivazhagan, and Hiroshi Araki. "New results and questions of lunar exploration from SELENE, Chang'E-1, Chandrayaan-1 and LRO/LCROSS". In: *Advances in Space Research* 52.2 (2013), pp. 285–305. ISSN: 02731177. DOI: 10.1016/j.asr.2012.11.022.

[16] R. S. Taylor. "Lunar Science: A Post-Apollo View". In: (1975).

[17] Venkatesan Sundararajan. "International Missions to the Moon: Space Exploration Goals, Programs and Economics". In: *Space 2006*. Reston, Virigina: American Institute of Aeronautics and Astronautics, 2006. ISBN: 978-1-62410-049-9. DOI: 10.2514/6.2006-7507.

[18] Anthony Colaprete et al. "An Overview of the Lunar Crater Observation and Sensing Satellite (LCROSS)". In: *Space Science Reviews* 167.1-4 (2012), pp. 3–22. ISSN: 0038-6308. DOI: 10.1007/s11214-012-9880-6.

[19] B. H. Foing et al. "SMART-1 mission to the Moon: Status, first results and goals". In: (2005).

[20] ZiYuan Ouyang et al. "Primary scientific results of Chang'E-1 lunar mission". In: *Science China Earth Sciences* 53.11 (2010), pp. 1565–1581. ISSN: 1674-7313. DOI: 10.1007/s11430-010-4056-2.

[21] Peter H. Schultz et al. "The LCROSS cratering experiment". In: *Science (New York, N.Y.)* 330.6003 (2010), pp. 468–472. ISSN: 0036-8075. DOI: 10.1126/science.1187454.

[22] J. A. Maxwell, L. C. Peck, and H. B. Wiik. "Chermical composition of APollo 11 lunar samples 10017, 10020, 10072 and 10084". In: ().

[23] G. V. Latham et al. "Passive seismic experiment". In: *Science (New York, N.Y.)* 167.3918 (1970), pp. 455–457. ISSN: 0036-8075. DOI: 10.1126/science.167.3918.455.

[24] Marshall Smith et al. "The Artemis Program: An Overview of NASA's Activities to Return Humans to the Moon". In: *2020 IEEE Aerospace Conference*. IEEE, 2020, pp. 1–10. ISBN: 978-1-7281-2734-7. DOI: 10.1109/AERO47225.2020.9172323.

[25] A. E. Ringwood. "The Earth-Moon Connection". In: (1989).

[26] G. Neukum, B. König, and J. Arkani-hamed. "A study of lunar impact crater size-distributions". In: (1974).

[27] Stephan Ulamec, Jens Biele, and Ed Trollope. "How to survive a Lunar night". In: ().

[28] P. Gläser et al. "Illumination conditions at the lunar south pole using high resolution Digital Terrain Models from LOLA". In: *Icarus* 243 (2014), pp. 78–90. ISSN: 00191035. DOI: 10.1016/j.icarus.2014.08.013.

[29] M. G. Jr. Langseth, S. J. Keihm, and J. L. Jr. Chute. "Heat-flow experiment. In Apollo 15 Preliminiry Science Report". In: NASA SP-330, 1973, 9-1 to 9–24.

[30] M. G. Jr. Langseth and S. J. Keihm. "In-situ measurements of lunar heat flow. In Soviet-American Conference on Geochemistry of the Moon and Planets". In: NASA SP-370, 1977, pp. 283–293.

[31] Yulia Akisheva and Yves Gourinat. "Utilisation of Moon Regolith for Radiation Protection and Thermal Insulation in Permanent Lunar Habitats". In: *Applied Sciences* 11.9 (2021), p. 3853. DOI: 10.3390/app11093853.

[32] Guenther Reitz, Thomas Berger, and Daniel Matthiae. "Radiation exposure in the moon environment". In: *Planetary and Space Science* 74.1 (2012), pp. 78–83. ISSN: 00320633. DOI: 10.1016/j.pss.2012.07.014.

[33] Alan L. Bean, Jr. Conrad Charles, and Richard F. Gordon. "Crew Observations". In: *NASA Special Publication*. Vol. 235. 1970, p. 29.

[34] Lawrence Taylor et al. “Lunar Dust Problem: From Liability to Asset”. In: *1st Space Exploration Conference: Continuing the Voyage of Discovery*. Reston, Virigina: American Institute of Aeronautics and Astronautics, 2005. ISBN: 978-1-62410-022-2. DOI: 10.2514/6.2005-2510.

[35] R L Bates and J A Jackson. “Glossary of geology”. In: (Jan. 1980). URL: https://www.osti.gov/biblio/5128638.

[36] Wayne J. Peeples et al. “Orbital radar evidence for lunar subsurface layering in Maria Serenitatis and Crisium”. In: *Journal of Geophysical Research* 83 (1978), pp. 3459–3468.

[37] J. J. Papike, S. B. Simon, and J. C. Laul. “The lunar regolith: Chemistry, mineralogy, and petrology”. In: *Reviews of Geophysics* 20.4 (1982), p. 761. ISSN: 8755-1209. DOI: 10.1029/RG020i004p00761.

[38] S.M. Gandhi and B.C. Sarkar. “Chapter 13 - Mineral Resources Classification”. In: *Essentials of Mineral Exploration and Evaluation*. Ed. by S.M. Gandhi and B.C. Sarkar. Elsevier, 2016, pp. 309–320. ISBN: 978-0-12-805329-4. DOI: https://doi.org/10.1016/B978-0-12-805329-4.00020-X. URL: https://www.sciencedirect.com/science/article/pii/B978012805329400020X.

[39] Alex Ellery. “Sustainable in-situ resource utilization on the moon”. In: *Planetary and Space Science* 184 (2020), p. 104870. ISSN: 00320633. DOI: 10.1016/j.pss.2020.104870.

[40] Alex Ellery. “Supplementing Closed Ecological Life Support Systems with In-Situ Resources on the Moon”. In: *Life (Basel, Switzerland)* 11.8 (2021). ISSN: 2075-1729. DOI: 10.3390/life11080770.

[41] W. H. Steurer. “Extraterrestrial Materials Processin”. In: (1982).

[42] B. D. Rao et al. *Extraction Processes for the Production of ALuminium, Titanium, Iron, Magnesium and Oxygen from Nonterrestrial Sources*. 1979. URL: https://books.google.de/books?id=JZQ9AQAAMAAJ&ots=woqC4ih3v1&dq=williams%20and%20erstfeld%201979&lr&pg=PA257#v=onepage&q=williams%20and%20erstfeld%201979&f=false.

[43] Gibson M. A. and Knudsen C. W. “Lunar Oxygen production from Ilmenite”. In: *Lunar bases and Space Activities of the 21st Century* (1985), pp. 543–550. URL: https://adsabs.harvard.edu/full/1985lbsa.conf..543G.

[44] G. G. Kersterke. *Electrowinning of Oxygen from Silicate Rocks*. 1971.

[45] William N. Agosto. “Electrostatic Separation and Sizing of Ilmenite in Lunar Soil Simulants and Samples”. In: 1984.

[46] Hobart M. King. *Ilmenite*. URL: https://geology.com/minerals/ilmenite.shtml.

[47] Campbell H. W., Hess P. C., and Rutherford M. J. “Ilmenite crystallization in non-mare basalts”. In: *Lunar and Planetary Science* IX (1978), pp. 149–151.

[48] Marc D. Norman and Graham Ryder. “Geochemical constraints on the igneous evolution of the lunar crust”. In: 1980.

[49] Rutherford M. J., Dixon S., and Hess P. “Ilmenite saturation at high pressure in KREEP basalts: Origin of KREEP and Hi-TiO2 in mare basalts”. In: *Lunar and Planetary Science* XI (1980), pp. 966–967.

[50] G. H. Heiken and D. T. Vaniman. “Characterization of lunar ilmenite resources”. In: (1990).

[51] Theodore E. Bunch et al. “Mining and beneficiation of lunar ores”. In: 1979.

[52] T. E. Erstfield and R. J. P. Williams. “High temperature electrolytic recovery of oxygen from gaseous effluents from the carbo-chlorination of lunar anorthite and the hydrogenation of ilmenite: A theoretical study”. In: 1979.

[53] Hossein Akbari et al. “A Beneficiation Study on a Low Grade Iron Ore by Gravity and Magnetic Separation”. In: *Russian Journal of Non-Ferrous Metals* 59.4 (2018), pp. 353–363. ISSN: 1067-8212. DOI: 10.3103/S1067821218040028.

[54] Mark Ma. “Froth Flotation of Iron Ores”. In: *International Journal of Mining Engineering and Mineral Processing* 1.2 (2012), pp. 56–61. ISSN: 2166-997X. DOI: 10.5923/j.mining.20120102.06.

[55] J. Svoboda and T. Fujita. “Recent developments in magnetic methods of material separation”. In: *Minerals Engineering* 16.9 (2003), pp. 785–792. ISSN: 08926875. DOI: 10.1016/S0892-6875(03)00212-7.

[56] R. R. Oder. “Beneficiation of lunar soils: Case studies in magnetics”. In: *Mining, Metallurgy & Exploration* 9.3 (1992), pp. 119–130. ISSN: 2524-3462. DOI: 10.1007/BF03402983.

[57] W. N. Agosto. “Beneficiation and powder metallurgical processing of lunar soil”. In: *4th Space manufacturing; Proceedings of the Fifth Conference*. Reston, Virigina: American Institute of Aeronautics and Astronautics, 1981. DOI: 10.2514/6.1981-3263.

[58] R. R. Oder. “Magnetic separation of lunar soils”. In: *IEEE Transactions on Magnetics* 27.6 (1991), pp. 5367–5370. ISSN: 0018-9464. DOI: 10.1109/20.278841.

[59] Berggren et al. “Lunar Soil Particle Separator”. In: *49th AIAA Aerospace Sciences Meeting including the New Horizons Forum and Aerospace Exposition*. Reston, Virigina: American Institute of Aeronautics and Astronautics, 2011. ISBN: 978-1-60086-950-1. DOI: 10.2514/6.2011-436.

[60] F. Fraas. “Electrostatic separation of granular materials”. In: *Bureau of Mines* (1962).

[61] W. N. Agosto. “Electrostatic Separation and sizing of Ilmenite in Lunar soil simulants and samples”. In: *Lunar and Planetary Institute* (1984).

[62] W. N. Agosto. “Electrostatic Concentration of Lunar minerals”. In: *Lunar and Planetary Institute* (1985).

[63] D. Carter. “Electrostatic Separation of Lunar Regolith for Size Beneficiation using Same-Material Tribocharging”. In: *NASA* (2015). URL: https://www.nasa.gov/feature/electrostatic-separation-of-lunar-regolith-for-size-beneficiation-using-same-material/.

[64] L. Dascalescu et al. “Electrostatic Separation Processes”. In: *IEEE Industry Applications Magazine* 10.6 (2004), pp. 19–25. ISSN: 1077-2618. DOI: 10.1109/MIA.2004.1353043.

[65] Hadler K. et al., eds. *A Universal flowsheet and terminology for In-situ Resource Utilization (ISRU)*. 2019. URL: https://www.hou.usra.edu/meetings/lpsc2019/pdf/2609.pdf.

[66] H. M. Sargeant et al. “Feasibility studies for hydrogen reduction of ilmenite in a static system for use as an ISRU demonstration on the lunar surface”. In: *Planetary and Space Science* 180 (2020), p. 104759. ISSN: 00320633. DOI: 10.1016/j.pss.2019.104759.

[67] Zhang Lu and Lv Jianguo. “Shear Properties of Lunar Regolith Simulants”. In: *Procedia Engineering* 73 (2014), pp. 178–185. ISSN: 18777058. DOI: 10.1016/j.proeng.2014.06.186.

[68] Kevin W. Farries et al. “Sintered or melted regolith for lunar construction: state-of-the-art review and future research directions”. In: *Construction and Building Materials* 296 (2021), p. 123627. ISSN: 09500618. DOI: 10.1016/j.conbuildmat.2021.123627.

[69] Lawrence A. Taylor, Carle M. Pieters, and Daniel Britt. “Evaluations of lunar regolith simulants”. In: *Planetary and Space Science* 126 (2016), pp. 1–7. ISSN: 00320633. DOI: 10.1016/j.pss.2016.04.005.

[70] L. Sibile and P. Carpenter. “Lunar Regolith Simulant Materials: Recommendations for Standardization, Production and Usage”. In: (2006).

[71] D. S. McKay et al. “JSC-1: A new lunar regolith simulant”. In: *Lunar and Planetary Exploration* (1993), pp. 963–964.

[72] J. Gaier. “The need for high fidelity lunar regolith simulants”. In: (2008).

[73] *Regolith simulants*. URL: https://exolithsimulants.com/.

[74] Exolith Lab. “LMS-1 Lunar Mare Simulant: Fact Sheet”. In: *Dictionary Geotechnical Engineering/Wörterbuch GeoTechnik*. Ed. by Helmut Herrmann and Herbert Bucksch. Berlin, Heidelberg: Springer Berlin Heidelberg, 2014, p. 603. ISBN: 978-3-642-41713-9. DOI: 10.1007/978-3-642-41714-6{\textunderscore}70933.

[75] Stefan Linke et al. “TUBS-M and TUBS-T based modular Regolith Simulant System for the support of lunar ISRU activities”. In: *Planetary and Space Science* 180 (2020), p. 104747. ISSN: 00320633. DOI: 10.1016/j.pss.2019.104747.

[76] Patrick Sean Quinn and Agnese Benzonelli. “XRD and Materials Analysis”. In: *The Encyclopedia of Archaeological Sciences*. Ed. by Sandra L. López Varela. Hoboken, NJ, USA: John Wiley & Sons, Inc, 2018, pp. 1–5. ISBN: 9780470674611. DOI: 10.1002/9781119188230.saseas0619.

[77] Walther J. Friedrich, Paul Knipping, and Max von Laue. “Interferenzerscheinungen bei Röntgenstrahlen”. In: *Annalen der Physik* 346 (), pp. 971–988.

[78] J. Epp. “X-ray diffraction (XRD) techniques for materials characterization”. In: *Materials Characterization Using Nondestructive Evaluation (NDE) Methods*. Elsevier, 2016, pp. 81–124. ISBN: 9780081000403. DOI: 10.1016/B978-0-08-100040-3.00004-3.

[79] Emmanuel Garnier. “Powder Diffraction. Theory and Practice. Edited by R. E. Dinnebier and S. J. L. Billinge. Cambridge: RSC Publishing, 2008. Pp. xxi + 582. Price (hardcover): GBP 59.00. ISBN (online): 978-1-84755-823-7 ; ISBN (print): 978-0-85404-231-9”. In: *Acta Crystallographica Section A Foundations of Crystallography* 65.1 (2009), p. 51. ISSN: 0108-7673. DOI: 10.1107/S010876730802850X.

[80] R. E. Dinnebier and S. J. L. Billinge. *Powder Diffraction*. Cambridge: Royal Society of Chemistry, 2008. ISBN: 978-0-85404-231-9. DOI: 10.1039/9781847558237.

[81] W. L. Bragg. “The diffraction of short electromagnetic waves by a crystal”. In: *Proceedings of the Cambridge Philosophical Society*. Vol. 17. 1913, pp. 43–57.

[82] L. Spieß et al. *Moderne Röntgenbeugung: Röntgendiffraktometrie für Materialwissenschaftler, Physiker und Chemiker*. 2., überarbeitete und erweiterte Auflage. Wiesbaden: Vieweg+Teubner Verlag / GWV Fachverlage GmbH Wiesbaden, 2009. ISBN: 978-3-8349-9434-9. DOI: 10.1007/978-3-8349-9434-9.

[83] Lothar Spieß et al. *Moderne Röntgenbeugung: Röntgendiffraktometrie für Materialwissenschaftler, Physiker und Chemiker*. 3., überarbeitete Auflage. Wiesbaden and Heidelberg: Springer Spektrum, 2019. ISBN: 978-3-8348-1219-3.

[84] ICDD. Aug. 2022. URL: https://www.icdd.com/.

[85] G. Will. *Powder Diffraction: The Rietveld Method and the Two Stage Method to Determine and Refine Crystal Structures from Powder Diffraction Data*. Berlin/Heidelberg: Springer-Verlag, 2006. ISBN: 3-540-27985-7. DOI: 10.1007/3-540-27986-5.

[86] *Technology readiness levels (TRL)*. URL: https://www.esa.int/Enabling_Support/Space_Engineering_Technology/Shaping_the_Future/Technology_Readiness_Levels_TRL.

[87] J. N. Rasera et al. “Experimental investigation of an optimised tribocharger design for space resource utilisation”. In: *Planetary and Space Science* 228 (2023), p. 105651. ISSN: 00320633. DOI: 10.1016/j.pss.2023.105651.

Appendix A

Appendix A: Experimental Measurements

A.1 Experimental analysis

List of symbols used in the analysis of results

Symbol	Description
F_i	Feeder intensity (%)
f	Feed rate (kg/hr)
M_i	Mass of input sample (g)
M_o	Mass of output (g)
$M_{ilm,i}$	Mass of ilmenite in input (g)
C_i	Ilmenite content ($wt.\%$)
$M_{ilm,o}$	Mass of ilmenite in output
ω_m	Rotational speed of magnetic separator (rpm)
V	Field voltage (kV)
Y	Yield of ilmenite in output ($wt.\%$)
R	Recovery of ilmenite in output ($wt.\%$)
G_i	Grade of ilmenite in input ($wt.\%$)
G_o	Grade of ilmenite in output ($wt.\%$)
ER	Enrichment ratio of ilmenite in output

A.1.1 Phase 0: Preliminary Experiments

Feed rate conversion experiment results

Table A.1: Vibratory feeder feed rate unit conversion experiment results

F_i	Feeding time (s)					Average feeding time (s)	Average feeding time (hr)	f
	Trial 1	Trial 2	Trial 3	Trial 4	Trial 5			
100	57.62	65.98	66.32	59.11	63.25	62.46	0.02	28.82
90	111.45	110.87	109.8	110.92	109.6	110.53	0.03	16.29
80	165.8	186.5	180.08	187.25	184.06	180.74	0.05	9.96
70	275.55	298	294.8	302.63	295.55	293.32	0.08	6.14
60	441.59	510.66	491.5	531.31	493.67	493.75	0.14	3.65
50	993.79	1023.78	1023.87	1030.62	1021.02	1018.62	0.28	1.77
40	1586.86	3045	2030.9	2041.1	2035.28	2147.82	0.60	0.84

A.1.2 Phase A: Optimisation of gravitational and magnetic beneficiation

A.1.2.1 List of samples tested: Phase A

Table A.2: Sample list for optimisation experiments: Phase A

ω_m	f	Simulant	Trial #	Sample type	Sample identifier
794	1.77	LMS-1	01	Non-magnetic	LMS-MB-21XXG-01
				Magnetic	LMS-MB-21XXH-01
			02	Non-magnetic	LMS-MB-21XXG-02
				Magnetic	LMS-MB-21XXH-02
			03	Non-magnetic	LMS-MB-21XXG-03
				Magnetic	LMS-MB-21XXH-03
	6.14		01	Non-magnetic	LMS-MB-41XXG-01
				Magnetic	LMS-MB-41XXH-01
			02	Non-magnetic	LMS-MB-41XXG-02
				Magnetic	LMS-MB-41XXH-02
			03	Non-magnetic	LMS-MB-41XXG-03
				Magnetic	LMS-MB-41XXH-03
	28.82		01	Non-magnetic	LMS-MB-71XXG-01
				Magnetic	LMS-MB-71XXH-01
			02	Non-magnetic	LMS-MB-71XXG-02
				Magnetic	LMS-MB-71XXH-02
			03	Non-magnetic	LMS-MB-71XXG-03
				Magnetic	LMS-MB-71XXH-03

A.1.2.2 Results: Phase A experiments

Table A.3: Results: Phase A

Sample	F_i	f	M_i	M_o	$M_{ilm,i}$	C_i	$M_{ilm,o}$	Y	R	G_i	G_o	ER
LMS-MB-21XXH-01	50	1.77	300	28.89	12.1	0.16	0.046	0.02	0.38	4.03	0.16	0.04
LMS-MB-21XXH-02	50	1.77	300	43.78	12.1	0.34	0.149	0.05	1.23	4.03	0.34	0.08
LMS-MB-21XXH-03	50	1.77	300	22.08	12.1	1.46	0.322	0.11	2.67	4.03	1.46	0.36
LMS-MB-21XXG-01	50	1.77	300	94.54	12.1	3.59	3.394	1.13	28.05	4.03	3.59	0.89
LMS-MB-21XXG-02	50	1.77	300	107.79	12.1	2.46	2.652	0.88	21.92	4.03	2.46	0.61
LMS-MB-21XXG-03	50	1.77	300	135.68	12.1	1.68	2.279	0.76	18.84	4.03	1.68	0.42
LMS-MB-41XXH-01	70	6.14	300	30.53	12.1	1.06	0.324	0.11	2.67	4.03	1.06	0.26
LMS-MB-41XXH-02	70	6.14	300	23.05	12.1	0.74	0.171	0.06	1.41	4.03	0.74	0.18
LMS-MB-41XXH-03	70	6.14	300	31.15	12.1	0.51	0.159	0.05	1.31	4.03	0.51	0.13
LMS-MB-41XXG-01	70	6.14	300	128.51	12.1	3.72	4.781	1.59	39.51	4.03	3.72	0.92
LMS-MB-41XXG-02	70	6.14	300	136.57	12.1	1.38	1.885	0.63	15.58	4.03	1.38	0.34
LMS-MB-41XXG-03	70	6.14	300	128.65	12.1	1.59	2.046	0.68	16.91	4.03	1.59	0.39
LMS-MB-71XXH-01	100	28.82	300	26.58	12.1	0.52	0.138	0.05	1.14	4.03	0.52	0.13
LMS-MB-71XXH-02	100	28.82	300	24.98	12.1	0.14	0.035	0.01	0.29	4.03	0.14	0.03
LMS-MB-71XXH-03	100	28.82	300	22.41	12.1	0.46	0.103	0.03	0.85	4.03	0.46	0.11
LMS-MB-71XXG-01	100	28.82	300	131.21	12.1	3.61	4.737	1.58	39.14	4.03	3.61	0.90
LMS-MB-71XXG-02	100	28.82	300	135.18	12.1	2.4	3.244	1.08	26.81	4.03	2.40	0.60
LMS-MB-71XXG-03	100	28.82	300	139.86	12.1	2.53	3.538	1.18	29.24	4.03	2.53	0.63

A.1.3 Phase B: Optimisation of electrostatic beneficiation (iteration 1)

A.1.3.1 List of samples tested: Phase B

Table A.4: Sample list for optimisation experiments: Phase B

ω_m	f	Simulant	V	Trial #	Collection bin	Sample identifier
794	6.14	LMS-1	5	01	2	LMS-EB4110B-01
					3	LMS-EB4110C-01
					4	LMS-EB4110D-01
				02	2	LMS-EB4110B-02
					3	LMS-EB4110C-02
					4	LMS-EB4110D-02
				03	2	LMS-EB4110B-03
					3	LMS-EB4110C-03
					4	LMS-EB4110D-03
			15	01	2	LMS-EB4130B-01
					3	LMS-EB4130C-01
				02	2	LMS-EB4130B-02
					3	LMS-EB4130C-02
				03	2	LMS-EB4130B-03
					3	LMS-EB4130C-03
			25	01	2	LMS-EB4150B-01
					3	LMS-EB4150C-01
					4	LMS-EB4150D-01
				02	2	LMS-EB4150B-02
					3	LMS-EB4150C-02
					4	LMS-EB4150D-02
				03	2	LMS-EB4150B-03
					3	LMS-EB4150C-03
					4	LMS-EB4150D-03

A.1.3.2 Results: Phase B

Table A.5: Results: Phase B

Sample #	V	M_i	Trial 1								
			M_o	$M_{ilm,i}$	C_i	$M_{ilm,o}$	Y	R	G_i	G_o	ER
LMS-EB4110B	5	300	5.61	12.1	6.22	0.349	0.12	2.88	4.03	6.22	1.54
LMS-EB4110C	5	300	71.99	12.1	2.14	1.541	0.51	12.73	4.03	2.14	0.53
LMS-EB4110D	5	300	45.55	12.1	1.31	0.597	0.20	4.93	4.03	1.31	0.32
LMS-EB4130B	15	300	65.9	12.1	12.94	8.527	2.84	70.47	4.03	12.94	3.21
LMS-EB4130C	15	300	37.72	12.1	1.64	0.619	0.21	5.11	4.03	1.64	0.41
LMS-EB4150B	25	300	23.88	12.1	8.96	2.140	0.71	17.68	4.03	8.96	2.22
LMS-EB4150C	25	300	102.09	12.1	0.82	0.837	0.28	6.92	4.03	0.82	0.20
LMS-EB4150D	25	300	4.35	12.1	0.25	0.011	0.00	0.09	4.03	0.25	0.06

Sample #	V	M_i	Trial 2								
			M_o	$M_{ilm,i}$	C_i	$M_{ilm,o}$	Y	R	G_i	G_o	ER
LMS-EB4110B	5	300	9.47	12.1	10.47	0.99	0.33	8.19	4.03	10.47	2.60
LMS-EB4110C	5	300	69.9	12.1	2.21	1.54	0.51	12.77	4.03	2.21	0.55
LMS-EB4110D	5	300	-	-	-	-	-	-	-	-	-
LMS-EB4130B	15	300	7.5	12.1	11.51	0.863	0.29	7.13	4.03	3.84	0.95
LMS-EB4130C	15	300	118.72	12.1	1.02	1.211	0.40	0.86	4.03	0.34	0.08
LMS-EB4150B	25	300	36.64	12.1	7.47	2.737	0.91	20.39	4.03	2.49	0.62
LMS-EB4150C	25	300	87.28	12.1	0.82	0.716	0.24	0.94	4.03	0.27	0.07
LMS-EB4150D	25	300	2.78	12.1	0	0.000	0.00	0.00	4.03	0.00	0.00

Table A.6: Results: Phase B

Sample #	V	M_i	Trial 3								
			M_o	$M_{ilm,i}$	C_i	$M_{ilm,o}$	Y	R	G_i	G_o	ER
LMS-EB4110B	5	300	5.72	12.1	9.2	0.526	0.18	4.35	4.03	9.20	2.28
LMS-EB4110C	5	300	120.97	12.1	0.87	1.052	0.35	8.70	4.03	0.87	0.22
LMS-EB4110D	5	300	-	-	-	-	-	-	-	-	-
LMS-EB4130B	15	300	18.79	12.1	11.37	2.136	0.71	17.66	4.03	11.37	2.82
LMS-EB4130C	15	300	111.24	12.1	1.2	1.335	0.44	11.03	4.03	1.20	0.30
LMS-EB4150B	25	300	28.52	12.1	8.5	2.424	0.81	20.03	4.03	8.50	2.11
LMS-EB4150C	25	300	94.9	12.1	0.43	0.408	0.14	3.37	4.03	0.43	0.11
LMS-EB4150D	25	300	1.32	12.1	1.08	0.014	0.00	0.12	4.03	1.08	0.27

Sample #	V	M_i	Average			
			Y	R	G_o	ER
LMS-EB4110B	5	300	0.21	5.14	8.63	2.14
LMS-EB4110C	5	300	0.46	11.40	1.74	0.43
LMS-EB4110D	5	300	0.20	4.93	1.31	0.32
LMS-EB4130B	15	300	1.28	31.76	9.38	2.33
LMS-EB4130C	15	300	0.35	5.67	1.06	0.26
LMS-EB4150B	25	300	0.81	19.37	6.65	1.65
LMS-EB4150C	25	300	0.22	3.74	0.51	0.13
LMS-EB4150D	25	300	0.00	0.07	0.44	0.11

A.1.4 Phase C: Optimisation of electrostatic beneficiation (iteration 2)

A.1.4.1 List of samples tested: Phase C

Table A.7: Sample list for optimisation experiments: Phase C

ω_m	f	Simulant	V	Trial #	Collection bin	Sample identifier
794	6.14	LMS-1	13	01	2	LMS-EB4126B-01
					3	LMS-EB4126C-01
				02	2	LMS-EB4126B-02
					3	LMS-EB4126C-02
				03	2	LMS-EB4126B-03
					3	LMS-EB4126C-03
			14	01	2	LMS-EB4128B-01
					3	LMS-EB4128C-01
				02	2	LMS-EB4128C-01
					3	LMS-EB4128C-02
				03	2	LMS-EB4128B-03
					3	LMS-EB4128C-03
			16	01	2	LMS-EB4132B-01
					3	LMS-EB4132C-01
				02	2	LMS-EB4132B-02
					3	LMS-EB4132C-02
				03	2	LMS-EB4132B-03
					3	LMS-EB4132C-03
			17	01	2	LMS-EB4134B-01
					3	LMS-EB4134C-01
				02	2	LMS-EB4134C-02
					3	LMS-EB4134C-02
				03	2	LMS-EB4134B-03
					3	LMS-EB4134C-03

A.1.4.2 Results: Phase C

Table A.8: Results: Phase C

Sample #	V	M_i	Trial 1								
			M_o	$M_{ilm,i}$	C_i	$M_{ilm,o}$	Y	R	G_i	G_o	ER
LMS-EB4126B	13	300	26	12.1	11.71	3.04	1.01	25.16	4.03	11.71	2.90
LMS-EB4126C	13	300	99.36	12.1	0.58	0.576	0.19	4.76	4.03	0.58	0.14
LMS-EB4128B	14	300	30.8	12.1	10.38	3.197	1.07	26.42	4.03	10.38	2.57
LMS-EB4128C	14	300	76.79	12.1	0.61	0.468	0.16	3.87	4.03	0.61	0.15
LMS-EB4132B	16	300	37.45	12.1	7.32	2.741	0.91	22.66	4.03	7.32	1.81
LMS-EB4132C	16	300	86.69	12.1	1.72	1.491	0.50	12.32	4.03	1.72	0.43
LMS-EB4134B	17	300	17.44	12.1	11.52	2.009	0.67	16.60	4.03	11.52	2.86
LMS-EB4134C	17	300	118.13	12.1	2.12	2.504	0.83	20.70	4.03	2.12	0.53

Sample #	V	M_i	Trial 2								
			M_o	$M_{ilm,i}$	C_i	$M_{ilm,o}$	Y	R	G_i	G_o	ER
LMS-EB4126B	13	300	15.59	12.1	11.75	1.832	0.61	15.14	4.03	11.75	2.91
LMS-EB4126C	13	300	100.68	12.1	0.67	0.675	0.22	5.57	4.03	0.67	0.17
LMS-EB4128B	14	300	41.51	12.1	13.19	5.475	1.83	45.25	4.03	13.19	3.27
LMS-EB4128C	14	300	76.49	12.1	0.59	0.451	0.15	3.73	4.03	0.59	0.15
LMS-EB4132B	16	300	50.24	12.1	9.63	4.838	1.61	39.98	4.03	9.63	2.39
LMS-EB4132C	16	300	78.17	12.1	2.14	1.673	0.56	13.83	4.03	2.14	0.53
LMS-EB4134B	17	300	22.94	12.1	11.88	2.725	0.91	22.52	4.03	11.88	2.95
LMS-EB4134C	17	300	122.57	12.1	3.97	4.866	1.62	40.22	4.03	3.97	0.98

Sample #	V	M_i	Trial 3								
			M_o	$M_{ilm,i}$	C_i	$M_{ilm,o}$	Y	R	G_i	G_o	ER
LMS-EB4126B	13	300	20.78	12.1	12.84	2.668	0.89	22.05	4.03	12.84	3.18
LMS-EB4126C	13	300	87.51	12.1	0.78	0.683	0.23	5.64	4.03	0.78	0.19
LMS-EB4128B	14	300	23.76	12.1	12.28	2.918	0.97	24.11	4.03	12.28	3.04
LMS-EB4128C	14	300	86.09	12.1	0.91	0.783	0.26	6.47	4.03	0.91	0.23
LMS-EB4132B	16	300	28.56	12.1	8.06	2.302	0.77	19.02	4.03	8.06	2.00
LMS-EB4132C	16	300	101.47	12.1	3.14	3.186	1.06	26.33	4.03	3.14	0.78
LMS-EB4134B	17	300	61.831	12.1	11.72	7.247	2.42	59.89	4.03	11.72	2.91
LMS-EB4134C	17	300	100.227	12.1	1.11	1.113	0.37	9.19	4.03	1.11	0.28

Sample #	V	M_i	Average			
			Y	R	G_o	ER
LMS-EB4126B	13	300	0.84	20.78	12.10	3.00
LMS-EB4126C	13	300	0.21	5.33	0.68	0.17
LMS-EB4128B	14	300	1.29	31.93	11.95	2.96
LMS-EB4128C	14	300	0.19	4.69	0.70	0.17
LMS-EB4132B	16	300	1.10	27.22	8.34	2.07
LMS-EB4132C	16	300	0.71	17.49	2.33	0.58
LMS-EB4134B	17	300	1.33	33.00	11.71	2.90
LMS-EB4134C	17	300	0.94	23.37	2.40	0.60

A.1.5 Phase D: Optimisation of electrostatic beneficiation (iteration 2)

A.1.5.1 List of samples tested: Phase D

Table A.9: Sample list for optimisation experiments: Phase D

ω_m	f	Simulant	V	Trial #	Collection bin	Sample identifier
794	6.14	TMIA4	14	01	2	TUB-EB-4128B-01
					3	TUB-EB-4128C-01
				02	2	TUB-EB-4128B-02
					3	TUB-EB-4128C-02
				03	2	TUB-EB-4128B-03
					3	TUB-EB-4128C-03

A.1.5.2 Results: Phase D

Table A.10: Results: Phase D

Sample #	V	M_i	Trial 1								
			M_o	$M_{ilm,i}$	C_i	$M_{ilm,o}$	Y	R	G_i	G_o	ER
TUB-EB-4128B	14	300	12.56	12.1	8.55	1.07	0.36	8.88	4.03	8.55	2.12
TUB-EB-4128C	14	300	113	12.1	7.07	7.99	2.66	66.03	4.03	7.07	1.75

Sample #	V	M_i	Trial 2								
			M_o	$M_{ilm,i}$	C_i	$M_{ilm,o}$	Y	R	G_i	G_o	ER
TUB-EB-4128B	14	300	68.75	12.1	7.97	5.48	1.83	45.28	4.03	7.97	1.98
TUB-EB-4128C	14	300	75.63	12.1	5.10	3.86	1.29	31.88	4.03	5.10	1.26

Sample #	V	M_i	Trial 3								
			M_o	$M_{ilm,i}$	C_i	$M_{ilm,o}$	Y	R	G_i	G_o	ER
TUB-EB-4128B	14	300	75.89	12.1	9.07	6.8	2.29	56.89	4.03	9.07	2.25
TUB-EB-4128C	14	300	91.24	12.1	4.74	4.32	1.44	35.74	4.03	4.74	1.18

Sample #	V	M_i	Average			
			Y	R	G_o	ER
TUB-EB-4128B	14	300	1.49	37.02	8.53	2.11
TUB-EB-4128C	14	300	1.80	44.55	5.64	1.40

Beneficiation energy consumption across experimental phases

Table A.11: Beneficiation energy consumption across experimental phases

Experimental Phase	Experiment	Feeder		
		Power (Watt)	Time (hr)	Energy (Watt-hr)
Phase A	LMS-MB-21XX	20	0.283	5.67
	LMS-MB-41XX	20	0.083	1.67
	LMS-MB-71XX	20	0.017	0.33
Phase B	LMS-EB-4110XX	20	0.083	1.67
	LMS-EB-4130XX	20	0.083	1.67
	LMS-EB-4150XX	20	0.083	1.67
Phase B	LMS-EB-4126XX	20	0.083	1.67
	LMS-EB-4128XX	20	0.083	1.67
	LMS-EB-4132XX	20	0.083	1.67
	LMS-EB-4134XX	20	0.083	1.67

Experimental Phase	Experiment	Sifter		
		Power (Watt)	Time (hr)	Energy (Watt-hr)
Phase A	LMS-MB-21XX	210	0.367	77
	LMS-MB-41XX	210	0.250	52.5
	LMS-MB-71XX	210	0.100	21
Phase B	LMS-EB-4110XX	210	0.250	52.5
	LMS-EB-4130XX	210	0.250	52.5
	LMS-EB-4150XX	210	0.250	52.5
Phase B	LMS-EB-4126XX	210	0.250	52.5
	LMS-EB-4128XX	210	0.250	52.5
	LMS-EB-4132XX	210	0.250	52.5
	LMS-EB-4134XX	210	0.250	52.5

Experimental Phase	Experiment	Magnetic separator motor		
		Power (Watt)	Time (hr)	Energy (Watt-hr)
Phase A	LMS-MB-21XX	11	0.450	4.95
	LMS-MB-41XX	11	0.250	2.7
	LMS-MB-71XX	11	0.183	2.02
Phase B	LMS-EB-4110XX	11	0.250	2.75
	LMS-EB-4130XX	11	0.250	2.75
	LMS-EB-4150XX	11	0.250	2.75
Phase B	LMS-EB-4126XX	11	0.250	2.75
	LMS-EB-4128XX	11	0.250	2.75
	LMS-EB-4132XX	11	0.250	2.75
	LMS-EB-4134XX	11	0.250	2.75

Experimental Phase	Experiment	Electrostatic high voltage power supply		
		Power (Watt)	Time (hr)	Energy (Watt-hr)
Phase A	LMS-MB-21XX	0	0	0
	LMS-MB-41XX	0	0	0
	LMS-MB-71XX	0	0	0
Phase B	LMS-EB-4110XX	2.5	0.33	0.83
	LMS-EB-4130XX	7.5	0.33	2.50
	LMS-EB-4150XX	12.5	0.33	4.17
Phase B	LMS-EB-4126XX	6.5	0.33	2.17
	LMS-EB-4128XX	7	0.33	2.33
	LMS-EB-4132XX	8	0.33	2.67
	LMS-EB-4134XX	8.5	0.33	2.83

Experimental Phase	Experiment	Total energy consumption (Watt-hr)
Phase A	LMS-MB-21XX	88
	LMS-MB-41XX	57
	LMS-MB-71XX	23
Phase B	LMS-EB-4110XX	58
	LMS-EB-4130XX	59
	LMS-EB-4150XX	61
Phase B	LMS-EB-4126XX	59
	LMS-EB-4128XX	59
	LMS-EB-4132XX	60
	LMS-EB-4134XX	60

Discrepancy Analysis: Expected vs. Actual experimental results

Table A.12: Discrepancy analysis: Expected vs. Actual experimental results

Parameter	Expected	LMS-1	TMIA4
Recovery of ilmenite (wt.%)	50	31.93	37.03
Grade of ilmenite (wt.%)	40	11.95	8.53
Enrichment ratio of ilmenite	4.5	2.90	2.11

Appendix B

Appendix B: Datasheets

B.1 Magnetic separator motor datasheet

RS PRO

RS PRO APPROVED

ENGLISH

Datasheet

RS PRO, 12 V dc, 640 gcm, Brushed DC Geared Motor, Output Speed 2900 rpm

Stock No: **454-0877**

Specifications:

Output Speed	2900 rpm
Supply Voltage	12 V dc
Maximum Output Torque	640 g.cm
DC Motor Type	Brushed
Shaft Diameter	6mm
Power Rating	19.8 W
Gearhead Type	Planetry
Length	76.5mm
Width	35.8mm
Current Rating	2.8 A
Weight	261g

rspro.com

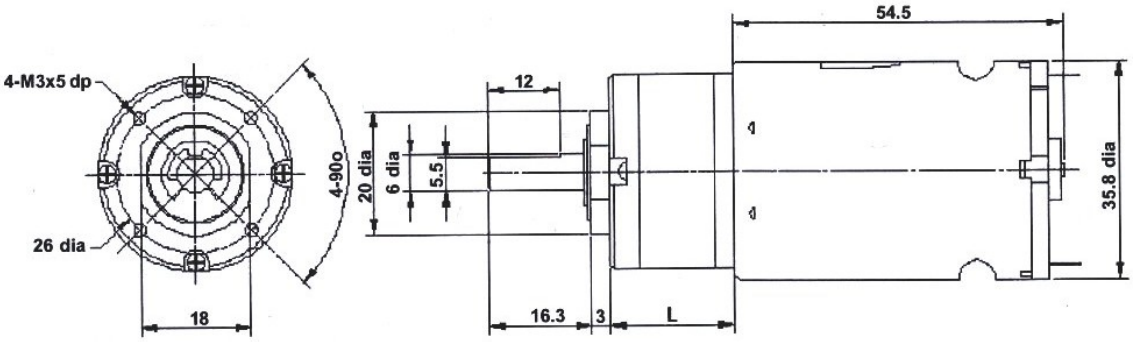

Operating relative humidity 20% ~ 85%
Operating temperature range -10°C ~ +60°C

Ratio	L
5:1	22.0mm

Gearbox Housing material	Metal
Backlash at no-load	< 2.5°
Bearing at output	Sleeve bearings
Radial load (10mm from flange)	< 3 kgf
Shaft axial load	< 2.5 kgf
Shaft press fit force max	< 10 kgf
Radial play of shaft	< 0.05mm
Thrust play of shaft	< 0.3mm

Reduction Ratio	Rated tolerance Torque	Max momentary Tolerance Torque	Efficiency
1/5	2 kgf-cm Max.	6 kgf-cm	80%

Reduction Table RPM SUPPLY VOLTAGE	4.5v	6v	9v	12v	15v
454-0877	1088	1450	2175	2900	3625

Note: Motor speeds may vary by (+) or (-) 12.5%

B.2 LMS-1 Factsheet

LMS-1 Lunar Mare Simulant | **Fact Sheet**

December, 2022

Simulant Name: LMS-1 Mare Simulant
Simulant Type: General purpose
Reference Material: Average lunar maria
Uncompressed Bulk Density: 1.56 g/cm^3
Mean Particle Size: 91 µm
Median Particle Size: 60 µm
Particle Size Range: <0.04 µm – 1000 µm

Geotechnical Properties

Grain Density: 2.92g/cm^3
Void Ratio: 0.8718
Porosity: 46.6%
[1]Max Angle of Repose: 38.3°
[2]Cohesion: 0.393 kPa
[2]Angle of Internal Friction: 34.84°

Geotechnical Property Sources

[1] (PDF) Comparing the Effects of Mineralogy and Particle Size Distribution on the Angle of Repose for Lunar Regolith Simulants (researchgate.net)

[2] 2038.PDF (usra.edu)

Mineralogy

As mixed.

Component	Wt.%
Pyroxene	32.8
Glass-rich basalt	32.0
Anorthosite	19.8
Olivine	11.1
Ilmenite	4.3

Safety

See SDS for details. Primary hazard is dust inhalation; wear a respirator in dusty conditions.

Bulk Chemistry

Relative abundances. Measured by XRF.

Oxide	Wt.%
SiO_2	46.9
TiO_2	3.6
Al_2O_3	12.4
FeO	8.6
MnO	0.2
MgO	16.8
CaO	7.0
Na_2O	1.7
K_2O	0.7
P_2O_5	0.2
LOI*	0.9
Total**	99.0

* Loss on ignition
** Excluding volatiles and trace elements

Photo credit Matthew Villegas. XRF data obtained by Hamilton Analytical Lab using fused bead sample preparation. Reflectance spectrum courtesy of Dr. Takahiro Hiroi, NASA RELAB, Brown University.

LMS-1 Lunar Mare Simulant | **Fact Sheet**

December, 2022

Trace Elements

Measured by XRF

Element	ppm
Ni	561
Cr	1728
V	155
Sc	20.7
Cu	26
Zn	66
Ga	18
Ba	173
Rb	14
Cs	0
Sr	265
Y	12
Zr	131
Hf	3.3
Nb	57.7
Ta	1
Mo	8
La	10
Ce	30
Nd	13
Sm	2.5
Dy	2.7
Yb	1.0
Th	3
U	3
Tl	0
Pb	15
Sn	1
Bi	0
Sb	1

Volatiles

Measured by XRF

Compound	Wt%
F	≥0.06
Cl	≥0.008
SO_3	≥0.01

Compound	ppm
Br	≥1
As	≥0

Reflectance Spectrum

Incidence angle 30°, emission angle 0°

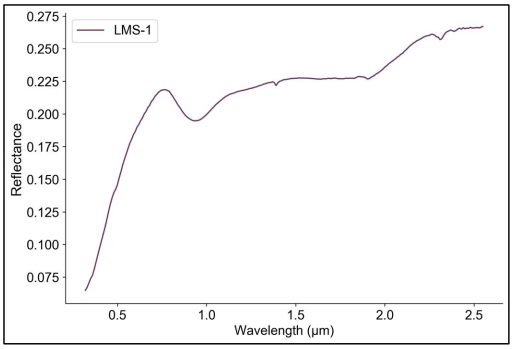

Mid-Infrared FTIR Spectrum

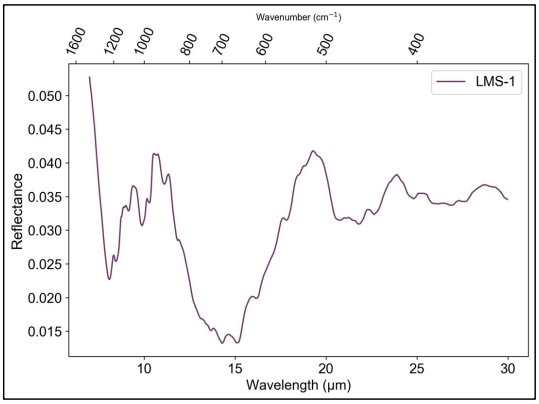

XRF data obtained by Hamilton Analytical Lab using fused bead sample preparation. FTIR spectrum courtesy of Dr. Takahiro Hiroi, NASA RELAB, Brown University.

LMS-1 Lunar Mare Simulant | **Fact Sheet**

December, 2022

Volumetric Particle Size Distribution

From CILAS 1190 laser diffraction particle size analyzer

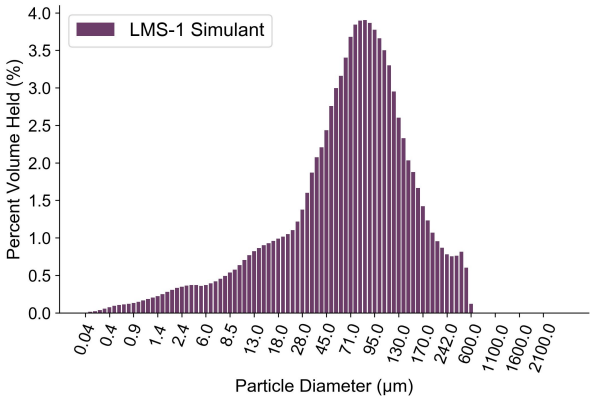

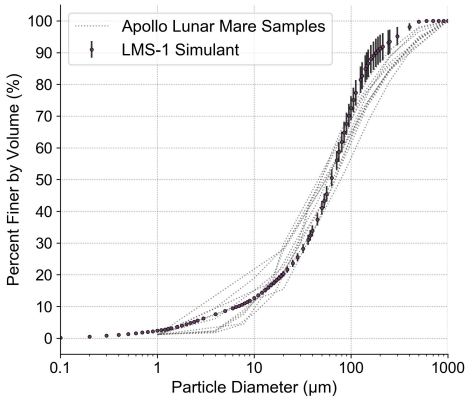

Sieve Analysis

Following ASTM Standard E11 using RO-TAP RX-30 sieve shaker

Sieve Number	Diameter (µm)	Mass of Soil Retained on Each Sieve (g)	Percent Retained by Mass (%)	Cumulative Retained by Mass (%)	Percent Finer by Mass (%)
18	1000	0.0	0.0%	0.0%	100.0%
25	710	82.2	8.3%	8.3%	91.7%
35	500	82.2	8.3%	16.6%	83.4%
45	355	84.8	8.6%	25.2%	74.8%
70	212	133.7	13.5%	38.7%	61.3%
140	106	239.7	24.2%	62.9%	37.1%
200	75	149.5	15.1%	78.1%	21.9%
270	53	133.5	13.5%	91.6%	8.4%
PAN		83.5	8.4%	100.0%	0.0%

Sieve analysis skews particle size larger, as many of the fines cling to the larger pieces of regolith. This is measured by mass percent rather than volume